NASA Technical Memorandum 112857

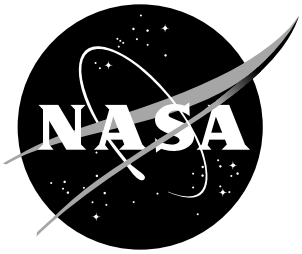

Results of Aerothermodynamic and Boundary Layer Transition Testing of 0.0362-Scale X-38 (Rev 3.1) Vehicle in NASA Langley 20-Inch Mach 6 Tunnel

Scott A. Berry, Thomas J. Horvath, V. Eric Roback, and George B. Williams, Jr.

September 1997

NASA Technical Memorandum 112857

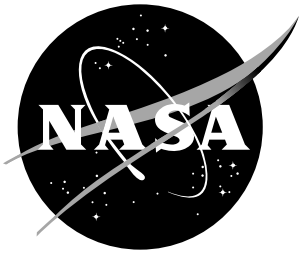

Results of Aerothermodynamic and Boundary Layer Transition Testing of 0.0362-Scale X-38 (Rev 3.1) Vehicle in NASA Langley 20-Inch Mach 6 Tunnel

Scott A. Berry, Thomas J. Horvath, V. Eric Roback, and George B. Williams, Jr.
Langley Research Center, Hampton, Virginia

National Aeronautics and
Space Administration

Langley Research Center
Hampton, Virginia 23681-2199

September 1997

Available from the following:

NASA Center for AeroSpace Information (CASI)
800 Elkridge Landing Road
Linthicum Heights, MD 21090-2934
(301) 621-0390

National Technical Information Service (NTIS)
5285 Port Royal Road
Springfield, VA 22161-2171
(703) 487-4650

Contents

Abstract

The aeroheating characteristics of the X-38 Revision 3.1 configuration have been experimentally examined in the Langley 20-Inch Mach 6 Tunnel. Global surface heat transfer distributions, surface streamline patterns, and shock shapes were measured on a 0.0362-scale model of a proposed Space Station Crew Return Vehicle at Mach 6 in air. Parametric variations include angles-of-attack of 20°, 30°, and 40°; Reynolds numbers based on model length of 0.9 to 3.7 million; and body-flap deflections of 0°, 20°, 25°, and 30°. The effects of discrete roughness elements, which included trip height, location, size, and orientation, as well as multiple-trip parametrics, were investigated. This document is intended to serve as a quick release of preliminary data to the X-38 program; analysis is limited to observations of the experimental trends in order to expedite dissemination.

Introduction

The International Space Station is currently scheduled to be fully operational by June, 2002, ushering in a new era of space exploration and space-based scientific research. When complete, the Space Station will be permanently occupied by a crew of six, which will, at least initially, rely on permanently docked Soyuz spacecrafts to serve as escape "lifeboats" in case of an emergency. The Soyuz utilizes a "ballistic" reentry which allows for little cross-range capability and maneuverability. In the event of a medical emergency, the Soyuz may be forced to loiter in space while seeking a ballistic entry corridor that will allow touchdown in the vicinity of appropriate medical facilities. A crew return vehicle based on lifting body technology could take advantage of the inherent cross-range capability to minimize on-orbit loiter time. A candidate Assured Crew Return Vehicle (ACRV) has been designed based on a derivative of the circa 1960 X-23/X-24A lifting body configurations. (See Ref. 1 and 2 for detailed descriptions and flight tests results from the X-23, also known as SV-5D PRIME, and X-24A programs, respectively.) A sketch comparing the differences between these two configurations is shown in Fig. 1. A full-scale, unpiloted flight test vehicle prototype, designated the X-38 (and has been also referred to as XCRV and X-35), is currently being designed for a space flight test in early 1999. References 3 and 4 provide additional detail about the X-38 program and results.

This report presents the preliminary results of wind tunnel tests T6735 and T6739, conducted in the NASA Langley Research Center (LaRC) 20-Inch Mach 6 Tunnel during December, 1996, and January, 1997, in support of the X-38 program. The purpose of these tests was to investigate the aeroheating characteristics of a proposed X-38 configuration (designated as Revision 3.1) and to examine the effect of discrete roughness elements on the windward surface boundary layer. Preliminary trajectory information (provided by Chuck Campbell of JSC) is presented in Fig. 2 and shows that the flight vehicle would experience a length Reynolds number (Re_L), based on a body length of 23-ft, of roughly 4 million at a freestream Mach number of 6. These conditions can be simulated in the LaRC 20-Inch Mach 6 Tunnel which has a Re_L range of 0.4 to 6.7 million for a model length of 10-in (thus the model is a 0.0362-scale of the 23-ft long flight vehicle). Test techniques that were utilized during these tests include thermographic phosphors which provides global surface heating images, oil-flow which provides surface streamline information, and schlieren which provide shock system details. Parametrics included in these tests were the effect of angle of attack (α of 20°, 30°, and 40°), Reynolds number (Re/ft between 1 and 6 million), body flap deflections (δ_{bf} of 0°, 20°, 25°, and 30°), and discrete roughness elements (which included height, location, orientation, and multiple-trip effects). The discrete roughness parametrics were included in these tests to provide information to develop a roughness transition correlation for the X-38 vehicle which would be similar to that which was established for the Shuttle Orbiter (Ref. 5) and would be used to provide surface roughness tolerances for the flight vehicle.

Nomenclature

M	Mach number
Re	unit Reynolds number (1/ft.)

Re_L	Reynolds number based on body length
α	model angle of attack (deg)
δ_{bf}	body flap deflection (deg)
p	pressure (psi)
T	temperature (°R)
x	longitudinal distance from the nose (in)
y	axial distance from the centerline (in)
z	height above the waterline (in)
L	reference length of model (10.25 in)
b	reference beam of the model (5.01 in)
h	heat transfer coefficient (lbm/ft^2-sec), $=q/(H_{aw} - H_w)$ where $H_{aw} = H_{t2}$
h_{F-R}	reference coefficient using Fay-Ridell calculation to stagnation point of a sphere
q	heat transfer rate (BTU/ft^2-sec)
H	enthalpy (BTU/lbm)
k	roughness element height (in)
W	roughness element diagonal width (in)
O	roughness element orintation (deg)
Subscripts	
∞	freestream static conditions
t1	reservoir conditions
t2	stagnation conditions behind normal shock
aw	adiabatic wall
w	model surface

Test Facility

The present experiment was conducted in the LaRC 20-Inch Mach 6 Tunnel (a schematic is provided in Fig. 3). A detailed description of this hypersonic blowdown facility which uses heated, dried, and filtered air as the test gas, is provided by Miller (Ref. 6). Typical operating conditions for the tunnel are stagnation pressures ranging from 30 to 500 psia, stagnation temperatures from 760° to 1000°R, and freestream unit Reynolds numbers from 0.5 to 8 million per foot. A two-dimensional, contoured nozzle is used to provide nominal freestream Mach numbers from 5.8 to 6.1. The test section is 20.5 by 20 inches; the nozzle throat is 0.399 by 20.5 inch. A bottom-mounted model injection system can insert models from a sheltered position to the tunnel centerline in less than 0.5-sec. Run times up to 15 minutes are possible with this facility, although for the current heat transfer and flow visualization tests, the model was exposed to the flow for only a few seconds. Flow conditions were determined from the measured reservoir pressure and temperature and the measured pitot pressure at the test section and were compared to a recent unpublished calibration of the facility.

Test Techniques

Surface Heating

The rapid advances in image processing technology which have occurred in recent years have made digital optical measurement techniques practical in the wind tunnel. One such optical acquisition method is two-color relative-intensity phosphor thermography, see Refs. 7, 8, and 9, (a diagram is shown in Fig. 4), which is currently being applied to aeroheating tests in the hypersonic wind tunnels of NASA Langley Research Center (for example, see Ref.

5, 10, or 11). With this technique, ceramic wind tunnel models are fabricated and coated with phosphors which fluoresce in two regions of the visible spectrum when illuminated with ultraviolet light. The fluorescence intensity is dependent upon the amount of incident ultraviolet light and the local surface temperature of the phosphors. By acquiring fluorescence intensity images with a color video camera of an illuminated phosphor model exposed to flow in a wind tunnel, surface temperature mappings can be calculated on the portions of the model which are in the field of view of the camera. A temperature calibration of the system conducted prior to the study provides the look-up tables which are used to convert the ratio of the green and red intensity images to global temperature mappings. With temperature images acquired at different times in a wind tunnel run, global heat transfer images are computed assuming one-dimensional heat conduction. The primary advantage of this technique is the global resolution of the quantitative heat transfer data. Such data can be used to identify the heating footprint of complex, three-dimensional flow phenomena (e.g., transition fronts, turbulent wedges, boundary layer vortices, etc.) that are extremely difficult to resolve by discrete measurement techniques. Phosphor thermography is routinely used in Langley's hypersonic facilities as quantitative global information is provided by models that can be fabricated much quicker and more economically than other "more conventional" techniques. Recent comparisons of heat transfer measurements obtained from phosphor thermography to conventional thin-film resistance gauges measurements (Ref. 11) and CFD predictions (Ref. 12) have shown excellent agreement.

Flow Visualization

Flow visualization techniques, in the form of schlieren and oil-flow, were used to complement the surface heating tests. The LaRC 20-Inch Mach 6 Tunnel is equipped with a pulsed white-light, Z-pattern, single-pass schlieren system with a field of view encompassing the entire 20-in test core. Images were recorded on 70-mm film and digitally scanned for incorporation in this report. Surface streamline patterns were obtained using the oil-flow technique. Backup ceramic models were spray-painted black to enhance contrast with the white pigmented oils used to trace streamline movement. A thin basecoat of clear silicon oil was first applied to the surface, then a mist of medium-sized pigmented-oil drops was sprayed onto the surface. After the model surface was prepared, the model was injected into the airstream and the development of the surface streamlines were recorded with a conventional video camera. The model was retracted immediately following flow establishment and formation of streamline patterns, and post-run digital photographs were recorded with a Kodak high-resolution camera.

Model Description

The X-38 model dimensions are shown in Fig. 5. A rapid prototyping technique was used to build a resin stereolithography (SLA) model with various, detachable lower-surface body flaps. The lower surface body flaps have separate left and right sections (with a flow-through gap in between) that, for the flight vehicle, are intended to be symmetrically deflected for pitch control or differentially deflected for lateral aerodynamic control. To simplify model construction, the body flaps were modeled as wedges, as oppossed to deflected flaps of finite wall thickness. The SLA model was then used with the various wedge body flaps as a pattern to cast several ceramic model configurations. Figure 6 is a photograph of the 6 model configurations that were cast with the various body flap deflections. The model designation numbers for these 6 models, including both primary "A" models used for heating and back-up "B" models used for flow visualization, are listed in Table 1 along with the windward surface contour measurement accuracies. Two casts of each configuration were made, with the primary ceramic shell being immediately prepared for testing (backfilled and phosphor coated) and the back-up shell held in reserve, in case of problems with the primary. Once the phosphor testing was completed, the backup models were spray-coated with a thin black glazing (to seal the surface), final fired in the kiln, and then back-filled for use as the oil-flow and schlieren models. The surface contour accuracies listed in Table 1 were determined from Quality Assurance measurements using a Brown and Sharpe Series 7300 Coordinate Measurement Machine (with quoted linear accuracies on the order of 0.0003 in. or better) and correspond to the difference between the actual surface measurement for each model and the original CAD geometry for the windward surface centerline. The values shown in the four "Surface Accuracy Measurements" columns of the table correspond to weighted-averaged surface accuracies over the first four 20% segments of the models' windward surfaces (the surface accuracy of the final 20% segment, which covers the body flap region, is incorporated in the body flap deflection accuracies). The body flap deflections were generally found to be accurate to within ± 1 deg.

In order to obtain accurate heat transfer data using the one-dimensional heat conduction equation, models need to

be made of a material with low thermal diffusivity and well defined, uniform, isotropic thermal properties. Also, the models must be durable for repeated use in the wind tunnel and not deform when thermally cycled. To meet these requirements, a unique, silica ceramic investment slip casting method has been developed and patented (Ref. 13). A hydraulically setting magnesia ceramic was used to backfill the ceramic shell, thus providing strength and support to the sting structure. The models were then coated with a mixture of phosphors suspended in a silica-based colloidal binder. This coating consisted of a 5:1 mixture of lanthanum oxysulfide (La_2O_2S) doped with trivalent europium and zinc cadmium sulfide (ZnCdS) doped with silver and nickel in a proprietary ratio. The coatings typically do not require refurbishment between runs in the wind tunnel and have been measured to be approximately 0.001 inches thick. Figure 7 shows photographs of one of the models installed in the 20-inch Mach 6 Tunnel. The final step in the fabrication process is to apply fiducial marks along the body to assist in determining spatial locations accurately. The fiducial marks used for the present study are shown in a sketch in Fig. 8 and the non-dimensional locations are listed in Table 2. The fiducial marks along the centerline designated with the letters "A" through "E" correspond to the roughness element locations.

The roughness elements used in this study were similar to the method used in Ref. 5 which were fabricated to simulate a raised Thermal Protection System (TPS) tile and were cut from 0.0025-inch thick Kapton tape. Variations on the roughness heights (k) were obtained by stacking multiple layers of Kapton tape (k = 0.0025, 0.0050, and 0.0075-inch). Roughness elements fabricated from Kapton tape were easily applied to the various locations of interest on the model without adversely affecting the phosphor coating. Kapton tape was chosen through a trial and error process based on the ease of fabrication and application of the roughness elements, as well as the durability of the material (and adhesive) to heat and shear stress loading. The simulated tile roughness elements were placed directly over the various fiducial marks which were previously located on the model. Presented in Fig. 9 is a sketch of a typical trip showing dimensions and orientation. A variation in roughness element width was investigated, ranging from the small sizes used in Ref. 5 to the approximate-size scaled TPS tile for the X-38 flight vehicle (0.050, 0.100, 0.200, and 0.400-inch square). Also, the orientation of the roughness elements was investigated, in 15° increments ranging from 0° to 45°. A few multiple trip configurations were also tested and these are shown in Fig. 10. The numbers assigned to the multiple trips shown in Fig. 10 correspond to the numbers listed in Table 4 under the "Multiple Trip Configuration" column.

Test Conditions

The LaRC 20-Inch Mach 6 Tunnel provides a freestream unit Reynolds number variation of 0.5 to 8.0 million per foot. For a 0.0362-scale model, this corresponds to a length Reynolds number of approximately 0.41 to 6.7 million. For the baseline data, the model angle of attack (α) was varied from 20° to 40° in 10° increments and the sideslip was maintained at zero for all the runs presented herein. Flow conditions, including run-to-run repeatability, are presented in Table 3. For each model configuration, the unit Reynolds number was varied between 1 and 4 million to obtain the smooth baseline data for comparison to the tripped data. The investigation of the effect of trips was conducted at $\alpha = 40°$ only. For the transition testing, the tunnel stagnation pressure and temperature were varied over a series of runs with the roughness element firmly applied to the location of interest. This was done to determine the maximum Reynolds number which still maintained laminar flow (the "incipient" value, if Bertin's[14] vernacular is adopted), the Reynolds number where significant non-laminar flow first appears downstream of the roughness element ("critical"), and finally the minimum Reynolds number where the transition front is fixed at the roughness element (Bertin's "effective" value).

Data Reduction

Heating rates were calculated from the global surface temperature measurements using one-dimensional semi-infinite solid heat-conduction equations, as discussed in detail in Refs. 8 and 9. Based on considerations presented in Ref. 9, phosphor system measurement error is believed to be better than $\pm 8\%$, with overall experimental uncertainty of $\pm 15\%$. Heating distributions are presented in terms of the ratio of heat-transfer coefficients $h/h_{F\text{-}R}$, where $h_{F\text{-}R}$ corresponds to the stagnation-point heating to a sphere with radius 0.4344-in (a 1-ft radius sphere scaled to the model size) and was calculated based on the theory of Fay and Ridell[15]. Repeatability for the normalized centerline heat transfer measurements was found to be generally better than $\pm 4\%$.

Results

Surface Heating

The phosphor thermography data was acquired in December, 1996, during Test 6735. The run log, which lists the parametrics that were investigated during 180 runs, is presented in Table 4 and the resulting global heating images are shown in chronological order by run number in Appendix A. All the images were acquired with the camera perpendicular to the model. General observations which can be made based on the baseline images are:

(1) As α increases from 20° to 40°, heating to the windward surface increases. (For example, see Run # 164 for α = 20°, Run # 146 for α = 30°, and Run # 12 for α = 40°.)

(2) As Re increases, the heating ratio $h/h_{F\text{-}R}$ remains relatively constant over the windward surface for laminar conditions. (For example, see Runs # 9 through 12)

(3) As the body flap deflection increases, the induced flap separation/reattachment produced significant heating levels on the body flap which were strongly affected by both α and Re; the highest flap heating case (Run # 19) was for α = 40°, Re_∞/ft = 4.4 million, and δ_{bf} = 30° and had local regions of heating that exceeded the reference value (corresponding to a strong shock impingement).

(4) Separation in front of the deflected body flap was generally fixed at the start of the windward surface expansion region at x/L = 0.7. (See, for example, Run # 174 for α = 20°, Run # 153 for α = 30°, and Run # 19 for α = 40°.)

(5) Differentially deflected flaps did not promote any significant crosstalk heating. (For example, compare Runs 24 and 27.)

General observations which can be made based on the boundary-layer transition images (Runs 32 through 130) obtained at α = 40° are:

(1) The roughness elements and locations that were used were successful in promoting transition for a wide range of Reynolds numbers.

(2) The turbulent wedge, resulting from a roughness element placed on the windward centerline, was a useful way of determining if the model was installed with a small amount of yaw or roll, as an asymmetric turbulent wedge implies a model attitude mis-alignment. (For example, compare Runs 33 and 34; Run 33 had a subtle amount of roll of the "dog-leg" strut used to hold the model at the proper α which promoted a less than 0.5° of yaw to the model.)

(3) Turbulence on the forebody reduced both the size of the separation region and the reattachment heating on the flap, in the localized region that is affected by the trip. (For example, compare Runs 23 and 124.)

(4) As the trips moved closer to the nose, the turbulent wedge behind the trip became harder to keep symmetric, most likely due to slight misalignments associated with the trip coupled with the lateral pressure gradient near the nose. (For example, see Runs 69 through 87.)

(5) The forward most trip station (Station A, x/L = 0.02) was the hardest location to trip. (For example, compare A-trips, Runs 83 through 87, to B-trips, Runs 67 through 82.)

(6) Trip effectiveness did not appear to change drastically as the width of the trip element was increased. (Compare Runs # 107, 113, 117, and 120.)

(7) The orientation of the trip was important, with a 45° trip being the most effective and the 0° trip being the least effective. (Compare Runs # 119, 126, 128, and 129.)

(8) Multiple roughness elements did not appear to promote transition any more effectively than a single trip element. (Compare Runs # 119, and 130 through 136.)

Flow Visualization

The flow visualization tests (both shock shapes and surface streamlines were acquired simultaneously) were performed in January, 1997, during Test 6739. The run log, which shows the 12 run matrix, is presented in Table 5. The schlieren images and oil-flow movement images are shown in chronological order in Appendices B and C, respectively. General observations on flow phenomenon which can be made based on the schlieren and oil-flow movement images are:

Windward Inflow/Outflow

1) As α increases from 30° to 40°, outflow (spreading of the surface streamlines) increases (see Runs 6 and 7 of Appendix C). For α = 20° (Run # 8), inflow of the windward surface streamlines was indicated.

(2) Changes in Re had little effect on inflow/outflow of surface streamlines (Runs 3, 1, and 2).

Windward Separation/Reattachment

(1) With the body flap deflected, the surface streamlines indicate the onset of separation at the expansion region. Both the separation and reattachment compression shocks are evident in the corresponding schlieren image (for example, see Run # 5).

(2) As α increases from 20° to 40°, the separation region appears to decrease slightly (for example, see Runs # 9, 5, and 1 of Appendix C).

(3) Likewise, as Re/ft increases from 1.1 million to 4.4 million, the separation region decreases slightly (see Runs # 3, 1, and 2 of Appendix C).

(4) For the body flap deflections tested, turbulence on the forebody (as indicated by the corresponding heating cases) did not appear to eliminate the separation region (see Runs # 2 and 11 of Appendix C and Run # 124 of Appendix A).

(5) On Run #11, a trip on the windward surface partially peeled off during the run. The schlieren image captured the disturbance wave that was created by this now large protuberance, which then reflected off the bow shock into the body flap area. The deflected disturbance was not picked up in the oil-flow.

Canopy Separation/Reattachment

(1) An imbedded shock or compression wave appears to emminate from the canopy region in the schlieren images for α = 20° and 30° (for example, see Runs # 8 and 6).

(2) As α increases, the separation/vortex region around the base of the canopy appears to become less distinct (for example, see Runs # 9, 5, and 4 of Appendix C).

Leeside Vortex

(1) A leeside vortex reattachment line is formed along the centerline between the canopy and the leeside flap, which, again, appears to become less distinct with increasing α (for example, see Runs # 9, 5, and 4 of Appendix C).

(2) The surface streamlines indicate that the leeside vortices impinge on the upper surface body flap: at α = 20° (Run 9), a stagnation point appears on the center of the leeside fin; while at α = 40° (Run 4), two reattachment lines appear on either side of the center stagnation point.

(3) The Reynolds number effect on the leeside vortices could not be determined from these images.

Fin Upwash

(1) Highly three-dimensional flow was evident on the outboard surface streamlines of the wing/fin which was stongly dependent on α (for example, see Runs # 8, 6, and 7 of Appendix C).

(2) At α = 20° (Run # 8), the surface streamlines along the fin leading edge appear to be moving from the leading edge towards the trailing edge, while at α = 40° (Run # 7), the fin upwash dominates such that the surface streamlines are curving up towards the leading edge.

(3) The surface streamlines are diverted around the leading-edge wing/body fillet for the range of α tested, which suggests that this juncture is a region of high pressure. For the α = 20˚ case only, this region appears to be the source of the embedded shock that is evident on the leeside of the schlieren image of Run # 8.

(4) At α = 20° (Run # 8), a low shear region appears in the middle of the outboard section of the fin.

(5) At higher α's, the flow over the fixed, deflected rudders appear to eminate from the windward surface (see, for example, Runs # 6 and 7 of Appendix C).

Conclusions

An experimental investigation of the aeroheating characteristics for a proposed X-38 configuration (Revision 3.1) has been conducted in the LaRC 20-Inch Mach 6 Tunnel. Phosphor thermography was used to provide global heating images of the windward surface for a variety of angles-of-attack, Reynolds numbers, and body flap deflections. Additionally, the effect of discrete roughness elements was investigated for α = 40°, which included trip location, height, width, and orientation parametrics. The aeroheating results were complemented with schlieren and oil-flow images which provided shock-shape and surface streamline information. As this report was intended to be a "quick-release" of the experimental data for review by the X-38 program, analysis was limited to observations of experimental results.

Acknowledgment

The following individuals were instrumental in the processes that were required to accomplish this experimental work: Mark Cagle of ETTD/MISB for model design; Mike Powers and Mark Griffith of FD/CMFSS for model construction; Ed Covington and Tom Burns of FD/QAIB for model surface inspection and verification; Grace Gleason, Rhonda Manis, and Johnny Ellis of FSSD/ASS, and Bert Senter of CSC for facility technical support; Glen Bittner of CSC and Ron Merski of AGDD/AB for test technique support; and Chuck Campbell of NASA JSC for program support.

References

1."SV-5D PRIME Final Flight Test Summary," Martin Marietta Engineering Report 14465, September 1967.

2.Mort, K. W. and Falarski, M. D., "Full-Scale Wind Tunnel Investigation of the Aerodynamic Characteristics of the X-24A Lifting Body Aircraft," NASA TN D-5932, August 1970.

3.Campbell, C. H., Caram, J. M., Li, C. P., and Madden, C. B., "Aerothermodynamic Enviroment Definition For an X-23/X-24A Derived Assured Crew Return Vehicle," AIAA Paper 96-1862, June 1996.

4.Campbell, C. H., Caram, J. M., Berry, S. A., DiFulvio, M., and Horvath, T. J., "Overview of X-38 Hypersonic Wind Tunnel Data and Comparison with Numerical Results," AIAA Paper 97-0567, Jan. 1997.

5.Berry, S. A., Bouslog, S. A., Brauckmann, G. J., and Caram, J. M., "Boundary-Layer Transition Due to Isolated Roughness: Shuttle Results From the LaRC 20-Inch Mach 6 Tunnel," AIAA Paper 97-0273, Jan. 1997.

6.Miller, C. G., "Langley Hypersonic Aerodynamic/Aerothermodynamic Testing Capabilities - Present and Future," AIAA Paper 90-1376, June 1990.

7.Buck, G. M., "Automated Thermal Mapping Techniques Using Chromatic Image Analysis," NASA TM 101554, April 1989.

8.Buck, G. M., "Surface Temperature/Heat Transfer Measurement Using A Quantitative Phosphor Thermography System," AIAA Paper 91-0064, Jan. 1991.

9.Merski, N. R., "A Relative-Intensity Two-Color Phosphor Thermography System," NASA-TM-104123, Sept. 1991.

10.Horvath, T. J., Rhode, M. N., and Buck, G. M., "Aerothermodynamic Measurements on a Proposed Assured Crew Return Vehicle (ACRV) Lifting Body Configuration at Mach 6 and 10 in Air," AIAA Paper 90-1744, June 1990.

11.Micol, J. R., "Aerothermodynamic Measurement and Prediction for a Modified Orbiter at Mach 6 and 10 in Air," *Journal of Spacecraft and Rockets*, Vol. 32, No. 5, 1995, pp. 737-748.

12.Loomis, M. P., Venkatapathy, E., Davies, C. B., Campbell, C. H., Berry, S. A., Horvath, T. J., and Merski, N. R., "Aerothmal CFD Validation and Prediction for the X-38 Program," AIAA Paper 97-2484, June 1997.

13.Buck, G. M. and Vasquez, P., "An Investment Ceramic Slip-Casting Technique for Net-Form, Precision, Detailed Casting of Ceramic Models," U. S. Patent 5,266,252, November 30, 1993.

14.Bertin, J. J., Hayden, T. E., and Goodrich, W. D., "Shuttle Boundary-Layer Transition Due to Distributed Roughness and Surface Cooling," *Journal of Spacecraft and Rockets*, Vol. 19, No. 5, 1982, pp. 389-396.

15.Fay, J. A., and Ridell, F. R., "Theory of Stagnation Point Heat Transfer in Dissociated Air," *Journal of Aeronautical Sciences*, Vol. 25, No. 2, 1958.

Table 1: Model configurations and windward surface accuracies.

Model Designation	Body Flap Deflections (Deg)		Surface Accuracy Measurements (in.)			
	δ_{RBF}	δ_{LBF}	0.0<x/L<0.2	0.2<x/L<0.4	0.4<x/L<0.6	0.6<x/L<0.8
A-1	0	0	±0.011	±0.012	±0.015	±0.019
A-2	20	20	±0.019	±0.011	±0.013	±0.019
A-3	25	25	±0.023	±0.010	±0.012	±0.015
A-4	30	30	±0.028	±0.014	±0.015	±0.026
A-5	20	25	±0.027	±0.011	±0.015	±0.012
A-6	0	25	±0.018	±0.015	±0.015	±0.012
B-1	0	0	±0.018	±0.010	±0.012	±0.027
B-2	20	20	±0.018	±0.010	±0.015	±0.019
B-3	25	25	±0.018	±0.011	±0.015	±0.030
B-4	30	30	±0.015	±0.011	±0.015	±0.017
B-5	20	25	±0.019	±0.010	±0.015	±0.026
B-6	0	25	±0.017	±0.011	±0.015	±0.029
	body flaps accurate to ±1 deg		accuracies listed above are weighted-averaged for each section			

Table 2: Trip locations and fiducial marks.

See Fig. 8	Fiducial	x/L	y/b	z/L
Windward trips	A/1	0.02	0	-
	B	0.1	0	-
	C	0.2	0	-
	D	0.3	0	-
	E	0.5	0	-
Windward	2	0.25	0	-
	3	0.55	0.25	-
	4	0.55	-0.25	-
	5	0.68	0	-
Leeward	6	0.02	0	-
	7	0.25	0	-
	8	0.55	0.25	-
	9	0.55	-0.25	-
	10	0.68	0	-
Port	11	0.02	-	0
	12	0.25	-	0
	13	0.68	-	0
	14	0.92	-	0.17

Table 3: Nominal flow conditions and run-to-run repeatability for 20-Inch Mach 6 Tunnel.

Re_∞ ($x10^6$/ft)	M_∞	P_{t1} (psi)	T_{t1} (°R)	H_{t1} (BTU/lbm)	P_{t2} (psi)
1.16±2.5%	5.88±0.03%	60.3±2.3%	880.0±0.4%	211.7±0.4%	1.95±1.5%
1.60±1.7%	5.90±0.02%	85.4±1.5%	885.7±0.5%	213.1±0.6%	2.71±1.1%
1.87±1.6%	5.92±0.03%	101.7±2.1%	894.8±0.3%	215.3±0.3%	3.19±1.9%
2.24±1.5%	5.94±0.02%	125.2±1.2%	906.3±0.5%	218.1±0.5%	3.88±1.1%
2.51±2.3%	5.95±0.03%	140.7±2.0%	905.8±0.8%	218.0±0.8%	4.33±1.7%
2.76±5.5%	5.95±0.06%	155.5±4.4%	906.3±0.7%	218.1±0.6%	4.76
3.20±1.0%	5.96±0.01%	181.1±1.0%	906.2±0.3%	218.1±0.3%	5.50±0.9%
3.73±1.9%	5.97±0.01%	211.9±1.1%	906.7±0.8%	218.2±0.8%	6.40±1.1%
4.42±2.1%	5.98±0.02%	252.2±1.2%	907.2±0.8%	218.4±0.9%	7.57±1.4%
5.52	6.00	329.7	929.4	223.9	9.81
6.71	6.01	402.2	928.6	223.6	11.86

Table 4: Run log for Test 6735 conducted in LaRC 20-Inch Mach 6 Tunnel.

Run	Date (1996)	Time	Model	AOA deg	Re $x10^6$/ft	P_0 psi	T_0 °R	Trip ❶					Notes ❷
								Location	k, in	W, in	O,deg	Multiple	
1	11/6		A-6	40	1	60.0	885						ESP run only
2	11/6		A-6	40	1	60.0	885						ESP run only
3	11/6		A-6	40	1	60.0	885						ESP run only
4	11/6		A-6	40	1	60.0	885						ESP run only
5	11/7		A-6	40	1	60.0	885						ESP run only
6	11/7		A-6	40									model injec run only
7	11/7		A-6	40	2	125.0	910						ESP run only
BASELINE DATA FOR ALL 6 MODELS AT AOA = 40°													
8	11/7		A-6	40	1	60.0	885						
9	11/7	21:30	A-1	40	1.14	59.4	880.0						
10	11/7	22:10	A-1	40	2.23	125.0	906.9						
11	11/7	22:40	A-1	40	4	250.0	910						lost FC, use calibrations
12	11/7	23:00	A-1	40	4.38	250.3	907.9						
13	11/7	23:10	A-1	40	6.71	402.2	928.5						
14	11/8	18:10	A-2	40	1.12	58.7	880.9						
15	11/8	18:45	A-2	40	2.22	124.5	906.5						
16	11/8	20:10	A-2	40	4.39	250.6	906.5						
17	11/8	21:15	A-4	40	1.14	59.6	882.0						
18	11/8	21:50	A-4	40	2.21	123.9	906.7						
19	11/8	22:30	A-4	40	4.42	250.9	903.9						
20	11/12	13:15	A-3	40	-	-	-						tunnel didnt reach FC
21	11/12	13:55	A-3	40	1.14	59.4	880.3						
22	11/12	14:40	A-3	40	2.24	124.7	904.0						
23	11/12	15:30	A-3	40	4.41	251.9	907.6						
24	11/12	16:25	A-5	40	1.17	61.0	881.1						
25	11/12	17:05	A-5	40	2.27	126.3	903.1						

Table 4: (Continued)

Run	Date (1996)	Time	Model	AOA deg	Re x10^6/ft	P_0 psi	T_0 °R	Trip ❶ Location	k, in	W, in	O,deg	Multiple	Notes ❷
26	11/12	17:35	A-5	40	4.40	251.8	908.6						
27	11/12	18:40	A-6	40	1.17	60.9	879.4						
28	11/12	19:10	A-6	40	2.25	125.7	905.1						
29	11/12	19:40	A-6	40	4.38	252.8	913.1						
30	11/12	20:50	A-2	40	-	-	-						TP system crash-lost data
31	11/12	21:20	A-2	40	4.43	253.2	906.9						
ROUGHNESS EFFECTS FOR MODEL #2 AT AOA = 40°													
32	11/12	22:30	A-2	40	4.45	254.2	906.8	E	0.0025	0.05	45		
33	11/12	23:00	A-2	40	4.44	253.7	907.5	E	0.005	0.05	45		slight model yaw?
34	11/13	13:05	A-2	40	4.39	251.8	909.1	E	0.005	0.05	45		fixed yaw, repeat R33
35	11/13	14:25	A-2	40	4.50	252.7	897.7						new baseline without trip
36	11/13	15:15	A-2	40	4.39	251.9	909.9	E	0.005	0.05	45		
37	11/13	15:45	A-2	40	3.21	181.2	904.9	E	0.005	0.05	45		
38	11/13	16:25	A-2	40	2.22	124.5	906.1	E	0.005	0.05	45		
39	11/13	17:00	A-2	40	2.73	154.4	907.1	E	0.005	0.05	45		
40	11/13	17:40	A-2	40	3.19	180.3	906.2	E	0.0075	0.05	45		
41	11/13	18:10	A-2	40	2.24	125.4	905.0	E	0.0075	0.05	45		
42	11/13	18:40	A-2	40	1.17	60.9	879.5	E	0.0075	0.05	45		
43	11/13	19:40	A-2	40	1.60	84.9	883.9	E	0.0075	0.05	45		
44	11/13	21:05	A-2	40	4.41	252.2	907.6	D	0.0025	0.05	45		
45	11/13	21:40	A-2	40	4.38	250.1	907.1	D	0.005	0.05	45		
46	11/13	22:10	A-2	40	3.22	181.3	903.3	D	0.005	0.05	45		
47	11/13	22:50	A-2	40	2.23	124.9	905.6	D	0.005	0.05	45		
48	11/14	18:10	A-2	40	2.78	156.7	905.4	D	0.005	0.05	45		
49	11/14	18:45	A-2	40	2.54	142.3	904.3	D	0.005	0.05	45		
50	11/14	19:20	A-2	40	3.22	182.9	907.1	D	0.0075	0.05	45		
51	11/14	19:55	A-2	40	2.27	126.5	903.1	D	0.0075	0.05	45		
52													run # skipped by mistake
53	11/14	21:20	A-2	40	1.17	61.4	881.3	D	0.0075	0.05	45		
54	11/14	22:00	A-2	40	1.63	86.7	883.7	D	0.0075	0.05	45		
55	11/15	9:35	A-2	40	4.44	253.0	905.4	C	0.0025	0.05	45		
56	11/15	10:35	A-2	40	3.21	181.4	905.6	C	0.0025	0.05	45		
57	11/15	11:25	A-2	40	3.68	211.6	912.1	C	0.0025	0.05	45		
58	11/15	12:40	A-2	40	4.45	252.9	903.9	C	0.0025	0.05	45		
59	11/15	14:00	A-2	40	3.75	212.6	904.2	C	0.0025	0.05	45		
60	11/15	15:00	A-2	40	3.18	180.4	907.0	C	0.005	0.05	45		
61	11/15	15:50	A-2	40	2.25	125.8	904.5	C	0.005	0.05	45		
62	11/15	16:45	A-2	40	1.59	84.7	885.1	C	0.005	0.05	45		
63	11/15	17:20	A-2	40	2.49	139.7	905.8	C	0.005	0.05	45		
64	11/15	18:05	A-2	40	2.24	125.6	906.6	C	0.0075	0.05	45		
65	11/15	19:05	A-2	40	1.15	60.1	879.2	C	0.0075	0.05	45		
66	11/15	20:20	A-2	40	1.61	85.7	883.8	C	0.0075	0.05	45		
67	11/15	21:00	A-2	40	4.40	250.9	906.3	B	0.0025	0.05	45		
68	11/15	21:35	A-2	40	5.52	329.7	929.4	B	0.0025	0.05	45		
69	11/15	22:15	A-2	40	3.18	180.2	906.6	B	0.005	0.05	45		
70	11/18	10:20	A-2	40	3.69	211.6	911.8	B	0.005	0.05	45		
71	11/18	11:05	A-2	40	2.24	125.1	903.7	B	0.0075	0.05	45		
72	11/18	11:30	A-2	40	1.60	84.9	884.4	B	0.0075	0.05	45		
73	11/18	13:10	A-2	40	3.20	180.8	905.6	B	0.0075	0.05	45		
74	11/18	14:00	A-2	40	4.44	252.0	903.7	B	0.0025	0.05	45		
75	11/18	16:20	A-2	40	3.20	181.2	906.2	B	0.0025	0.05	45		

Table 4: (Continued)

Run	Date (1996)	Time	Model	AOA deg	Re x10^6/ft	P_0 psi	T_0 °R	Trip ❶					Notes ❷
								Location	k, in	W, in	O,deg	Multiple	
76	11/18	17:20	A-2	40	-	-	-	-	-	-	-	-	TP system crash-lost data
77	11/18	18:00	A-2	40	-	-	-	-	-	-	-	-	TP system crash-lost data
78	11/18	18:40	A-2	40	2.23	125.5	909.3	B	0.005	0.05	45		
79	11/18	20:30	A-2	40	-	-	-	-	-	-	-	-	TP system crash-lost data
80	11/18	21:00	A-2	40	3.22	182.2	906.1	B	0.005	0.05	45		
81	11/18	22:00	A-2	40	3.79	213.4	900.5	B	0.005	0.05	45		
82	11/18	22:35	A-2	40	4.47	253.7	904.0	B	0.005	0.05	45		
83	11/19	13:45	A-2	40	4.26	248.6	919.7	A	0.0025	0.05	45		
84	11/19	14:25	A-2	40	4.41	252.4	907.7	A	0.005	0.05	45		
85	11/19	15:30	A-2	40	-	-	-	-	-	-	-	-	TP system crash-lost data
86	11/19	18:00	A-2	40	4.41	250.6	904.5	A	0.0075	0.05	45		
87	11/19	18:45	A-2	40	3.18	180.4	906.8	A	0.0075	0.05	45		
ROUGHNESS REPEATS FOR MODEL # 2													
88	11/19	20:50	A-2	40	3.71	210.6	905.8	E	0.005	0.05	45		
89	11/19	21:35	A-2	40	2.49	139.9	906.2	E	0.005	0.05	45		
90	11/19	22:20	A-2	40	2.23	124.6	905.9	E	0.005	0.05	45		
91	11/19	23:05	A-2	40	1.59	85.3	888.8	E	0.005	0.05	45		
92	11/20	16:20	A-2	40	2.54	141.7	902.0	D	0.0075	0.05	45		
93	11/20	16:50	A-2	40	1.87	102.0	894.7	D	0.0075	0.05	45		
94	11/20	17:35	A-2	40	1.17	61.5	881.3	D	0.0075	0.05	45		
95	11/20	18:15	A-2	40	3.76	213.8	906.3	B	0.0025	0.05	45		
96	11/20	18:40	A-2	40	3.18	180.2	907.5	B	0.0025	0.05	45		
ROUGHNESS REPEATS ON MODEL # 1													
97	11/20	20:00	A-1	40	4.48	255.7	906.8						
98	11/20	20:30	A-1	40	3.71	211.9	909.0	E	0.005	0.05	45		
99	11/20	21:10	A-1	40	2.45	140.0	450	E	0.005	0.05	45		lost pitot, use calibration
100	11/20	21:40	A-1	40	2.52	142.0	907.0	E	0.005	0.05	45		trip fell off prior to run...
101	11/20	22:30	A-1	40	2.48	141.1	911.9	E	0.005	0.05	45		lost trip again, kapton not sticking to this model
ROUGHENESS REPEATS ON MODEL # 3													
102	11/21	15:35	A-3	40	3.70	211.2	909.3	E	0.005	0.05	45		
103	11/21	16:35	A-3	40	2.48	139.1	906.2	E	0.005	0.05	45		
104	11/21	17:15	A-3	40	3.19	179.9	904.3	E	0.005	0.05	45		
105	11/21	17:50	A-3	40	3.20	181.1	905.6	D	0.005	0.05	45		
106	11/21	18:30	A-3	40	2.24	125.7	906.4	D	0.005	0.05	45		
107	11/21	19:00	A-3	40	1.60	85.2	885.6	D	0.005	0.05	45		
108	11/21	20:20	A-3	40	3.73	212.0	906.5	D	0.005	0.05	45		
109	11/21	20:55	A-3	40	3.72	211.3	906.1	B	0.005	0.05	45		
110	11/21	21:30	A-3	40	2.51	140.1	902.7	B	0.005	0.05	45		
111	11/21	22:05	A-3	40	2.24	124.6	903.4	B	0.005	0.05	45		
TRIP SIZE EFFECTS ON MODEL # 3													
112	11/21	22:55	A-3	40	2.25	126.0	904.9	D	0.005	0.1	45		
113	11/22	10:30	A-3	40	1.62	85.8	883.0	D	0.005	0.1	45		
114	11/22	11:10	A-3	40	1.17	60.8	877.7	D	0.005	0.1	45		
115	11/22	12:40	A-3	40	3.70	210.2	906.6	D	0.005	0.1	45		
116	11/22	13:15	A-3	40	2.24	124.6	903.0	D	0.005	0.2	45		
117	11/22	14:35	A-3	40	1.59	85.2	887.0	D	0.005	0.2	45		
118	11/22	15:15	A-3	40	3.74	211.6	903.8	D	0.005	0.2	45		
119	11/22	15:50	A-3	40	2.25	126.2	906.9	D	0.005	0.4	45		
120	11/22	16:25	A-3	40	1.60	85.4	888.0	D	0.005	0.4	45		
121	11/22	17:00	A-3	40	1.86	101.3	894.8	D	0.005	0.4	45		

Table 4: (Continued)

Run	Date (1996)	Time	Model	AOA deg	Re x10^6/ft	P_0 psi	T_0 °R	Trip ❶					Notes ❷
								Location	k, in	W, in	O,deg	Multiple	
122	11/22	17:35	A-3	40	3.76	213.5	905.0	D	0.005	0.4	45		
123	11/22	18:10	A-3	40	3.21	181.9	907.4	D	0.005	0.4	45		
124	11/22	18:45	A-3	40	4.48	254.5	903.6	D	0.005	0.4	45		
125	11/22	20:15	A-3	40	1.60	86.1	889.1	D	0.005	0.1	45		
TRIP ORIENTATION EFFECTS ON MODEL # 3													
126	11/22	20:50	A-3	40	2.25	126.4	906.5	D	0.005	0.4	0		
127	11/22	21:20	A-3	40	3.19	181.2	907.5	D	0.005	0.4	0		
128	11/22	21:50	A-3	40	2.24	125.8	907.1	D	0.005	0.4	15		
129	11/22	22:25	A-3	40	2.26	126.3	904.2	D	0.005	0.4	30		
MULTIPLE TRIP EFFECTS ON MODEL # 3													
130	11/22	23:15	A-3	40	2.26	126.0	904.6	D	0.005	0.4	45	1,2	
131	11/25	9:20	A-3	40	2.22	125.0	908.3	D	0.005	0.4	45	1,2,3	
132	11/25	10:20	A-3	40	2.23	124.7	906.3	D	0.005	0.4	45	1,3,4	
133	11/25	11:30	A-3	40	2.23	125.1	908.0	D,C	0.005	0.4	45	1,3,4,5	
134	11/25	12:50	A-3	40	2.21	125.0	910.9	D	0.005	0.4	45	3,4	
135	11/25	13:20	A-3	40	2.24	125.5	905.8	D	0.005	0.4	45	3,4,6	
136	11/25	14:00	A-3	40	2.23	125.4	908.6	D	0.005	0.4	45	1,3,4,6	
137	11/25	15:10	A-3	40	2.25	126.4	907.6	D	0.005	0.4	0		
138	11/26	9:10	A-3	40	2.22	125.0	908.2	D	0.005	0.4	0	1,2	
139	11/26	10:10	A-3	40	2.22	125.1	908.4	D	0.005	0.4	0	1,2,3	
140	11/26	11:10	A-3	40	2.21	125.3	912.1	D,E,C	0.005	0.4	0	1,2,3,4	
BASELINE DATA FOR ALL 6 MODELS AT AOA = 30 °													
141	11/26	13:51	A-3	30	1.17	60.8	877.9						
142	11/26	14:30	A-3	30	2.25	125.9	906.7						
143	11/26	15:03	A-3	30	4.35	249.9	910.9						
144	11/27	9:15	A-1	30	1.15	60.2	882.9						
145	11/27	10:17	A-1	30	2.24	125.8	906.3						
146	11/27	10:44	A-1	30	4.39	251.5	908.2						
147	11/27	11:11	A-2	30	1.14	60.0	883.6	B	0.0025	0.05	45		
148	12/2	10:21	A-2	30	1.16	60.5	878.4						
149	12/2	10:53	A-2	30	2.21	124.6	908.9						
150	12/2	11:18	A-2	30	4.34	249.9	911.8						
151	12/2	13:01	A-4	30	1.14	59.8	881.8						
152	12/2	13:43	A-4	30	2.24	125.3	906.5						
153	12/2	14:25	A-4	30	4.42	251.9	905.3						
154	12/2	14:56	A-5	30	1.16	60.3	879.7						
155	12/2	15:40	A-5	30	-	-	-	-	-	-	-	-	TP system did not trigger
156	12/2	16:20	A-5	30	2.21	124.5	909.8						
157	12/2	16:55	A-5	30	4.35	251.1	913.2						
158	12/2	17:30	A-6	30	1.16	60.3	877.6						
159	12/2	18:15	A-6	30	2.21	124.0	906.4						
160	12/2	18:40	A-6	30	4.40	251.6	908.1						
BASELINE DATA FOR ALL 6 MODELS AT AOA = 20°													
161	12/2	21:16	A-1	20	1.17	61.0	877.9						
162	12/2	22:15	A-1	20	1.15	60.2	880.3						
163	12/2	22:52	A-1	20	1.15	59.9	880.1						
164	12/3	9:53	A-1	20	4.44	251.0	901.1						
165	12/3	10:45	A-1	20	2.24	124.5	902.9						
166	12/3	11:14	A-2	20	1.17	61.0	877.9						
167	12/3	12:38	A-2	20	2.25	125.5	904.2						
168	12/3	13:16	A-2	20	4.47	252.7	901.9						

Table 4: (Continued)

Run	Date (1996)	Time	Model	AOA deg	Re x10^6/ft	P_0 psi	T_0 °R	Trip ❶					Notes ❷
								Location	k, in	W, in	O,deg	Multiple	
169	12/3	13:45	A-3	20	1.15	60.1	879.7						
170	12/3	14:29	A-3	20	2.22	123.7	903.1						
171	12/3	15:01	A-3	20	4.39	250.3	905.7						
172	12/3	15:31	A-4	20	1.15	60.2	879.7						
173	12/3	16:02	A-4	20	2.23	124.6	906.2						
174	12/3	16:32	A-4	20	4.40	253.2	910.7						

❶Refer to Fig. 8 and/or Table 2 for x/L value of locations; Refer to Fig. 10 for sketch of multiple trip configurations; k is the trip height, W is the trip width, and O is the trip orientation

❷FC refers to tunnel flow conditions, TP refers to thermographic phosphors

Table 5: Run log of Test 6739 conducted in the LaRC 20-Inch Mach 6 Tunnel.

Run	Date (1997)	Model	AOA deg	Re x10^6/ft	P_0 psi	T_0 °R	Trip ❶					Notes ❷
							Location	k, in	W, in	O,deg	Multiple	
1	1/23	B-3	40	2.2	125	910						
2	1/23	B-3	40	4.4	250	910						
3	1/23	B-3	40	1.1	60	885						
4	1/23	B-3	40	2.2	125	910						leeside only
5	1/23	B-3	30	2.2	125	910						
6	1/24	B-1	30	2.2	125	910						
7	1/24	B-1	40	2.2	125	910						
8	1/24	B-1	20	2.2	125	910						
9	1/24	B-3	20	2.2	125	910						
10	1/24	B-3	40	2.2	125	910	D	0.005	0.4	45		
11	1/24	B-3	40	4.4	250	910	D	0.005	0.4	45		Trip peeled up during run
12	1/24	B-3	40	2.2	125	910	C	0.005	0.05	45		

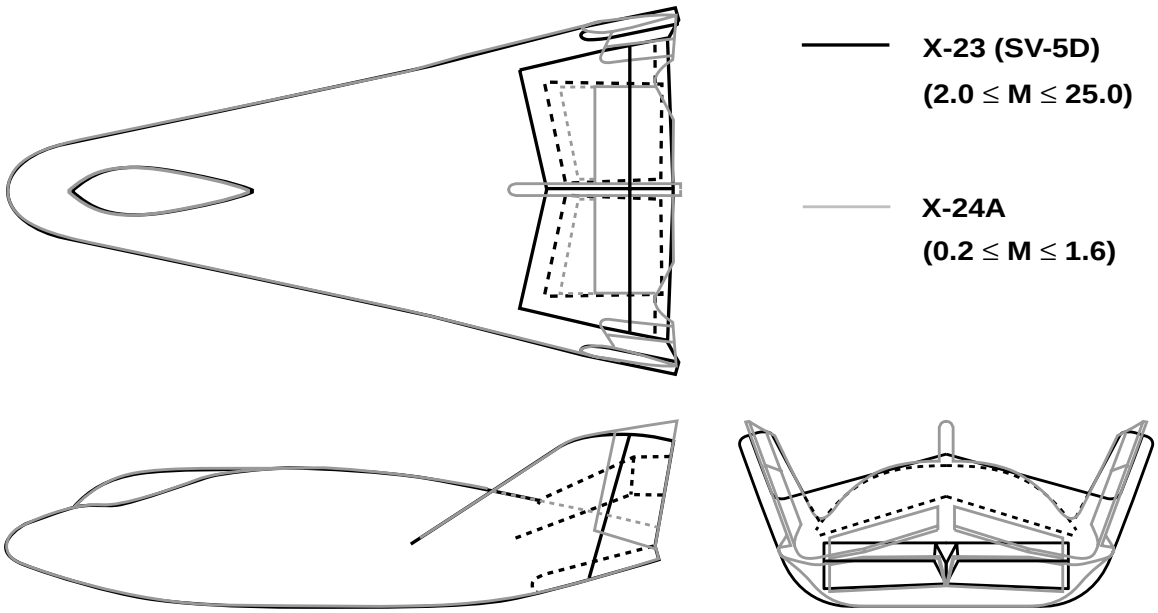

Figure 1. Comparison of X-23 and X-24A flight vehicles.

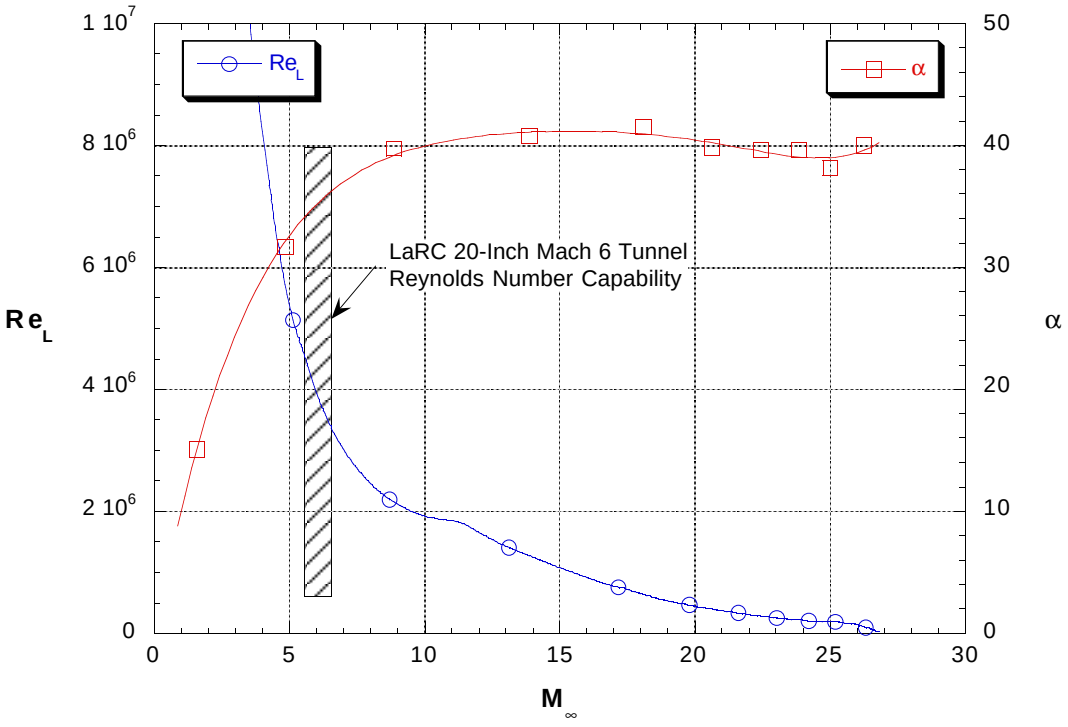

Figure 2. Preliminary X-38 trajectory

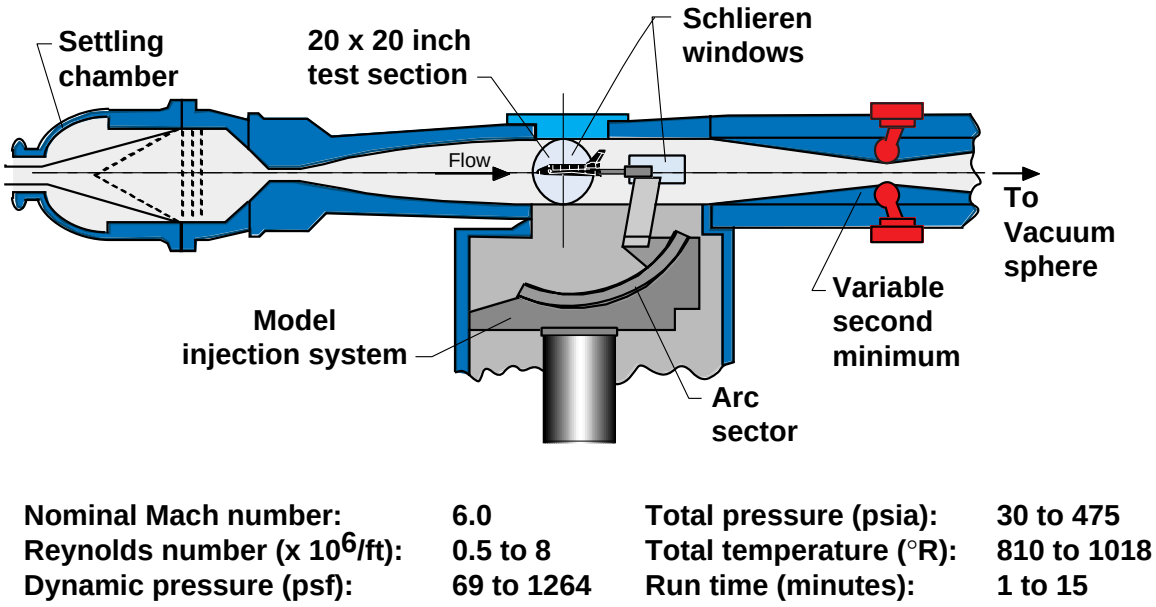

Figure 3. Schematic of NASA Langley 20-Inch Mach 6 Tunnel.

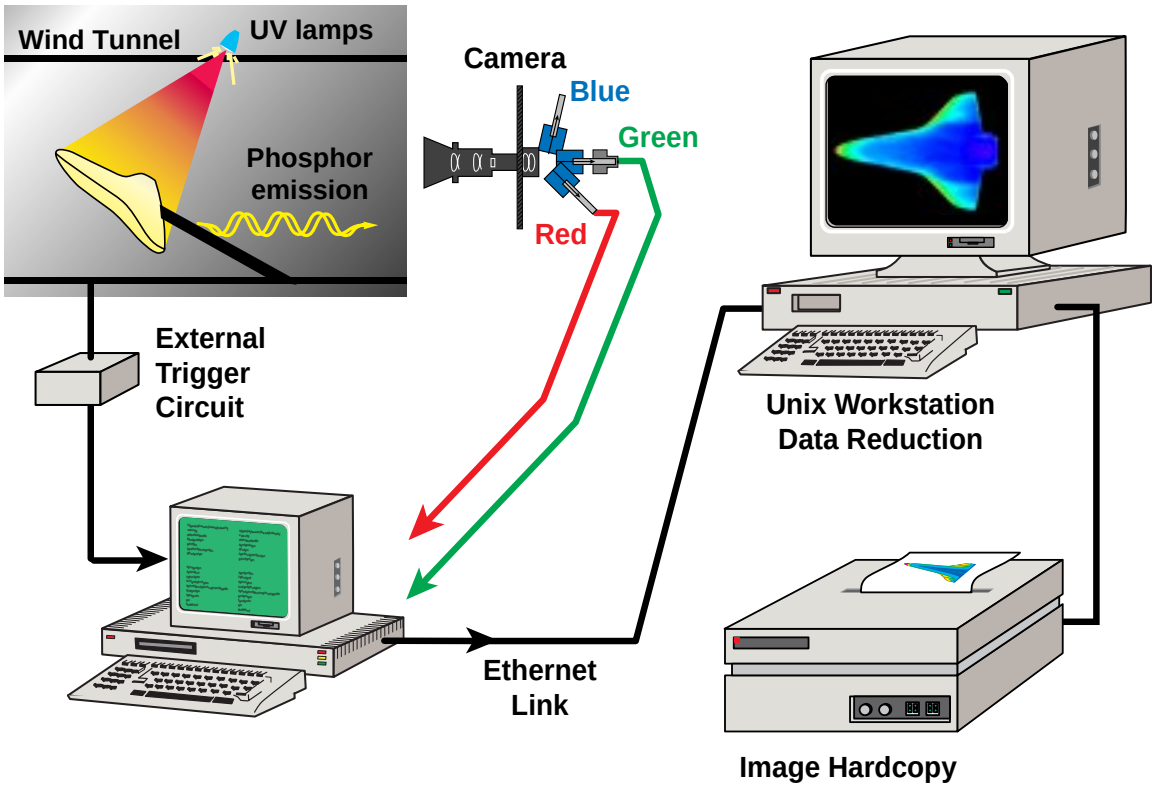

Figure 4. Schematic of phosphor thermography system.

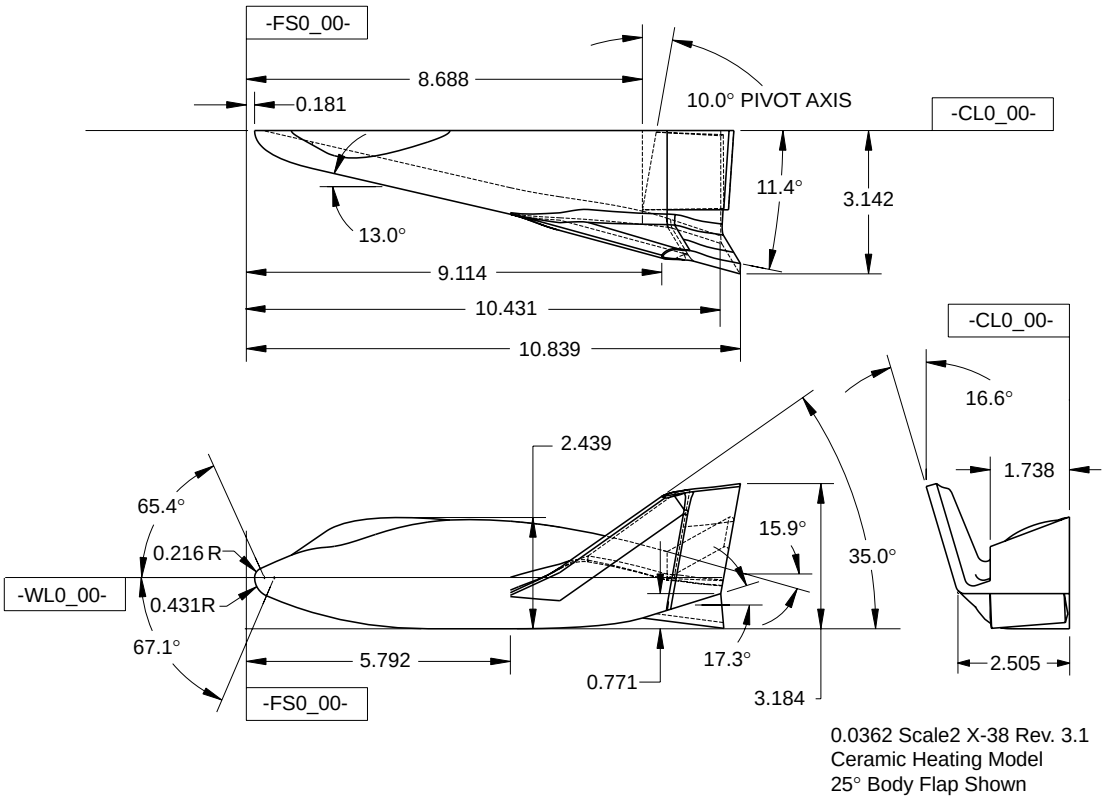

Figure 5. X-38 model dimension.

Figure 6. Photograph of the 6 model configurations.

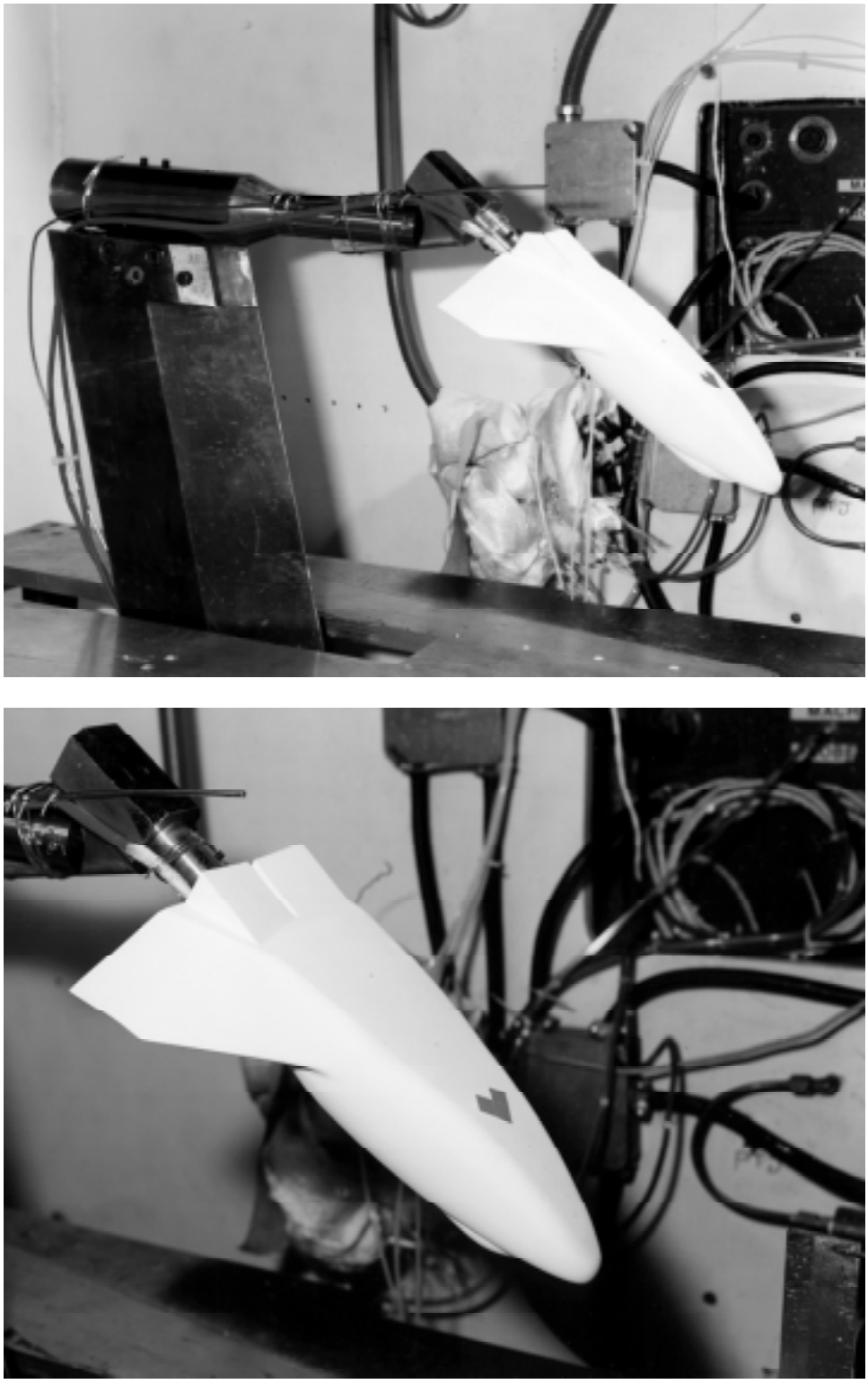

Figure 7. Photographs of a model installed in the 20-Inch Mach 6 Tunnel.

Notes: (1) See Table 2 for fiducial mark locations
(2) Waterline is defined as being through the nose and parallel to Windward surface flat
(3) Numbered fiducials were applied with a coordinate measurement machine prior to testing using the reference dimensions L=10.25 in and b=5.01 in
(4) Lettered fiducials correspond to trip locations, most were added during the tunnel entry and measured post-test

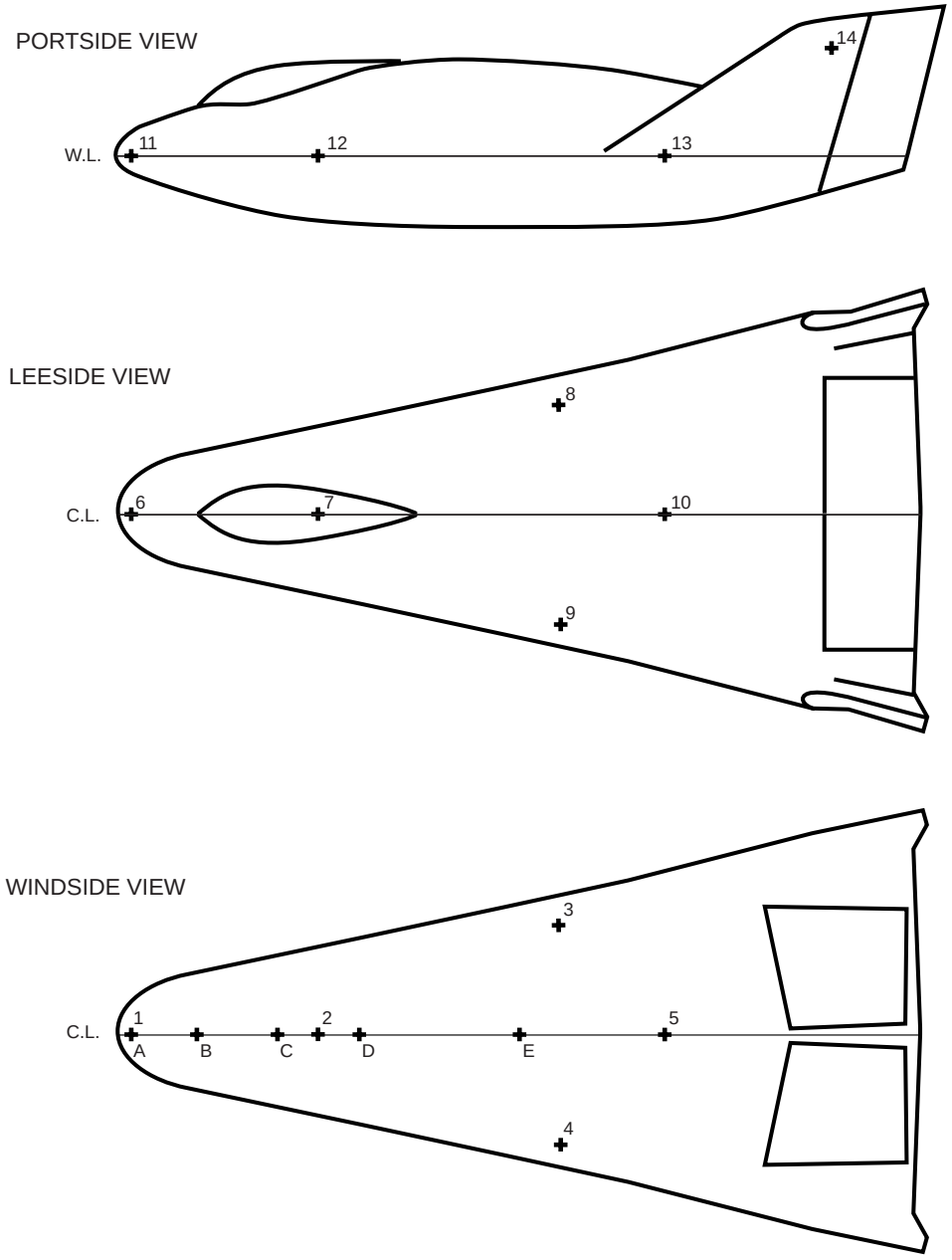

Figure 8. Sketch of trip locations and fiducial marks.

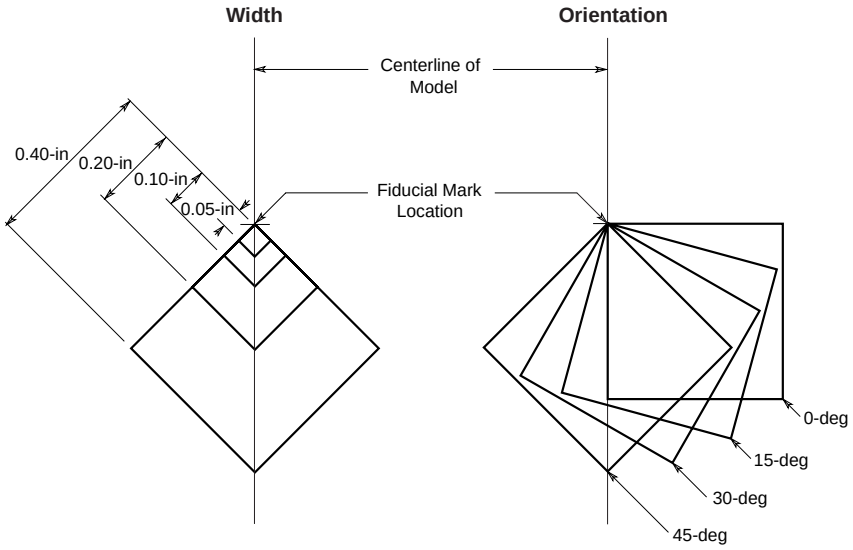

Figure 9. Sketch of trips showing size and orientation.

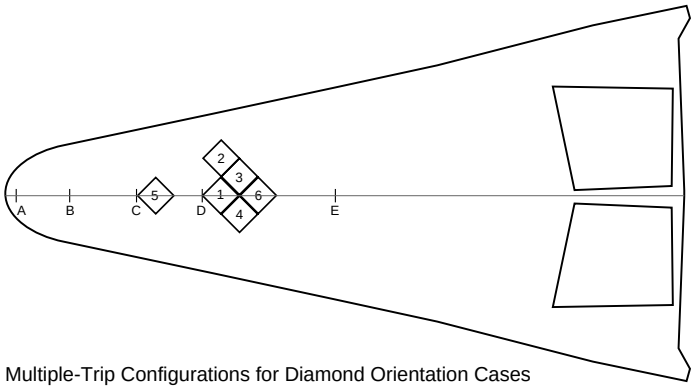

Multiple-Trip Configurations for Diamond Orientation Cases
T6735 Runs 130-136

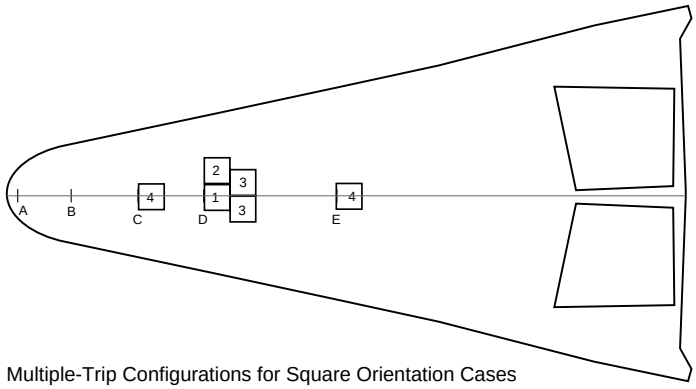

Multiple-Trip Configurations for Square Orientation Cases
T6735 Runs 137-140

Figure 10. Sketch of multiple trip configurations.

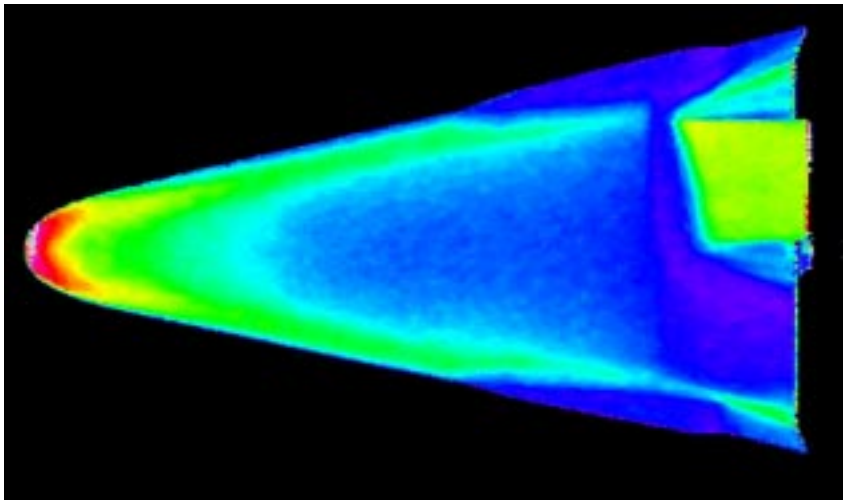

Run # 8
Windward View
Model # 6
LBF @ 25°
$\alpha = 40°$
$Re_\infty/ft = 1.1x10^6$
Baseline, no trip

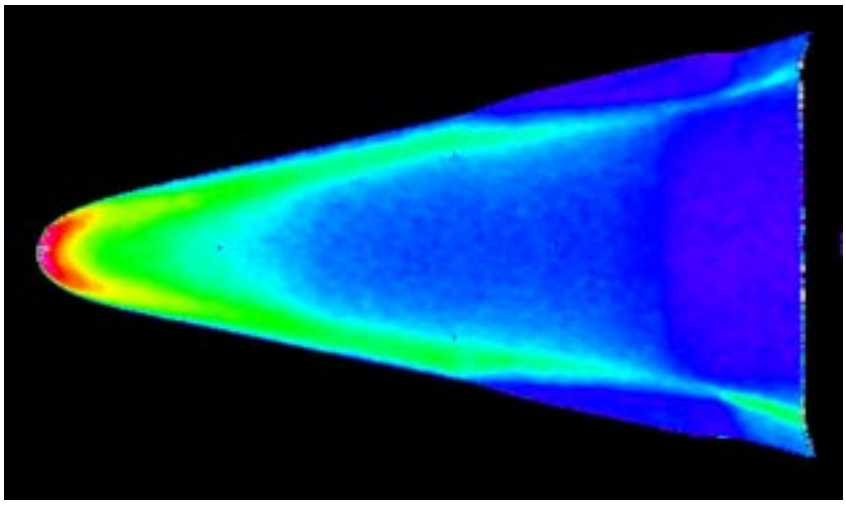

Run # 9
Windward View
Model # 1
BF @ 0°
$\alpha = 40°$
$Re_\infty/ft = 1.1x10^6$
Baseline, no trip

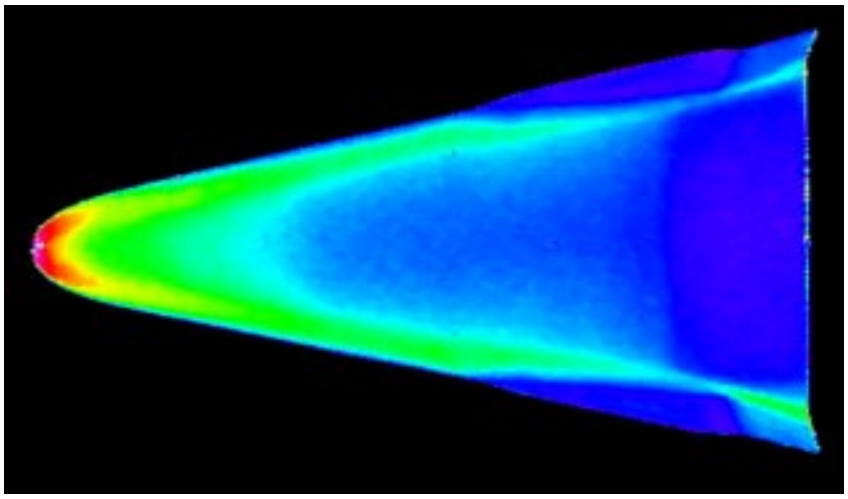

Run # 10
Windward View
Model # 1
BF @ 0°
$\alpha = 40°$
$Re_\infty/ft = 2.2x10^6$
Baseline, no trip

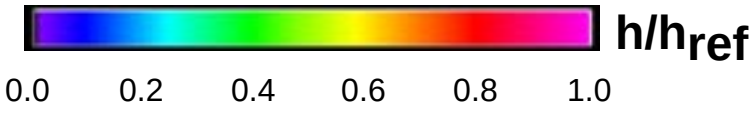

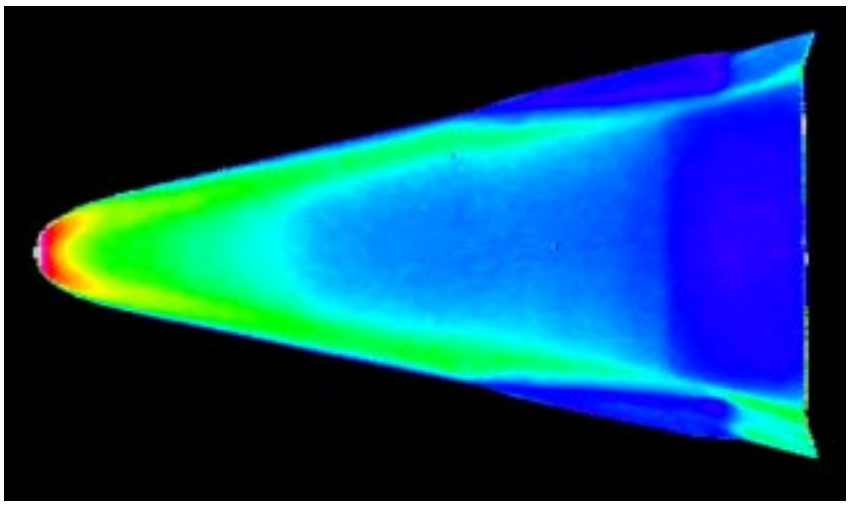

Run # 12
Windward View
Model # 1
BF @ 0°
$\alpha = 40°$
$Re_\infty/ft = 4.4x10^6$
Baseline, no trip

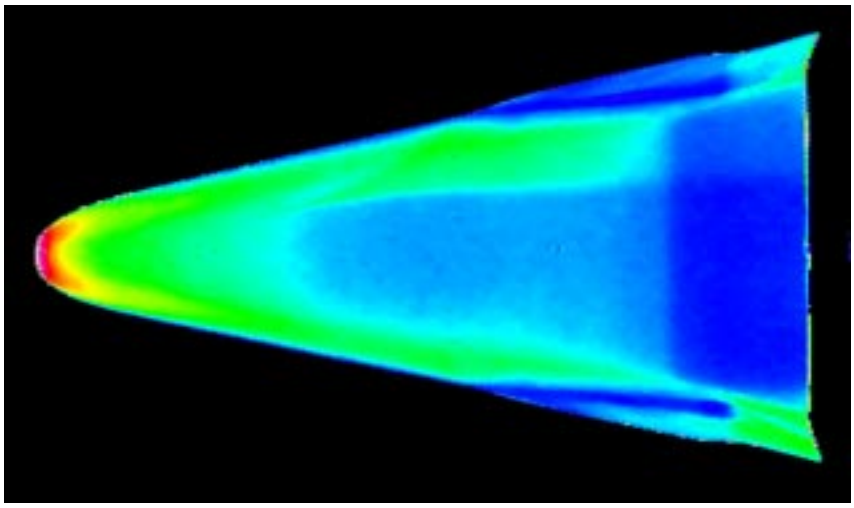

Run # 13
Windward View
Model # 1
BF @ 0°
$\alpha = 40°$
$Re_\infty/ft = 6.7x10^6$
Baseline, no trip

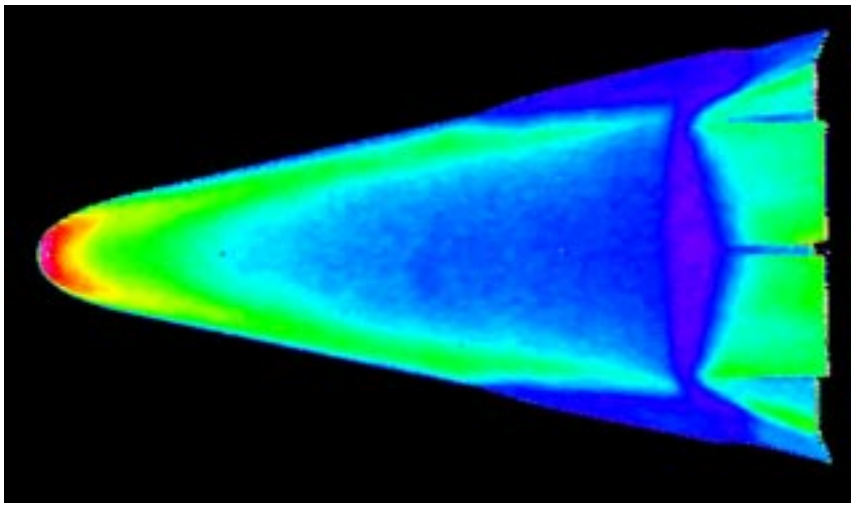

Run # 14
Windward View
Model # 2
BF @ 20°
$\alpha = 40°$
$Re_\infty/ft = 1.1x10^6$
Baseline, no trip

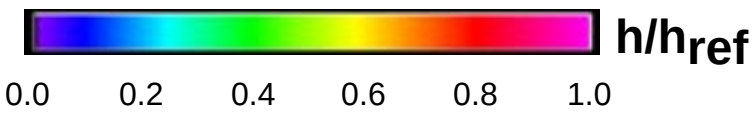

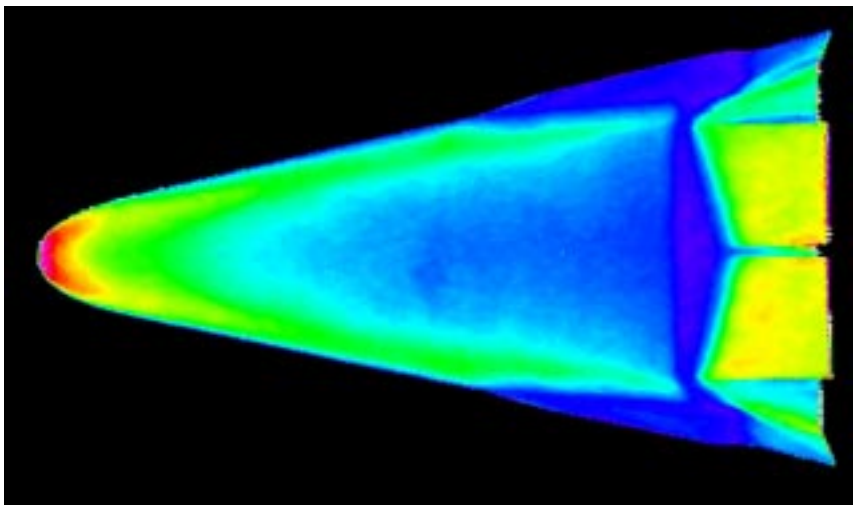

Run # 15
Windward View
Model # 2
BF @ 20°
$\alpha = 40°$
$Re_\infty/ft = 2.2x10^6$
Baseline, no trip

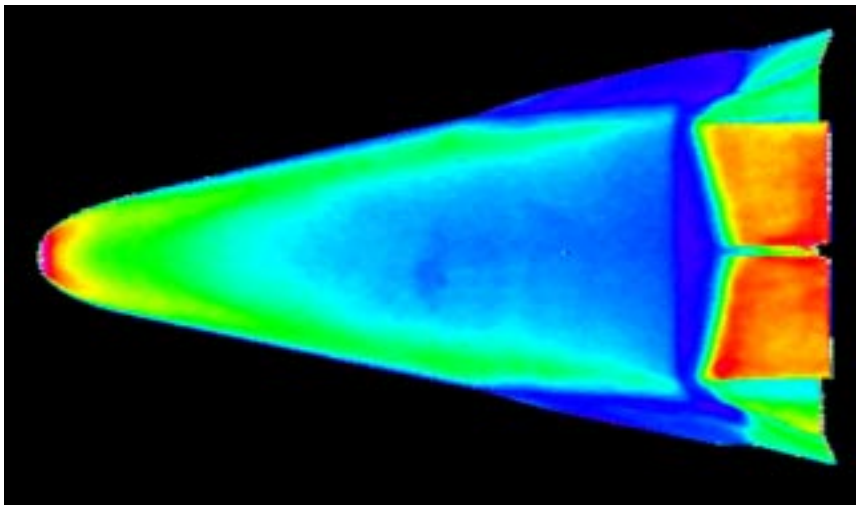

Run # 16
Windward View
Model # 2
BF @ 20°
$\alpha = 40°$
$Re_\infty/ft = 4.4x10^6$
Baseline, no trip

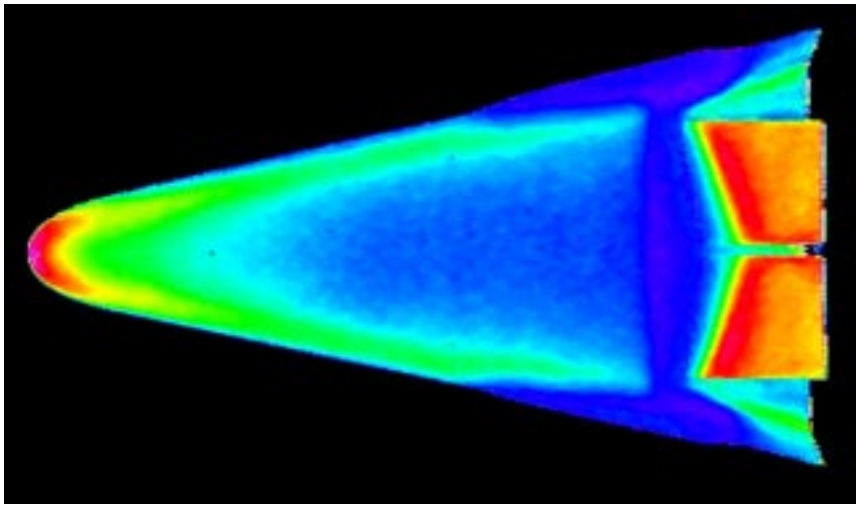

Run # 17
Windward View
Model # 4
BF @ 30°
$\alpha = 40°$
$Re_\infty/ft = 1.1x10^6$
Baseline, no trip

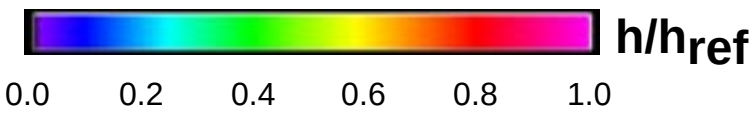

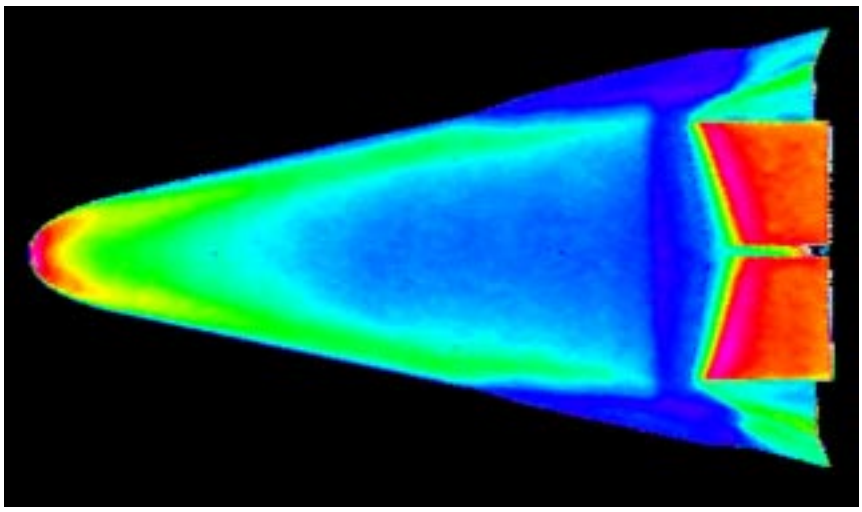

Run # 18
Windward View
Model # 4
BF @ 30°
$\alpha = 40°$
$Re_\infty/ft = 2.2x10^6$
Baseline, no trip

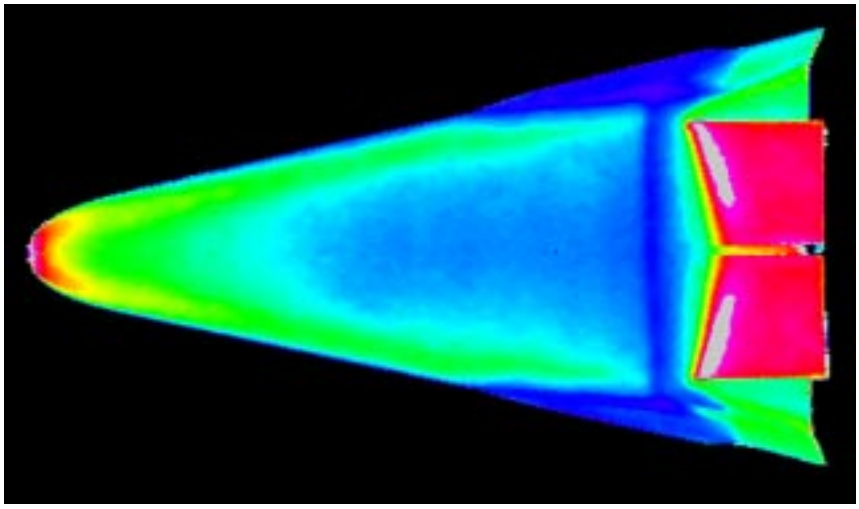

Run # 19
Windward View
Model # 4
BF @ 30°
$\alpha = 40°$
$Re_\infty/ft = 4.4x10^6$
Baseline, no trip

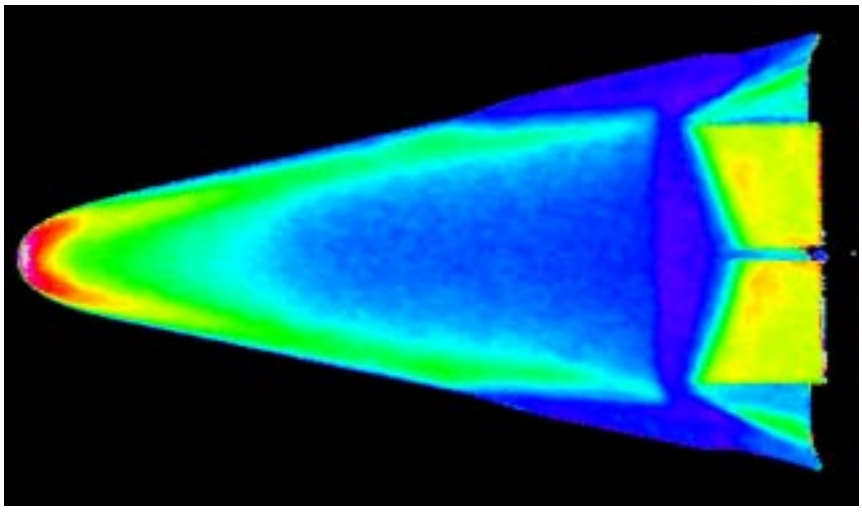

Run # 21
Windward View
Model # 3
BF @ 25°
$\alpha = 40°$
$Re_\infty/ft = 1.1x10^6$
Baseline, no trip

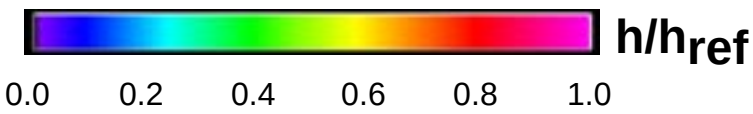

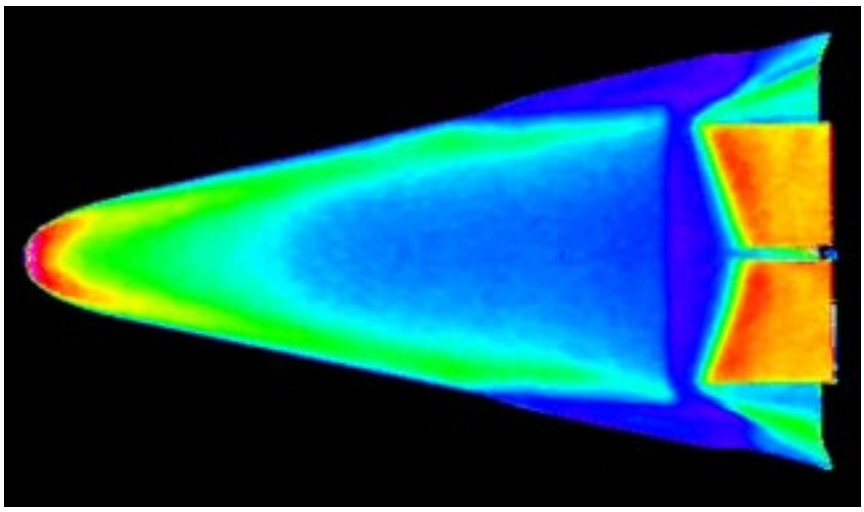

Run # 22
Windward View
Model # 3
BF @ 25°
$\alpha = 40°$
$Re_\infty/ft = 2.2x10^6$
Baseline, no trip

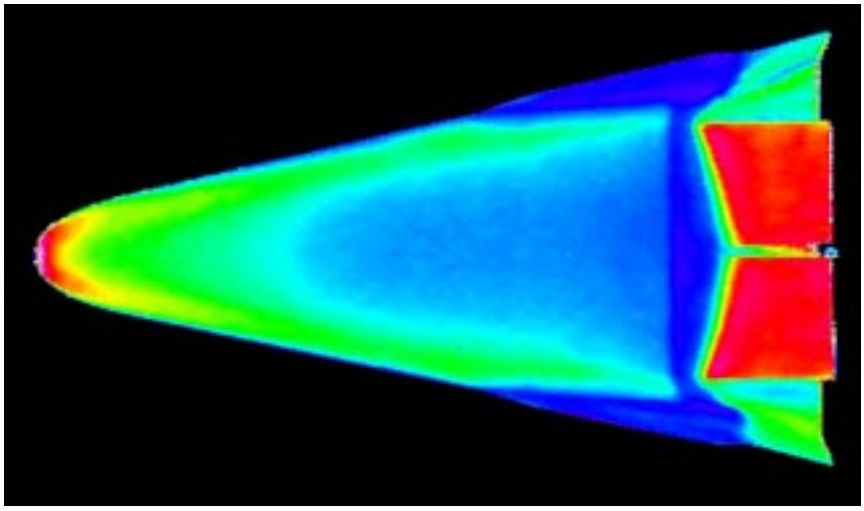

Run # 23
Windward View
Model # 3
BF @ 25°
$\alpha = 40°$
$Re_\infty/ft = 4.4x10^6$
Baseline, no trip

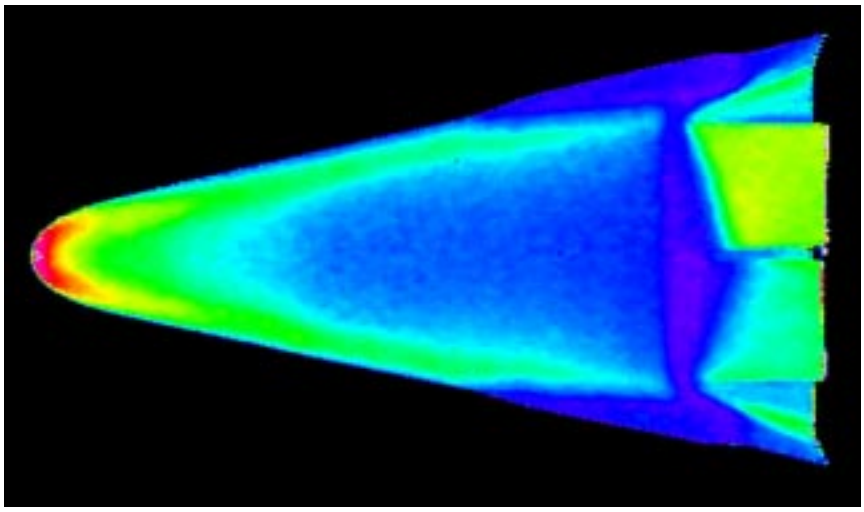

Run # 24
Windward View
Model # 5
RBF @ 20°
LBF @ 25°
$\alpha = 40°$
$Re_\infty/ft = 1.1x10^6$
Baseline, no trip

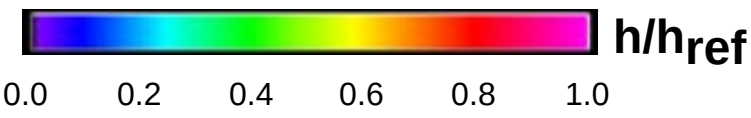

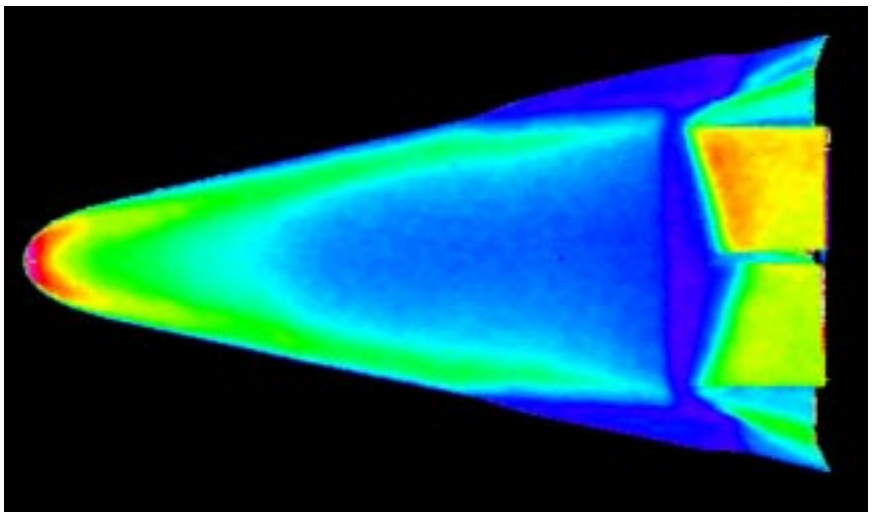

Run # 25
Windward View
Model # 5
RBF @ 20°
LBF @ 25°
$\alpha = 40°$
$Re_\infty/ft = 2.2x10^6$
Baseline, no trip

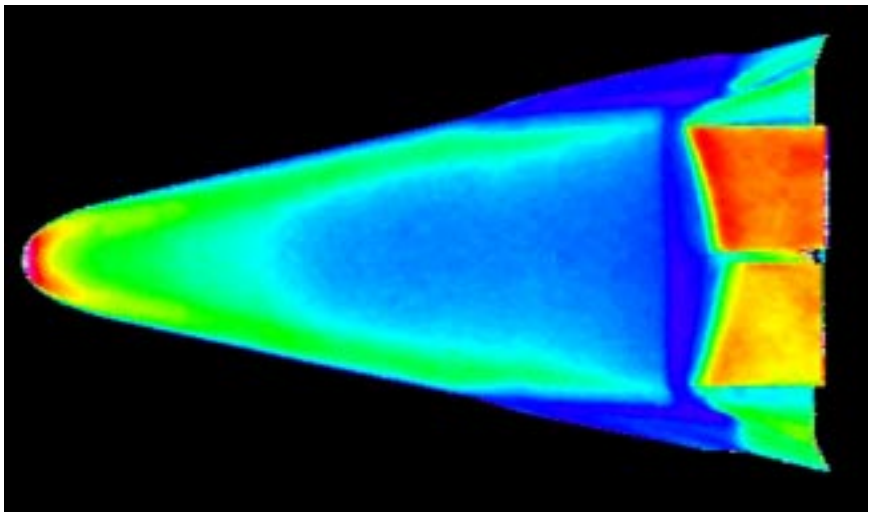

Run # 26
Windward View
Model # 5
RBF @ 20°
LBF @ 25°
$\alpha = 40°$
$Re_\infty/ft = 4.4x10^6$
Baseline, no trip

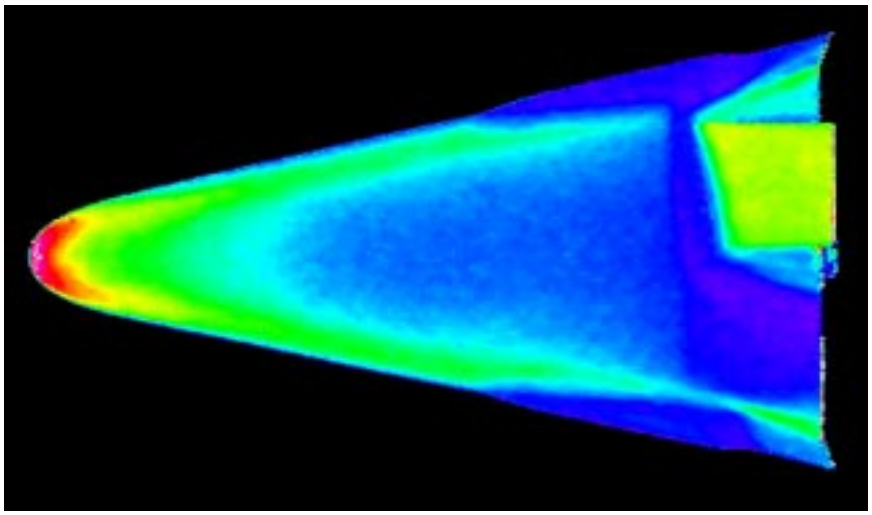

Run # 27
Windward View
Model # 6
RBF @ 0°
LBF @ 25°
$\alpha = 40°$
$Re_\infty/ft = 1.1x10^6$
Baseline, no trip

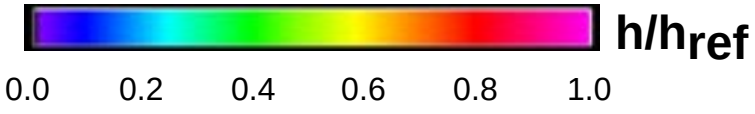

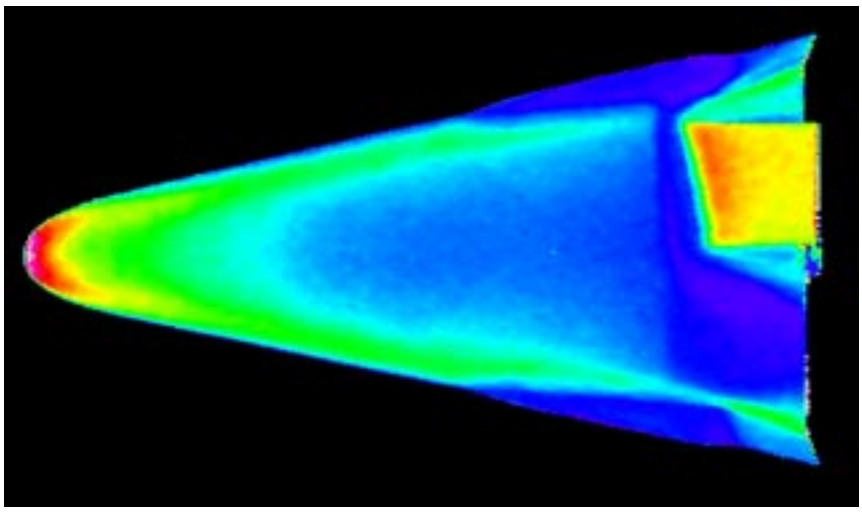

Run # 28
Windward View
Model # 6
RBF @ 0°
LBF @ 25°
$\alpha = 40°$
$Re_\infty/ft = 2.2x10^6$
Baseline, no trip

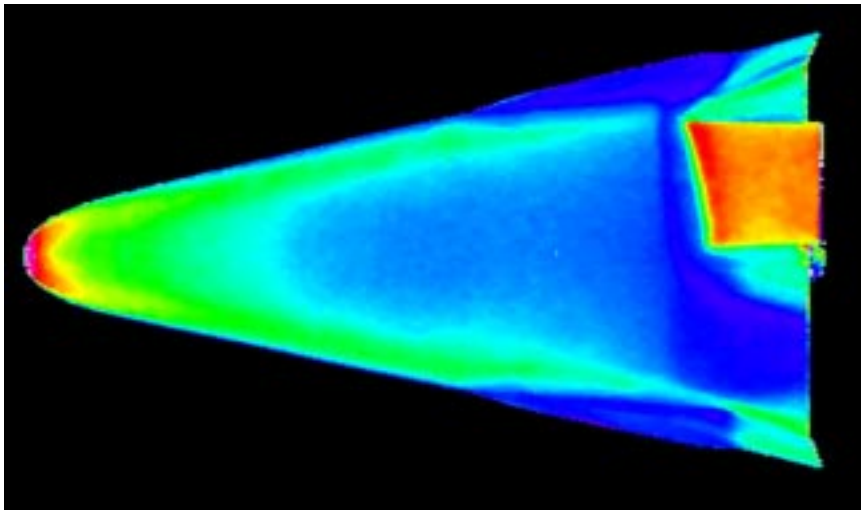

Run # 29
Windward View
Model # 6
RBF @ 0°
LBF @ 25°
$\alpha = 40°$
$Re_\infty/ft = 4.4x10^6$
Baseline, no trip

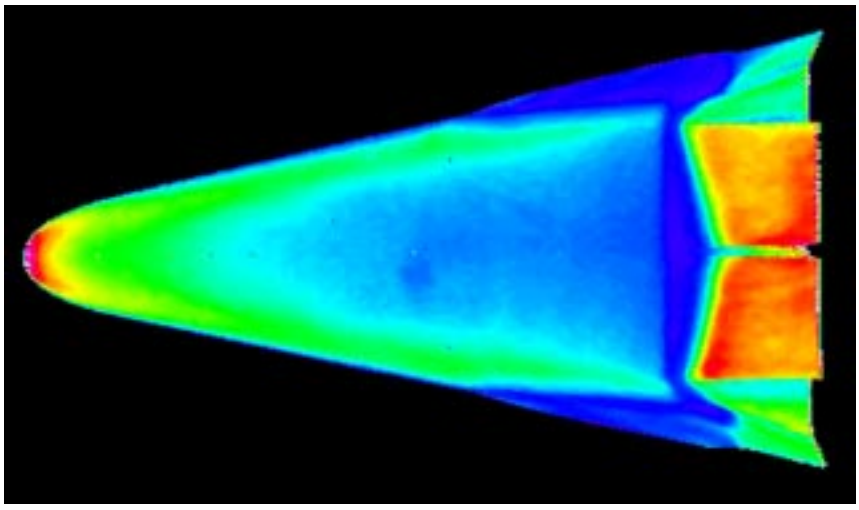

Run # 31
Windward View
Model # 2
BF @ 20°
$\alpha = 40°$
$Re_\infty/ft = 4.4x10^6$
Baseline, no trip
Repeat of Run 16

h/h_{ref}

0.0 0.2 0.4 0.6 0.8 1.0

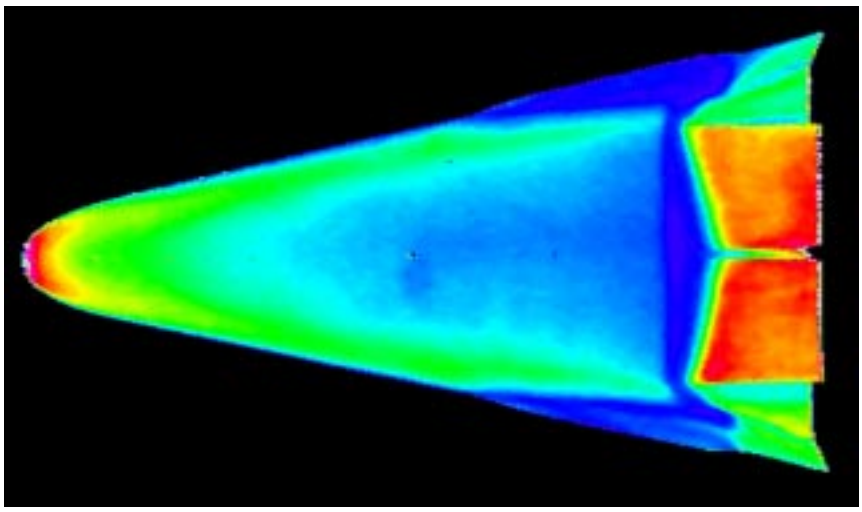

Run # 32
Windward View
Model # 2
BF @ 20°
$\alpha = 40°$
$Re_\infty/ft = 4.4x10^6$
0.0025-in. Trip
@ x/L = 0.5

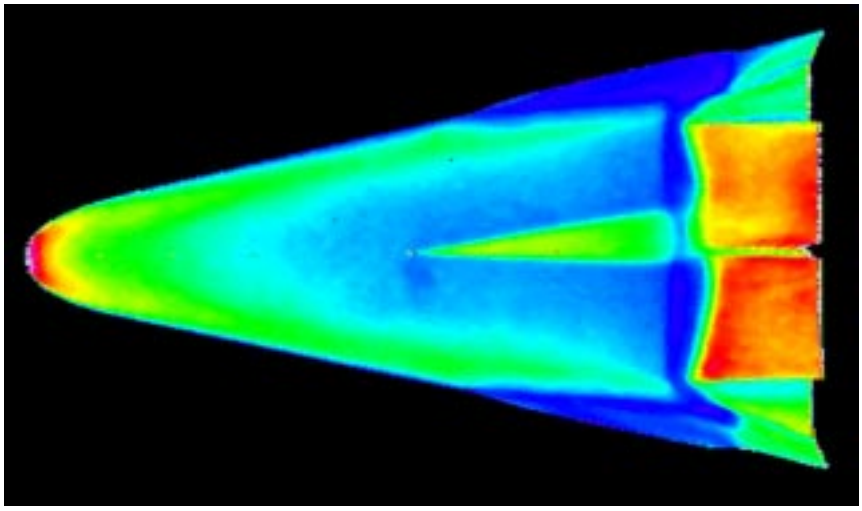

Run # 33
Windward View
Model # 2
BF @ 20°
$\alpha = 40°$
$Re_\infty/ft = 4.4x10^6$
0.0050-in. Trip
@ x/L = 0.5

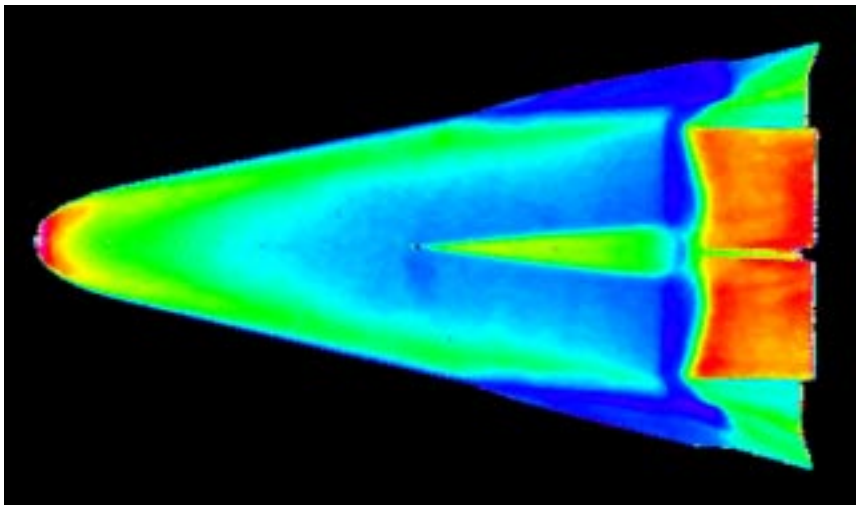

Run # 34
Windward View
Model # 2
BF @ 20°
$\alpha = 40°$
$Re_\infty/ft = 4.4x10^6$
0.0050-in. Trip
@ x/L = 0.5
Fixed yaw

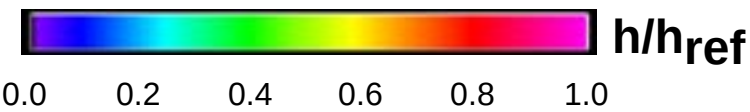

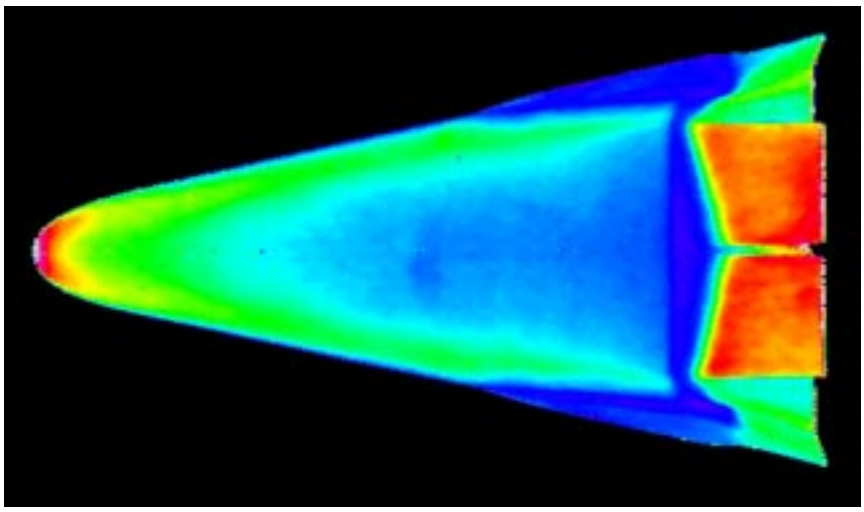

Run # 35
Windward View
Model # 2
BF @ 20°
$\alpha = 40°$
$Re_\infty/ft = 4.4x10^6$
Baseline repeat

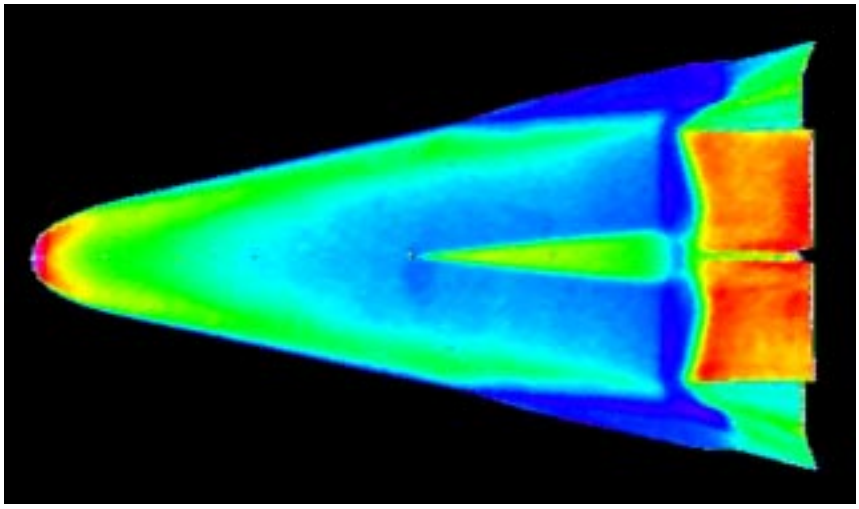

Run # 36
Windward View
Model # 2
BF @ 20°
$\alpha = 40°$
$Re_\infty/ft = 4.4x10^6$
0.0050-in. Trip
@ x/L = 0.5
Repeat Run 34

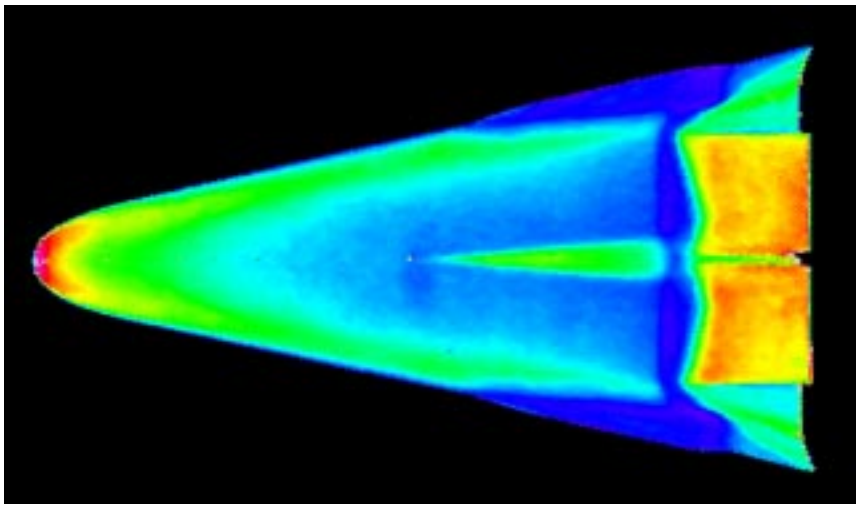

Run # 37
Windward View
Model # 2
BF @ 20°
$\alpha = 40°$
$Re_\infty/ft = 3.3x10^6$
0.0050-in. Trip
@ x/L = 0.5

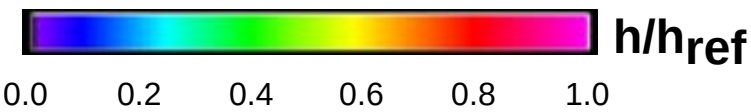

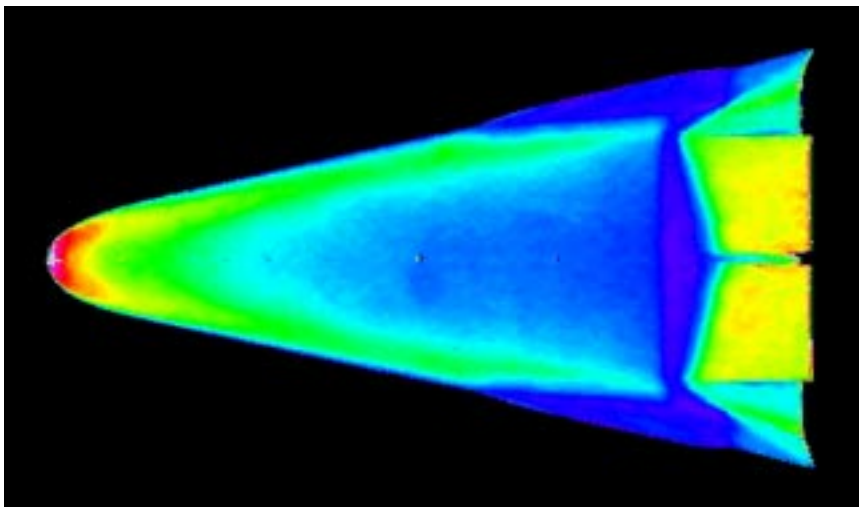

Run # 38
Windward View
Model # 2
BF @ 20°
$\alpha = 40°$
$Re_\infty/ft = 2.2x10^6$
0.0050-in. Trip
@ x/L = 0.5

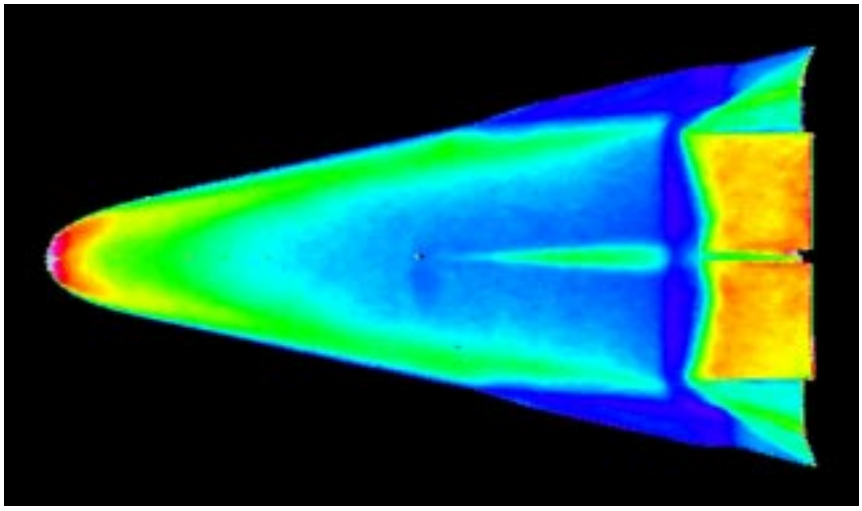

Run # 39
Windward View
Model # 2
BF @ 20°
$\alpha = 40°$
$Re_\infty/ft = 2.7x10^6$
0.0050-in. Trip
@ x/L = 0.5

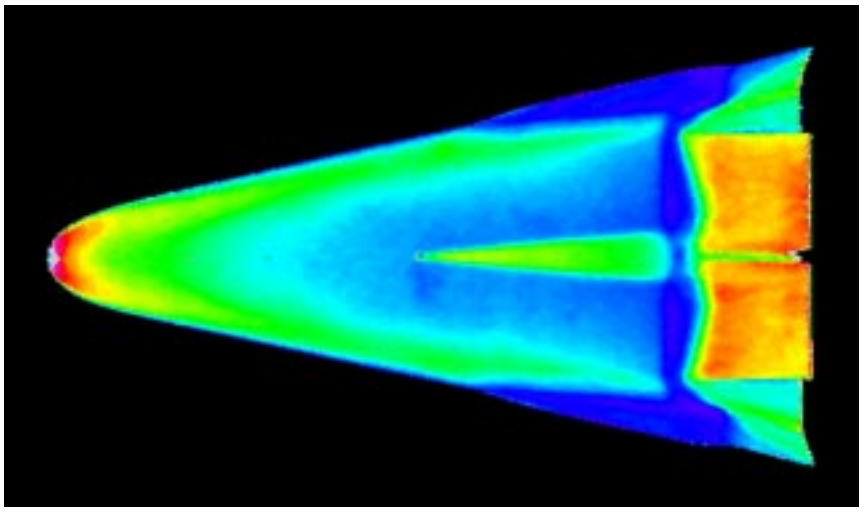

Run # 40
Windward View
Model # 2
BF @ 20°
$\alpha = 40°$
$Re_\infty/ft = 3.3x10^6$
0.0075-in. Trip
@ x/L = 0.5

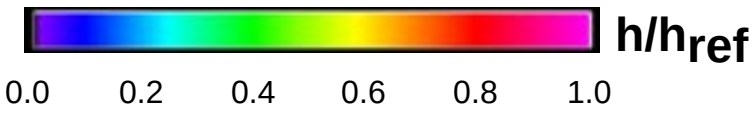

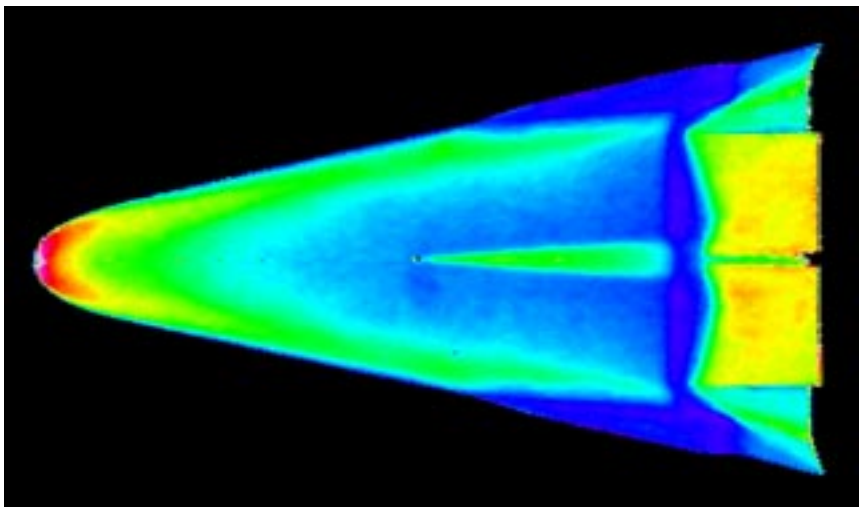

Run # 41
Windward View
Model # 2
BF @ 20°
$\alpha = 40°$
$Re_\infty/ft = 2.2x10^6$
0.0075-in. Trip
@ x/L = 0.5

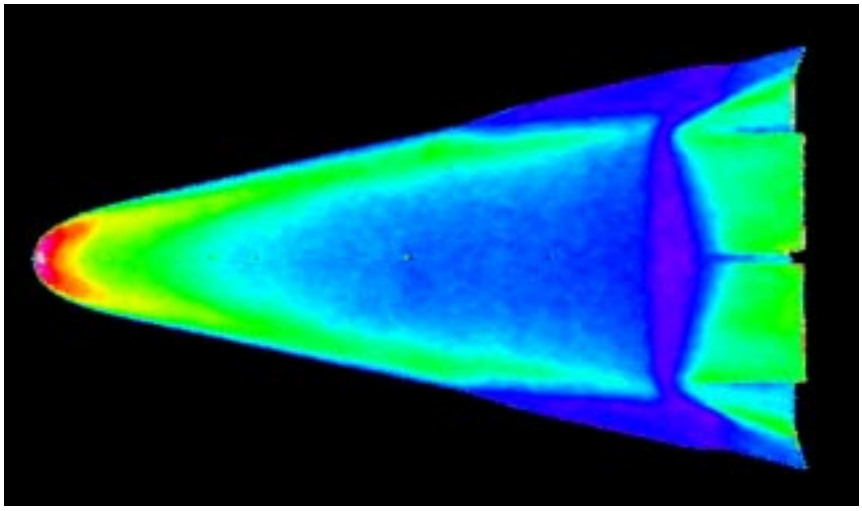

Run # 42
Windward View
Model # 2
BF @ 20°
$\alpha = 40°$
$Re_\infty/ft = 1.1x10^6$
0.0075-in. Trip
@ x/L = 0.5

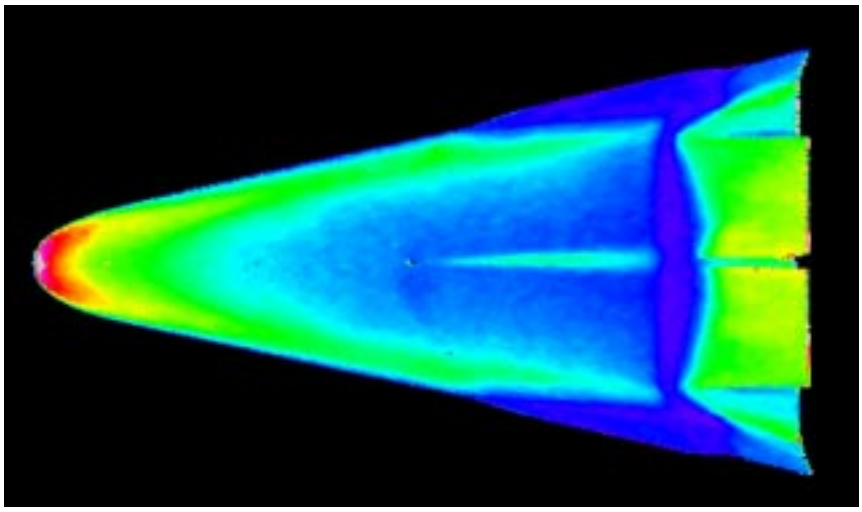

Run # 43
Windward View
Model # 2
BF @ 20°
$\alpha = 40°$
$Re_\infty/ft = 1.6x10^6$
0.0075-in. Trip
@ x/L = 0.5

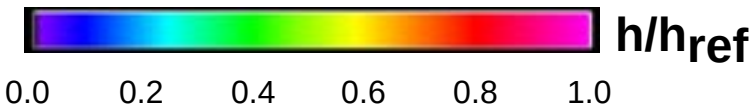

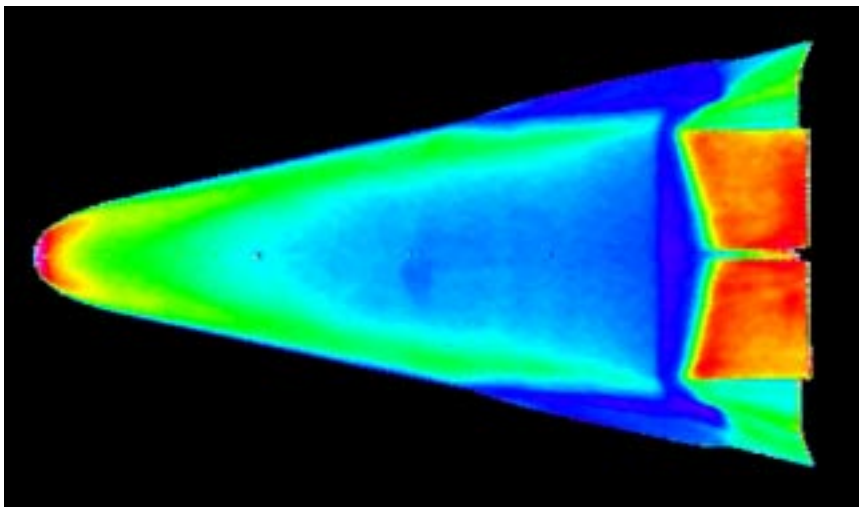

Run # 44
Windward View
Model # 2
BF @ 20°
$\alpha = 40°$
$Re_\infty/ft = 4.4x10^6$
0.0025-in. Trip
@ x/L = 0.3

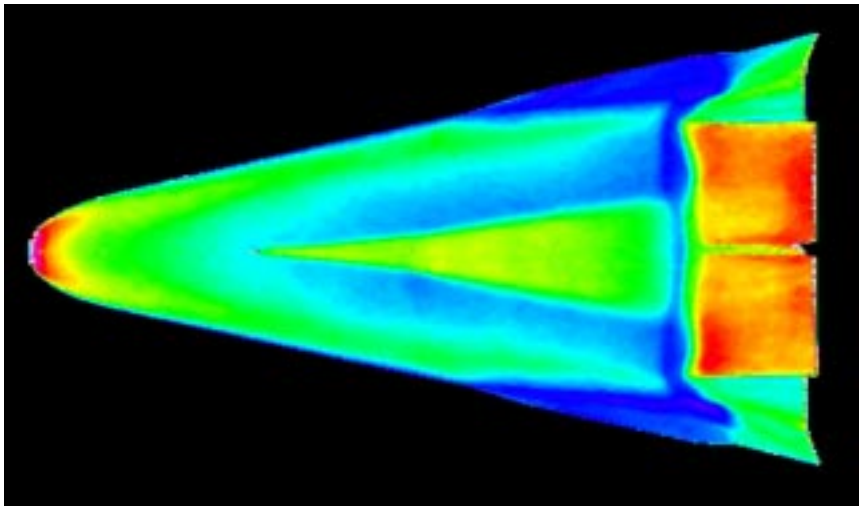

Run # 45
Windward View
Model # 2
BF @ 20°
$\alpha = 40°$
$Re_\infty/ft = 4.4x10^6$
0.0050-in. Trip
@ x/L = 0.3

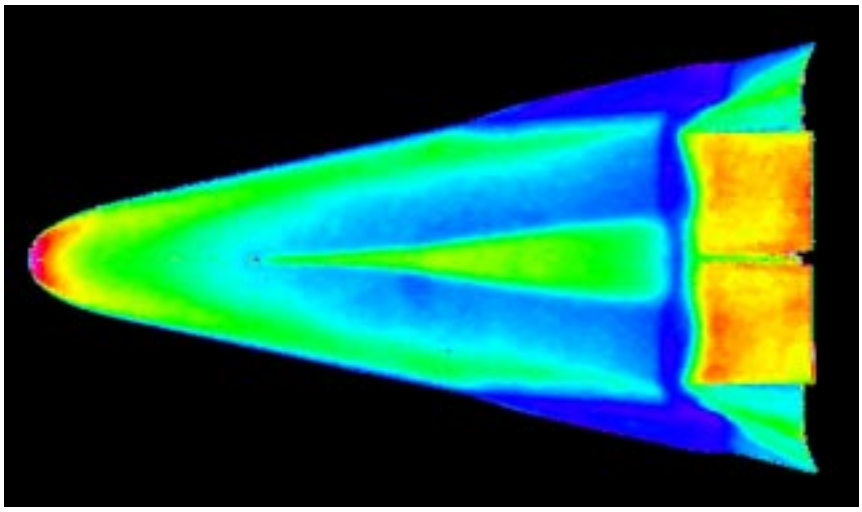

Run # 46
Windward View
Model # 2
BF @ 20°
$\alpha = 40°$
$Re_\infty/ft = 3.3x10^6$
0.0050-in. Trip
@ x/L = 0.3

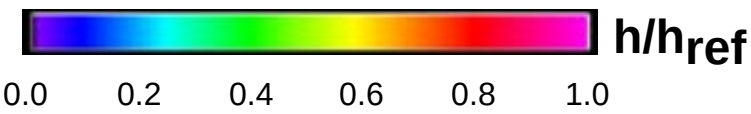

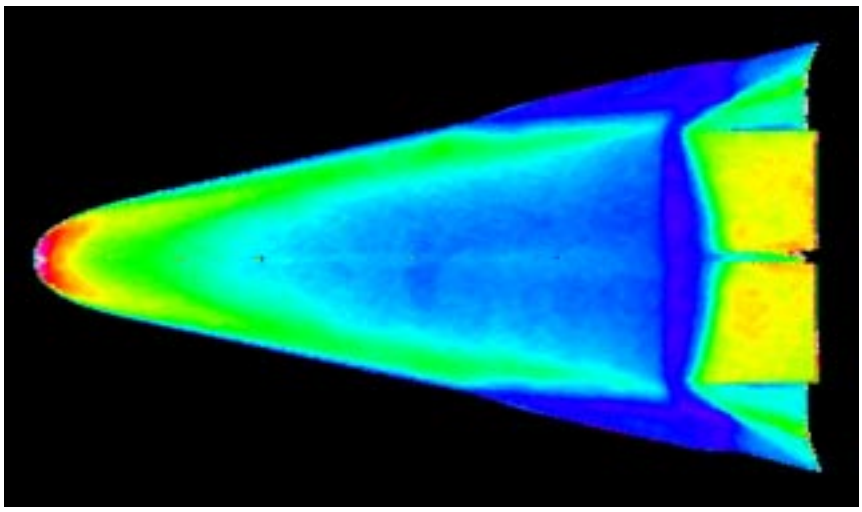

Run # 47
Windward View
Model # 2
BF @ 20°
$\alpha = 40°$
$Re_\infty/ft = 2.2x10^6$
0.0050-in. Trip
@ x/L = 0.3

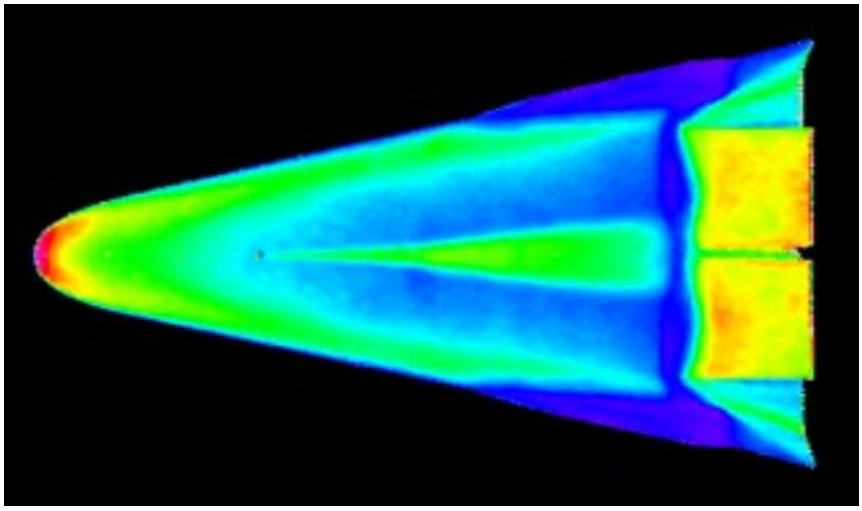

Run # 48
Windward View
Model # 2
BF @ 20°
$\alpha = 40°$
$Re_\infty/ft = 2.8x10^6$
0.0050-in. Trip
@ x/L = 0.3

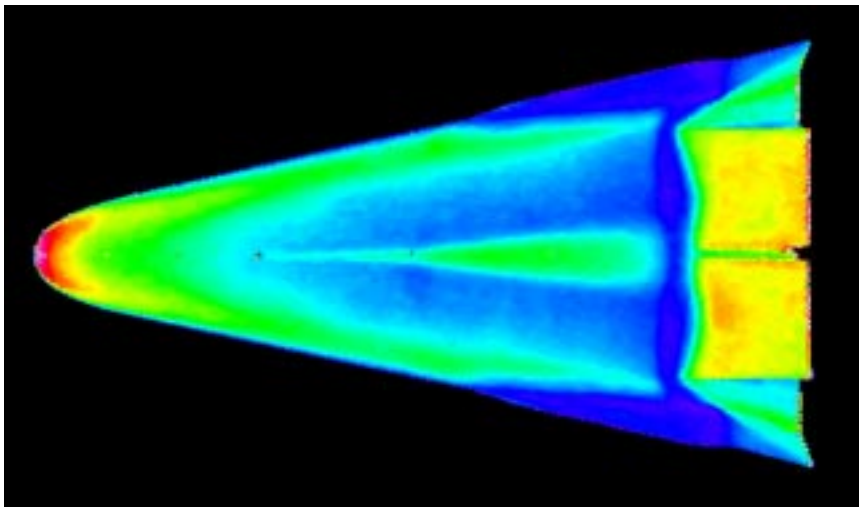

Run # 49
Windward View
Model # 2
BF @ 20°
$\alpha = 40°$
$Re_\infty/ft = 2.4x10^6$
0.0050-in. Trip
@ x/L = 0.3

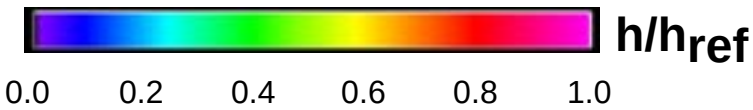

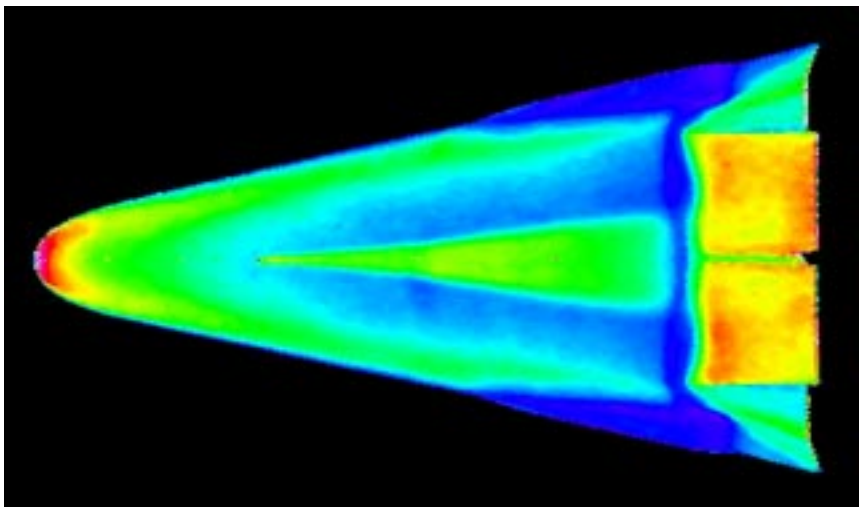

Run # 50
Windward View
Model # 2
BF @ 20°
$\alpha = 40°$
$Re_\infty/ft = 3.3x10^6$
0.0075-in. Trip
@ x/L = 0.3

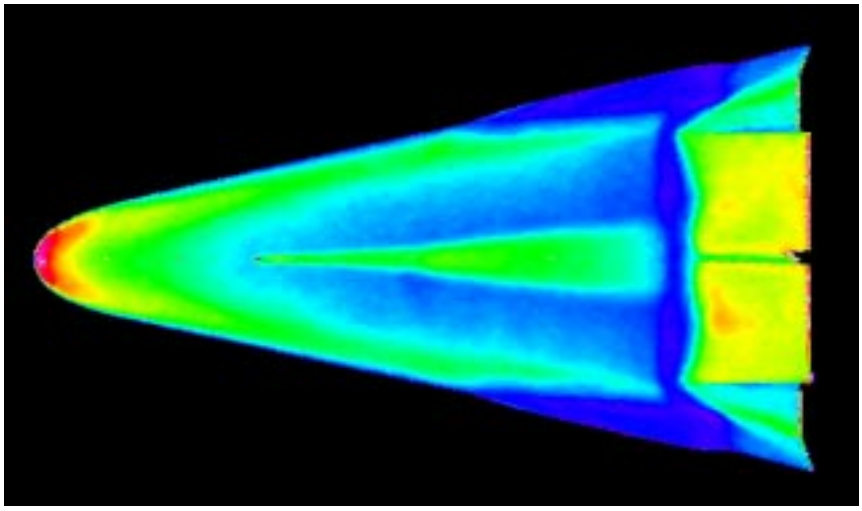

Run # 51
Windward View
Model # 2
BF @ 20°
$\alpha = 40°$
$Re_\infty/ft = 2.2x10^6$
0.0075-in. Trip
@ x/L = 0.3

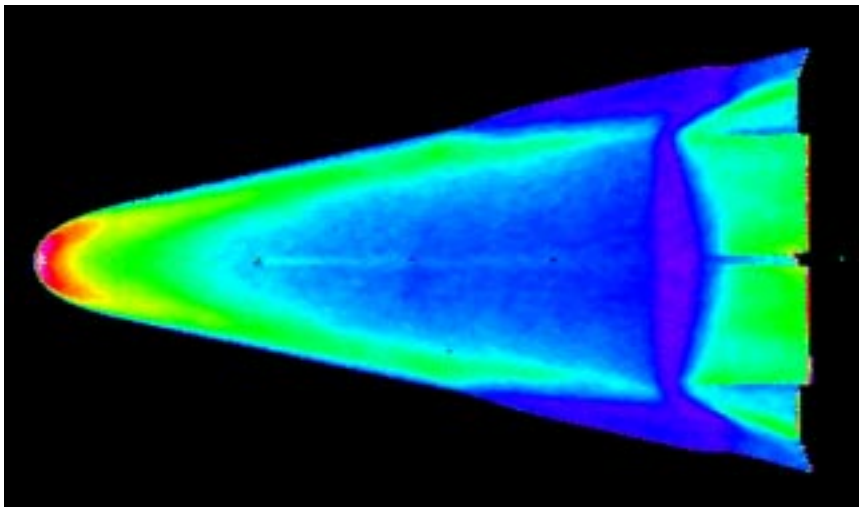

Run # 53
Windward View
Model # 2
BF @ 20°
$\alpha = 40°$
$Re_\infty/ft = 1.1x10^6$
0.0075-in. Trip
@ x/L = 0.3

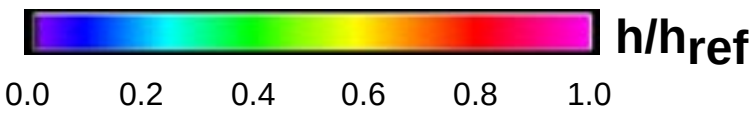

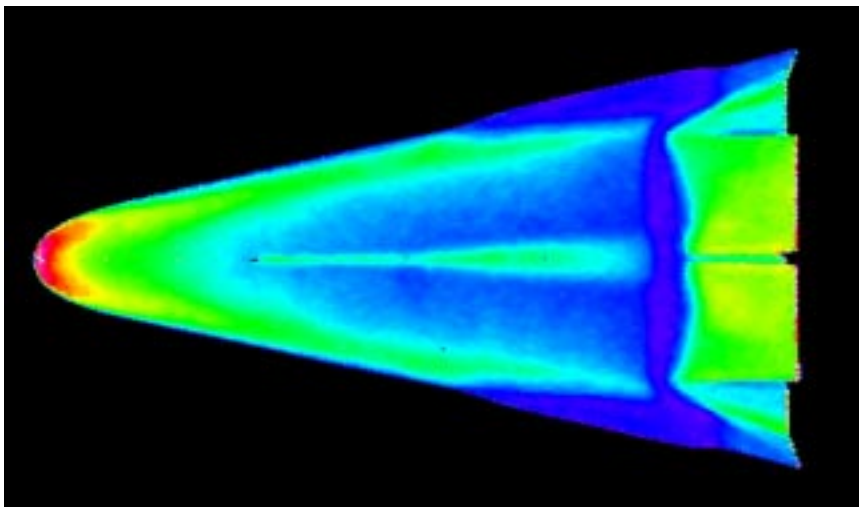

Run # 54
Windward View
Model # 2
BF @ 20°
$\alpha = 40°$
$Re_\infty/ft = 1.6x10^6$
0.0075-in. Trip
@ x/L = 0.3

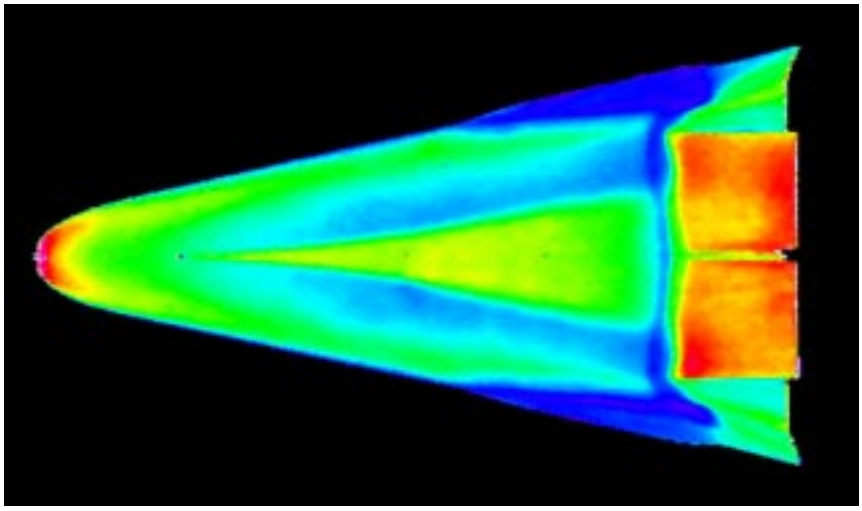

Run # 55
Windward View
Model # 2
BF @ 20°
$\alpha = 40°$
$Re_\infty/ft = 4.4x10^6$
0.0025-in. Trip
@ x/L = 0.2

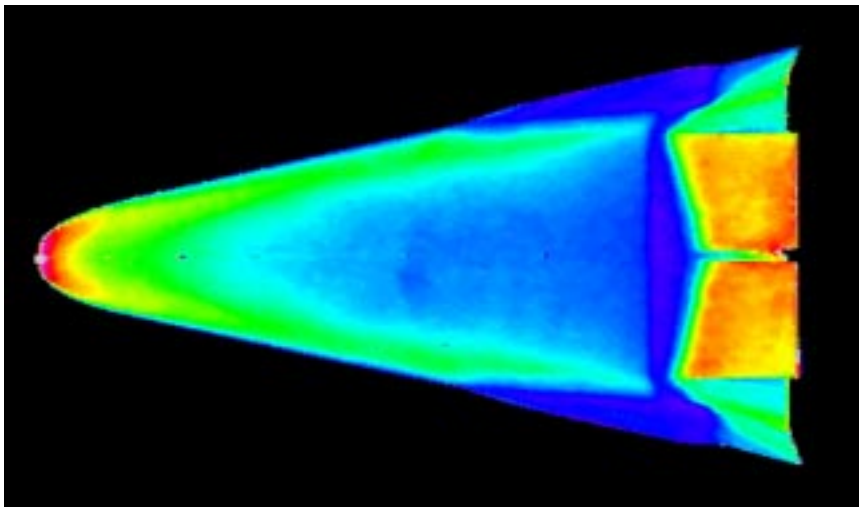

Run # 56
Windward View
Model # 2
BF @ 20°
$\alpha = 40°$
$Re_\infty/ft = 3.3x10^6$
0.0025-in. Trip
@ x/L = 0.2

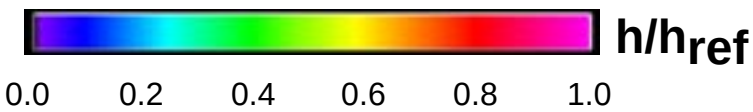

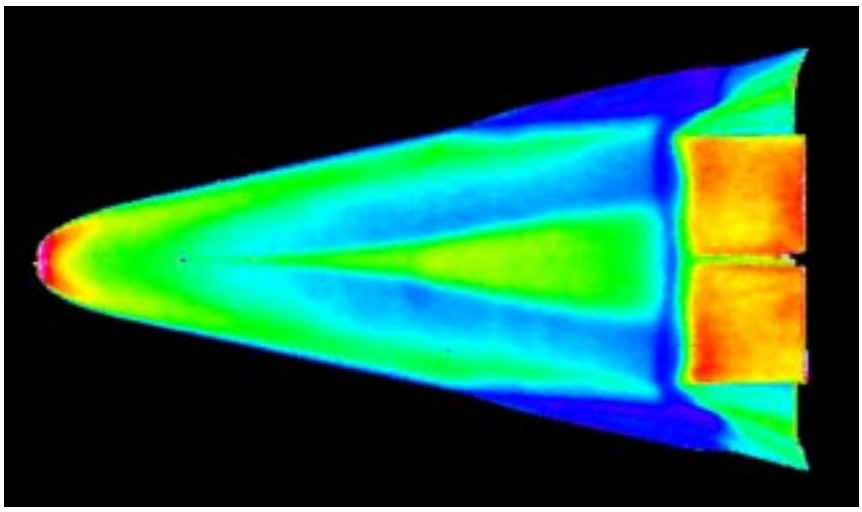

Run # 57
Windward View
Model # 2
BF @ 20°
$\alpha = 40°$
$Re_\infty/ft = 3.8x10^6$
0.0025-in. Trip
@ x/L = 0.2

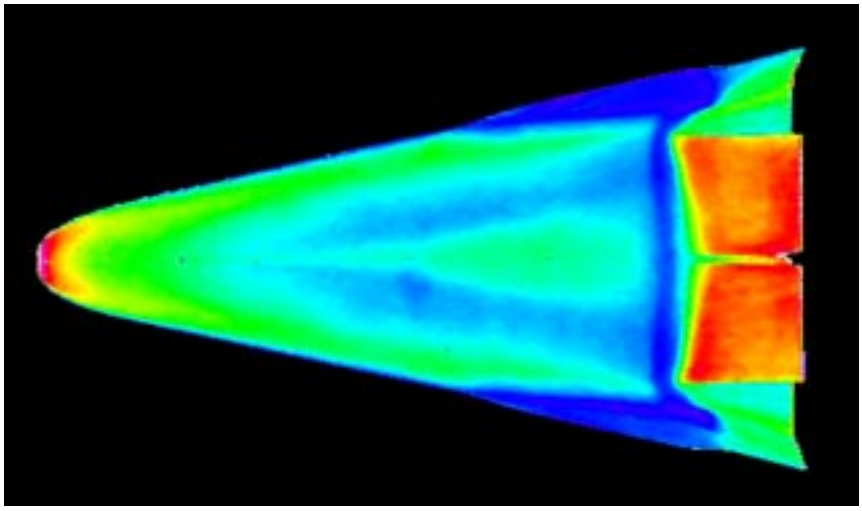

Run # 58
Windward View
Model # 2
BF @ 20°
$\alpha = 40°$
$Re_\infty/ft = 4.4x10^6$
New 0.0025-in. Trip
@ x/L = 0.2

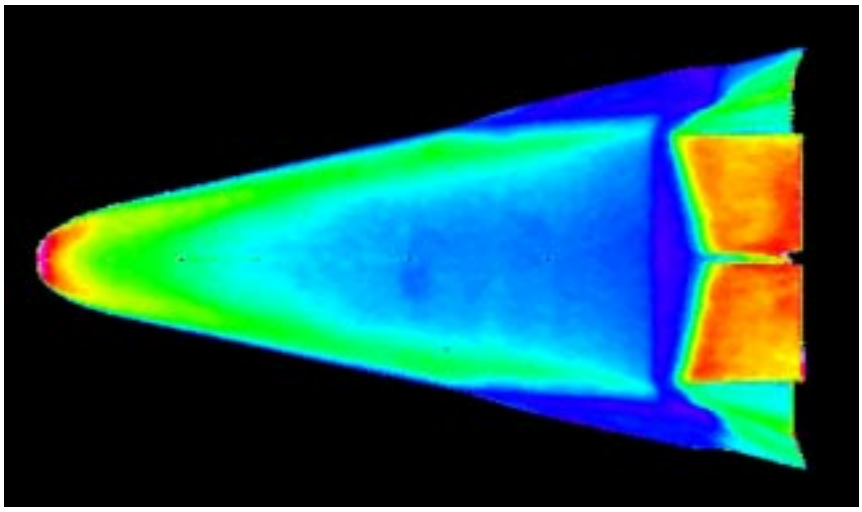

Run # 59
Windward View
Model # 2
BF @ 20°
$\alpha = 40°$
$Re_\infty/ft = 3.8x10^6$
New 0.0025-in. Trip
@ x/L = 0.2

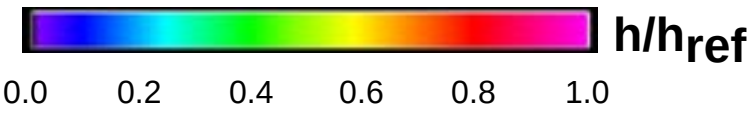

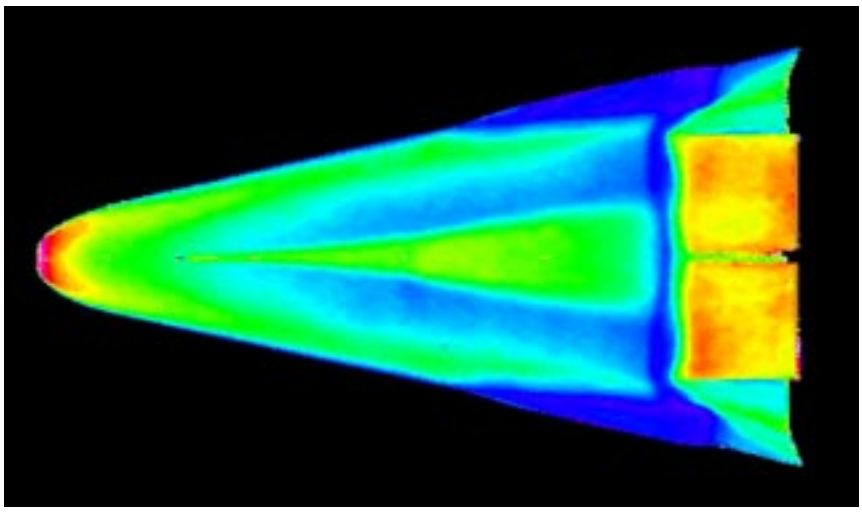

Run # 60
Windward View
Model # 2
BF @ 20°
$\alpha = 40°$
$Re_\infty/ft = 3.3x10^6$
0.0050-in. Trip
@ x/L = 0.2

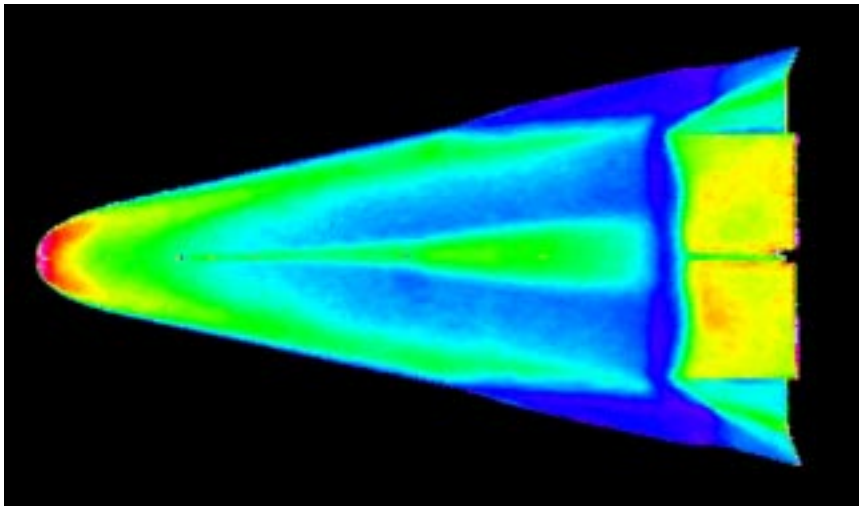

Run # 61
Windward View
Model # 2
BF @ 20°
$\alpha = 40°$
$Re_\infty/ft = 2.2x10^6$
0.0050-in. Trip
@ x/L = 0.2

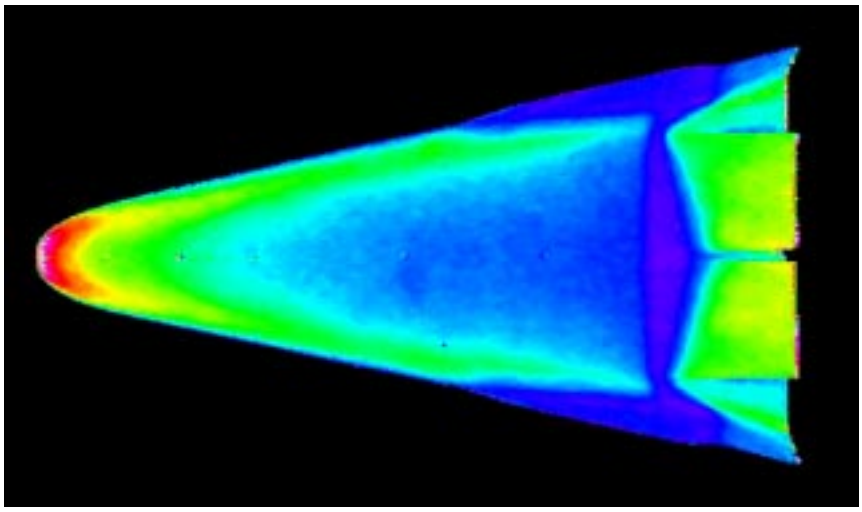

Run # 62
Windward View
Model # 2
BF @ 20°
$\alpha = 40°$
$Re_\infty/ft = 1.6x10^6$
0.0050-in. Trip
@ x/L = 0.2

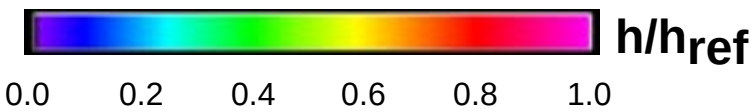

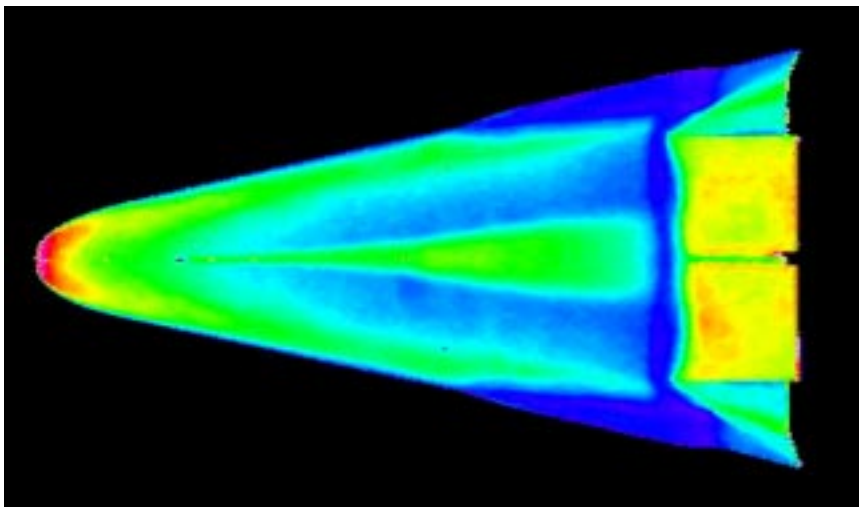

Run # 63
Windward View
Model # 2
BF @ 20°
$\alpha = 40°$
$Re_\infty/ft = 2.5x10^6$
0.0050-in. Trip
@ x/L = 0.2

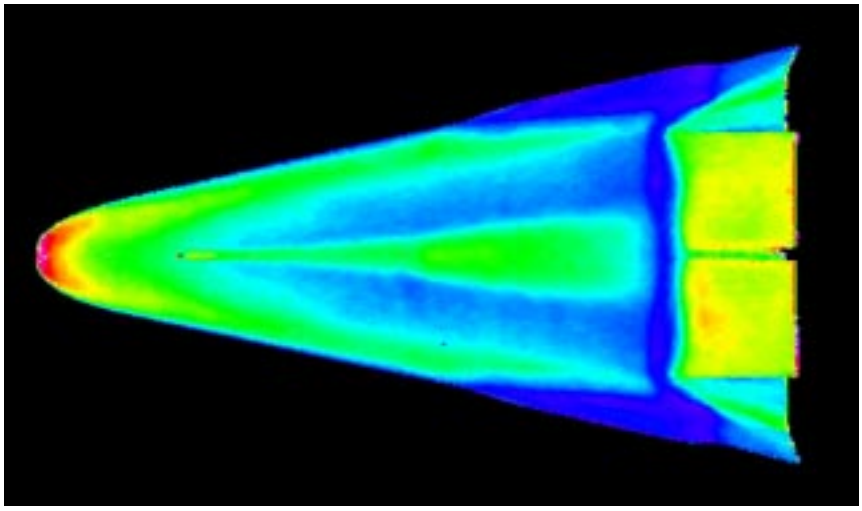

Run # 64
Windward View
Model # 2
BF @ 20°
$\alpha = 40°$
$Re_\infty/ft = 2.2x10^6$
0.0075-in. Trip
@ x/L = 0.2

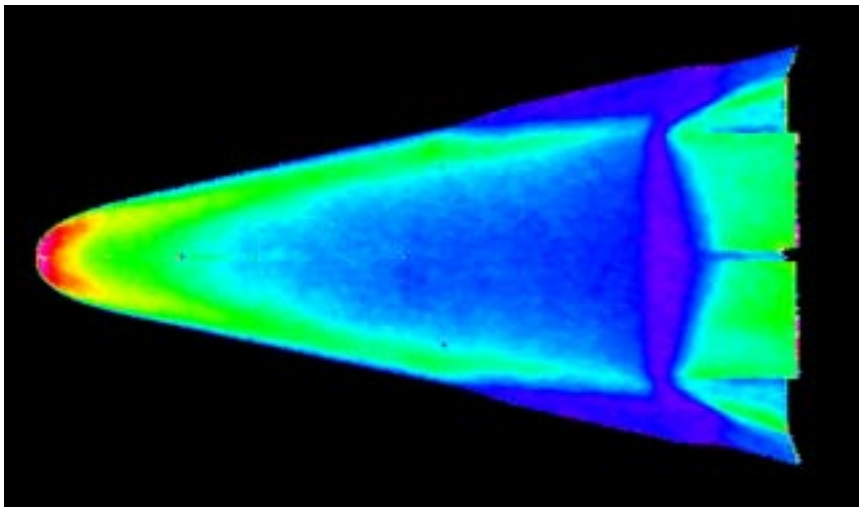

Run # 65
Windward View
Model # 2
BF @ 20°
$\alpha = 40°$
$Re_\infty/ft = 1.1x10^6$
0.0075-in. Trip
@ x/L = 0.2

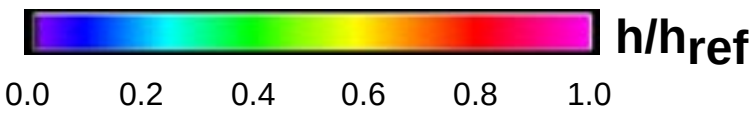

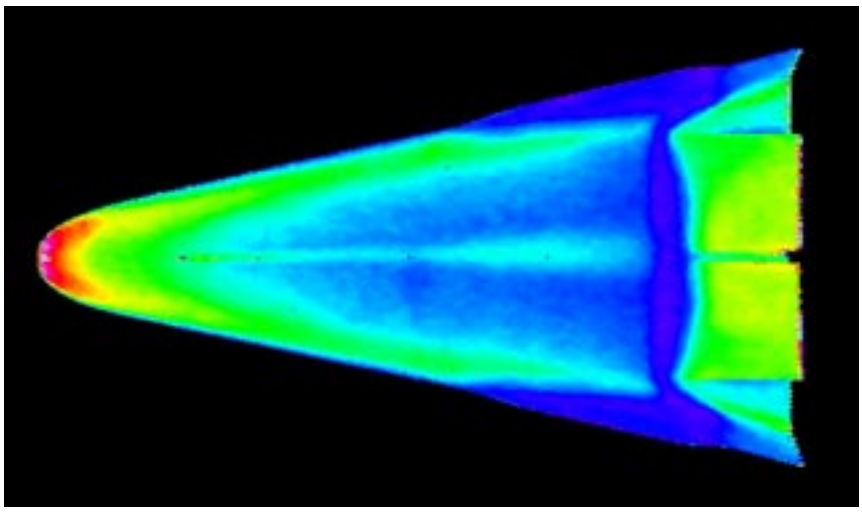

Run # 66
Windward View
Model # 2
BF @ 20°
$\alpha = 40°$
$Re_\infty/ft = 1.6x10^6$
0.0075-in. Trip
@ x/L = 0.2

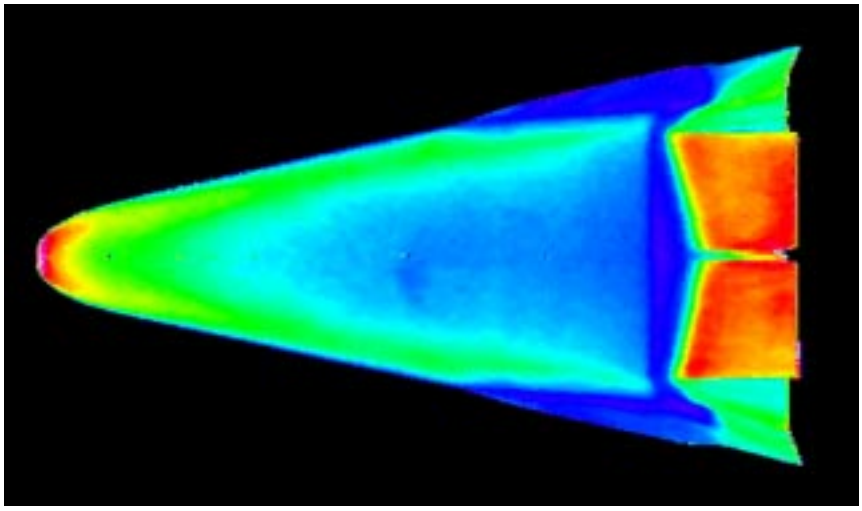

Run # 67
Windward View
Model # 2
BF @ 20°
$\alpha = 40°$
$Re_\infty/ft = 4.4x10^6$
0.0025-in. Trip
@ x/L = 0.1

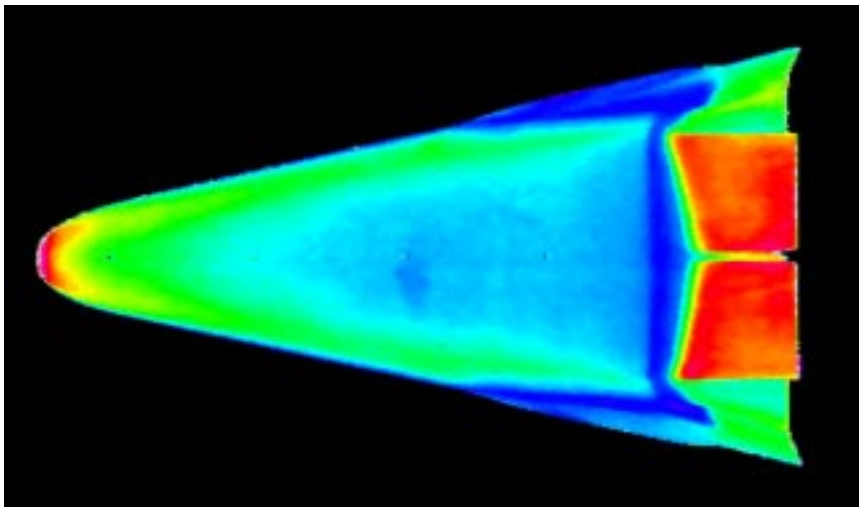

Run # 68
Windward View
Model # 2
BF @ 20°
$\alpha = 40°$
$Re_\infty/ft = 5.4x10^6$
0.0025-in. Trip
@ x/L = 0.1

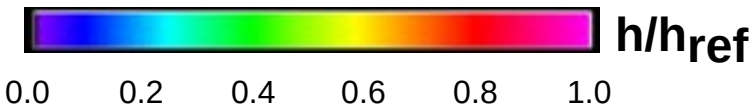

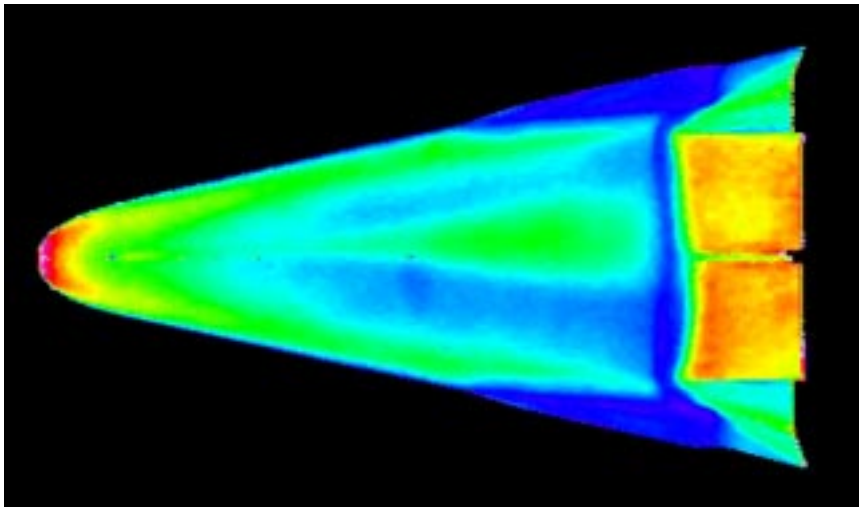

Run # 69
Windward View
Model # 2
BF @ 20°
$\alpha = 40°$
$Re_\infty/ft = 3.3x10^6$
0.0050-in. Trip
@ x/L = 0.1

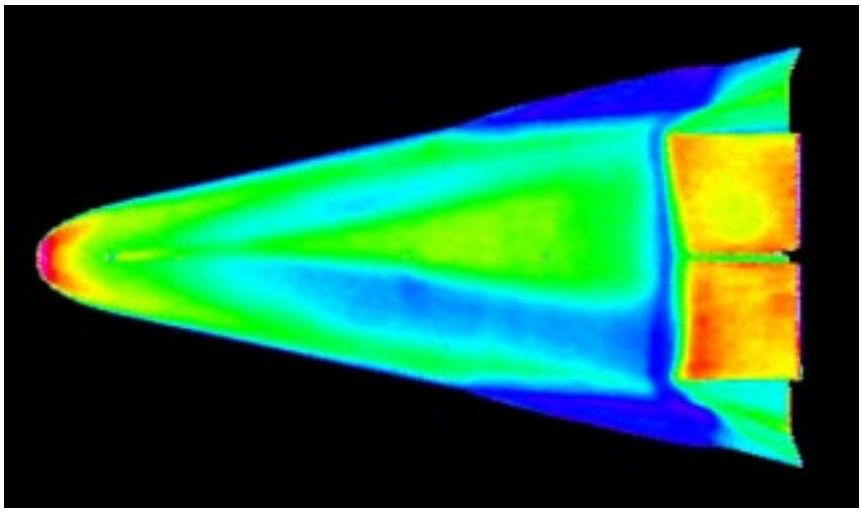

Run # 70
Windward View
Model # 2
BF @ 20°
$\alpha = 40°$
$Re_\infty/ft = 4.4x10^6$
0.0050-in. Trip
@ x/L = 0.1

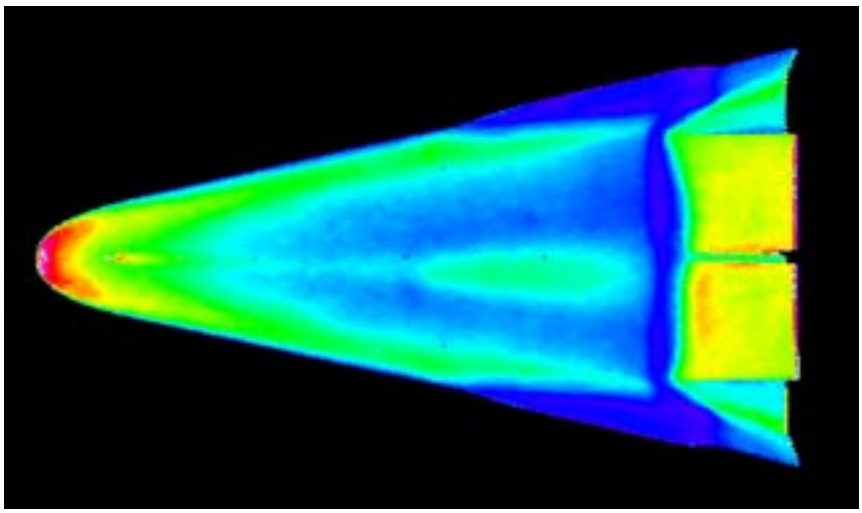

Run # 71
Windward View
Model # 2
BF @ 20°
$\alpha = 40°$
$Re_\infty/ft = 2.2x10^6$
0.0075-in. Trip
@ x/L = 0.1

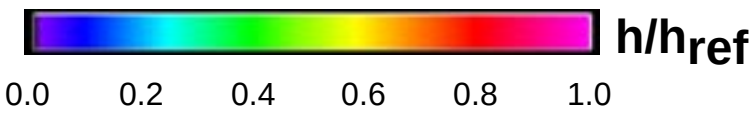

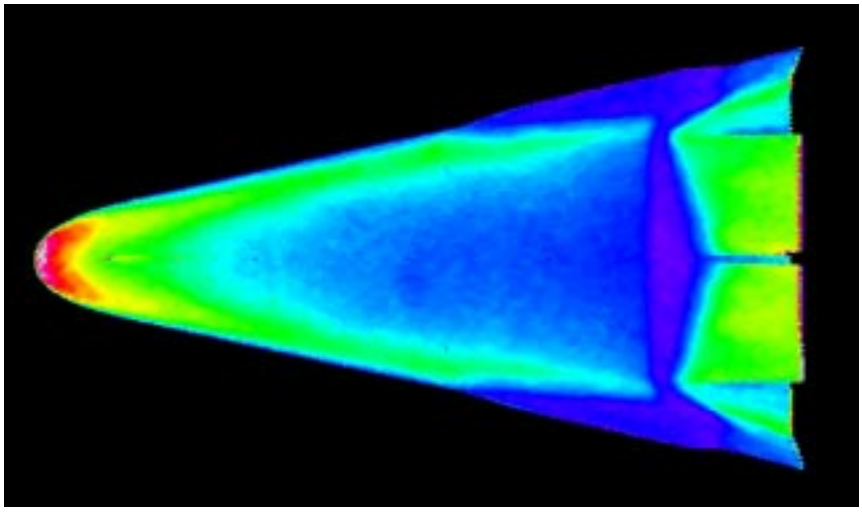

Run # 72
Windward View
Model # 2
BF @ 20°
$\alpha = 40°$
$Re_\infty/ft = 1.6x10^6$
0.0075-in. Trip
@ x/L = 0.1

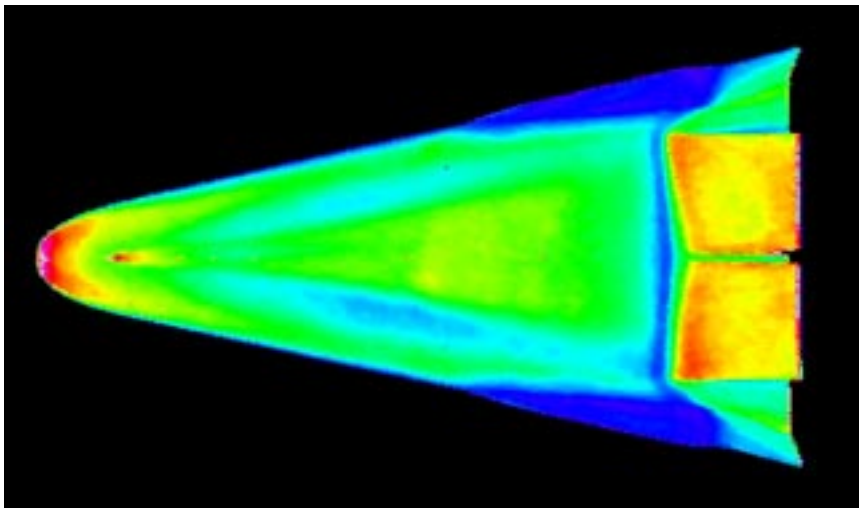

Run # 73
Windward View
Model # 2
BF @ 20°
$\alpha = 40°$
$Re_\infty/ft = 3.3x10^6$
0.0075-in. Trip
@ x/L = 0.1

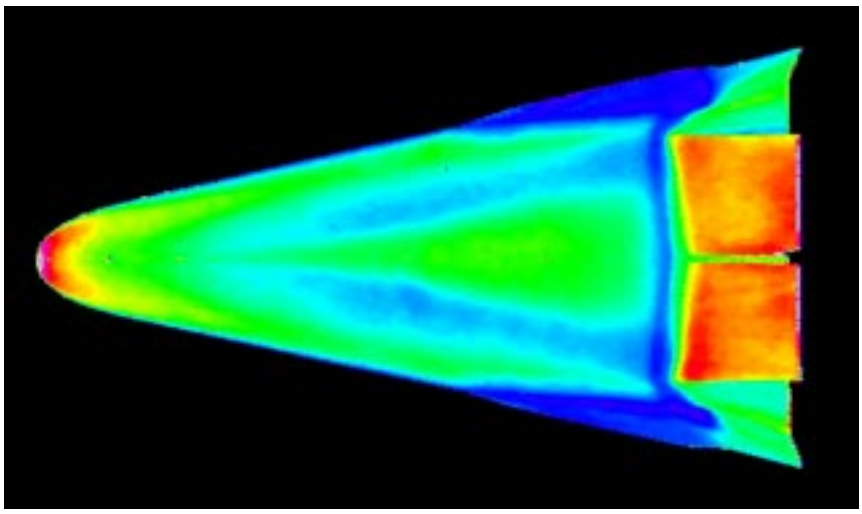

Run # 74
Windward View
Model # 2
BF @ 20°
$\alpha = 40°$
$Re_\infty/ft = 4.4x10^6$
0.0025-in. Trip
@ x/L = 0.1

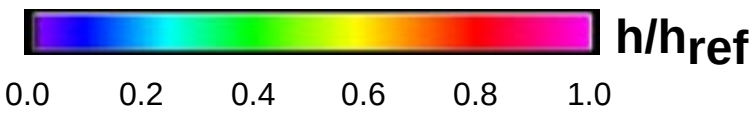

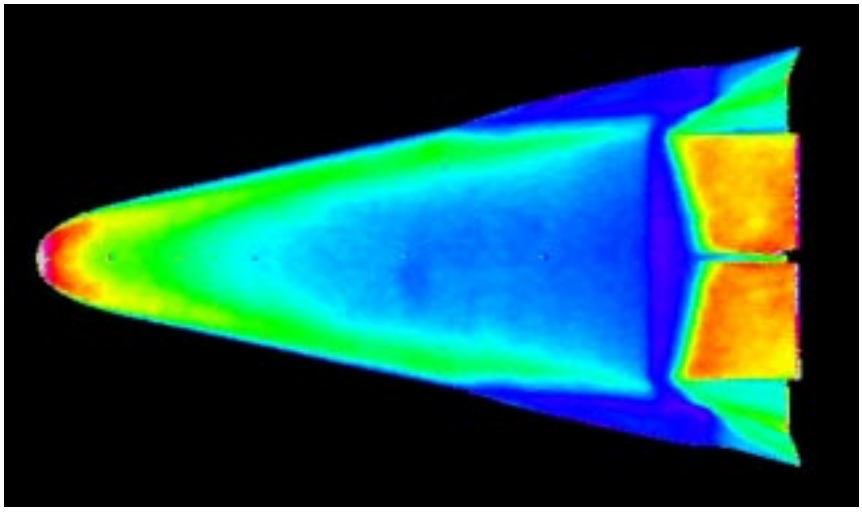

Run # 75
Windward View
Model # 2
BF @ 20°
$\alpha = 40°$
$Re_\infty/ft = 3.3x10^6$
0.0025-in. Trip
@ x/L = 0.1

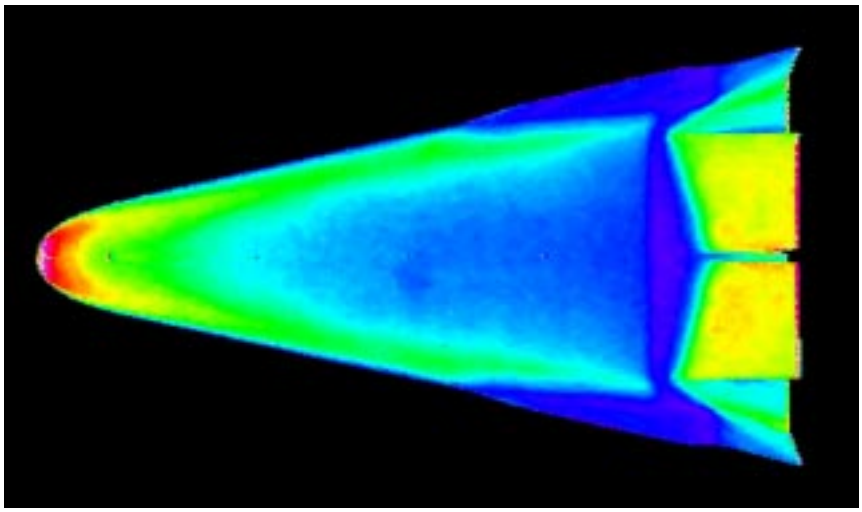

Run # 78
Windward View
Model # 2
BF @ 20°
$\alpha = 40°$
$Re_\infty/ft = 2.2x10^6$
0.0050-in. Trip
@ x/L = 0.1

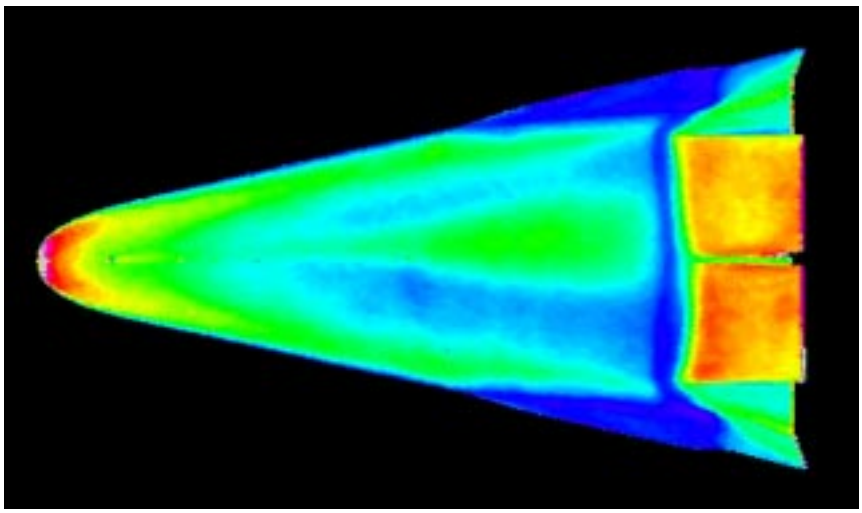

Run # 80
Windward View
Model # 2
BF @ 20°
$\alpha = 40°$
$Re_\infty/ft = 3.3x10^6$
0.0050-in. Trip
@ x/L = 0.1

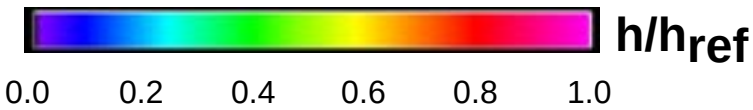

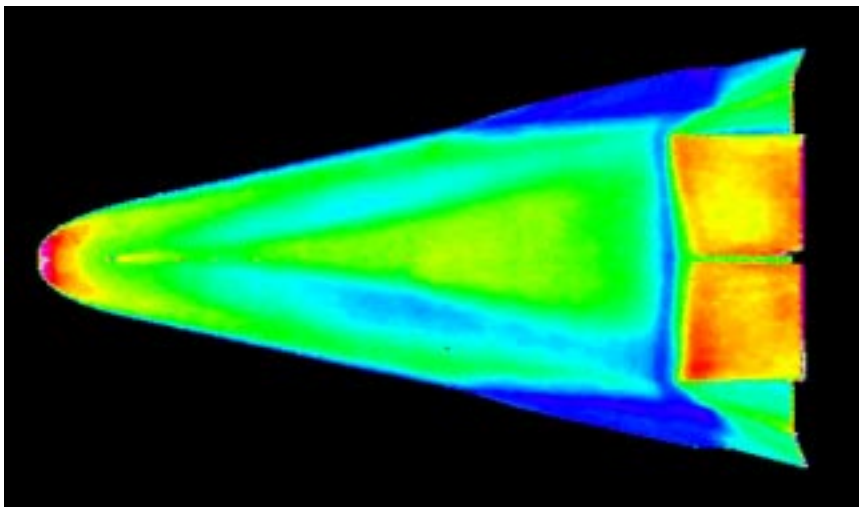

Run # 81
Windward View
Model # 2
BF @ 20°
$\alpha = 40°$
$Re_\infty/ft = 3.8x10^6$
0.0050-in. Trip
@ x/L = 0.1

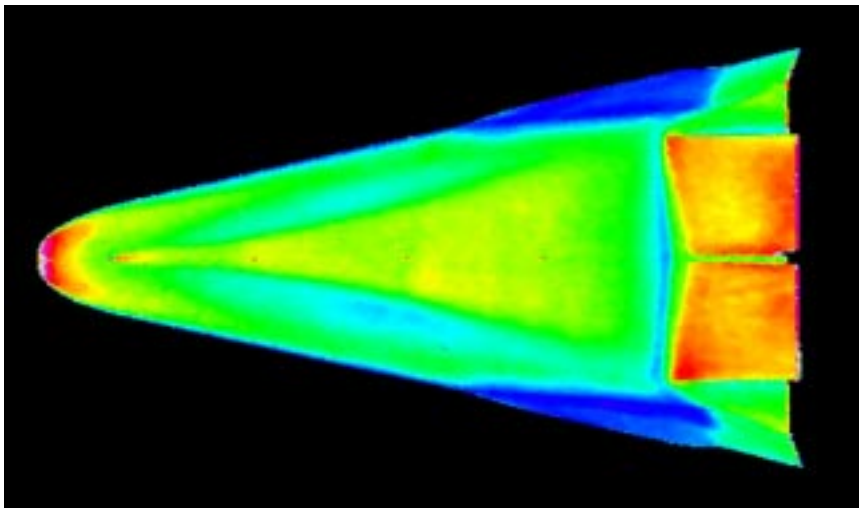

Run # 82
Windward View
Model # 2
BF @ 20°
$\alpha = 40°$
$Re_\infty/ft = 4.4x10^6$
0.0050-in. Trip
@ x/L = 0.1

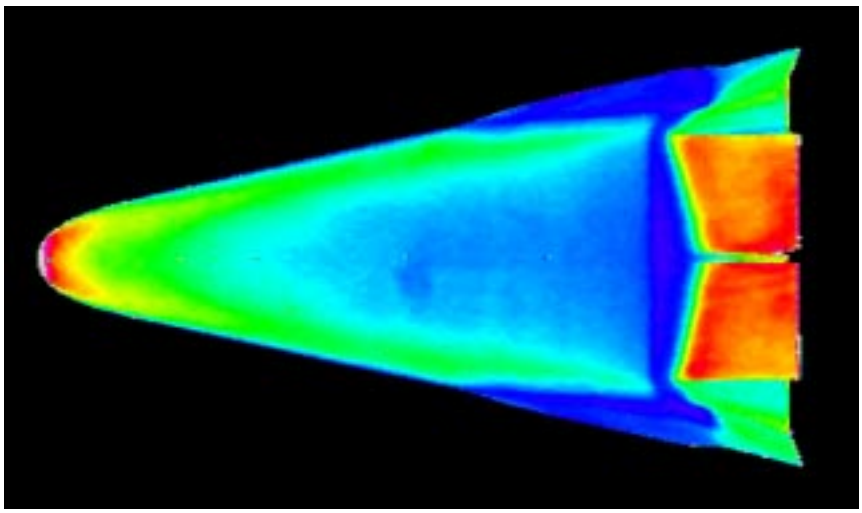

Run # 83
Windward View
Model # 2
BF @ 20°
$\alpha = 40°$
$Re_\infty/ft = 4.4x10^6$
0.0025-in. Trip
@ x/L = 0.02

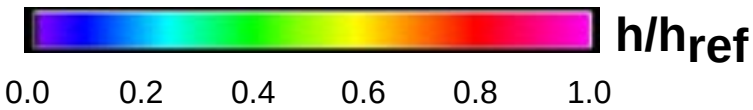

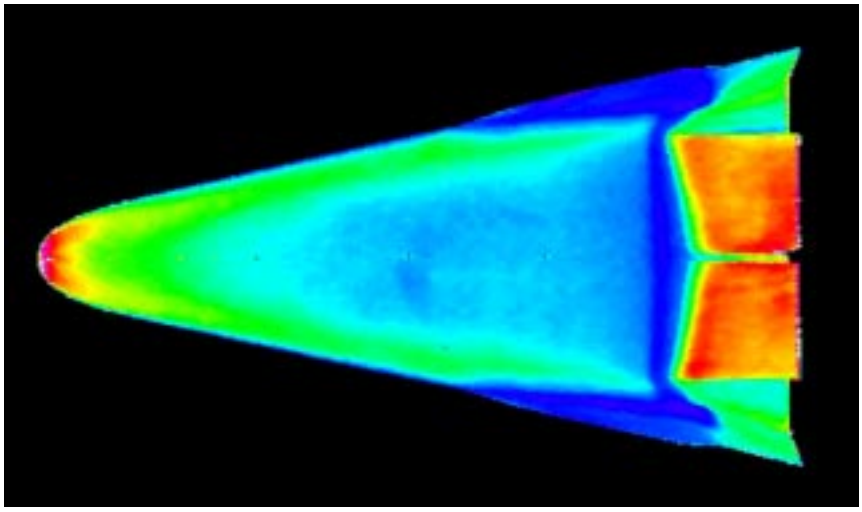

Run # 84
Windward View
Model # 2
BF @ 20°
$\alpha = 40°$
$Re_\infty/ft = 4.4x10^6$
0.0050-in. Trip
@ x/L = 0.02

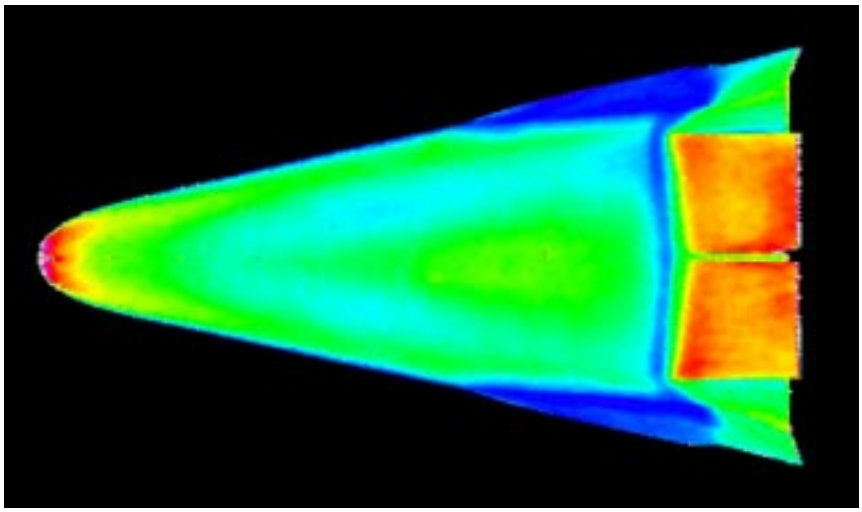

Run # 86
Windward View
Model # 2
BF @ 20°
$\alpha = 40°$
$Re_\infty/ft = 4.4x10^6$
0.0075-in. Trip
@ x/L = 0.02

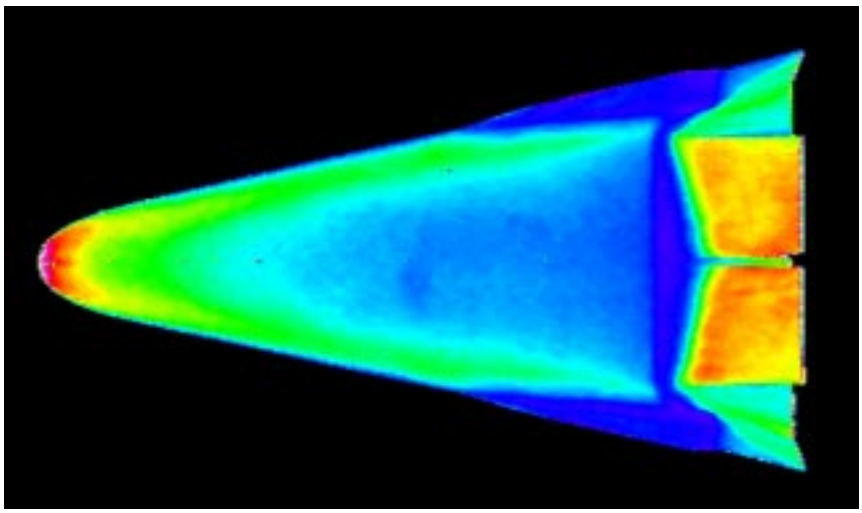

Run # 87
Windward View
Model # 2
BF @ 20°
$\alpha = 40°$
$Re_\infty/ft = 3.3x10^6$
0.0075-in. Trip
@ x/L = 0.02

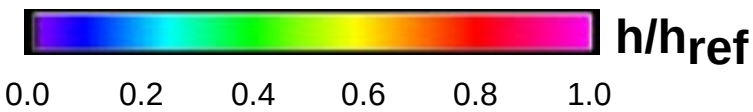

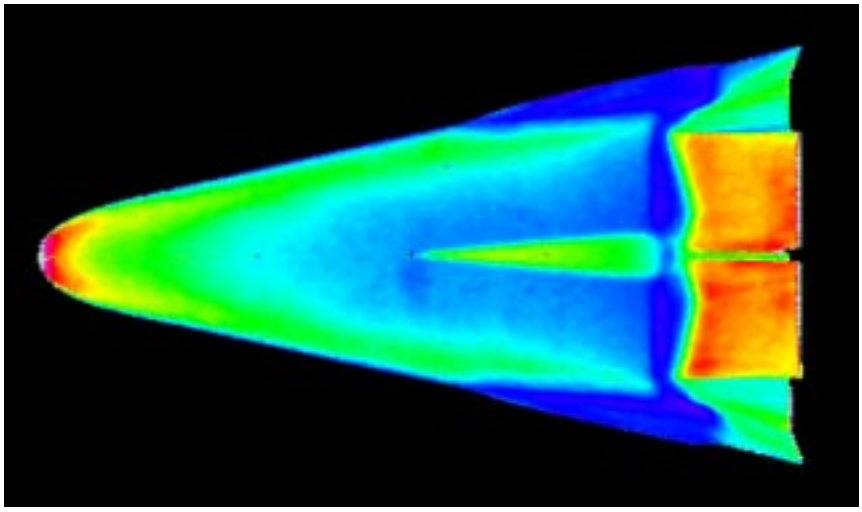

Run # 88
Windward View
Model # 2
BF @ 20°
$\alpha = 40°$
$Re_\infty/ft = 3.8x10^6$
0.0050-in. Trip
@ x/L = 0.5

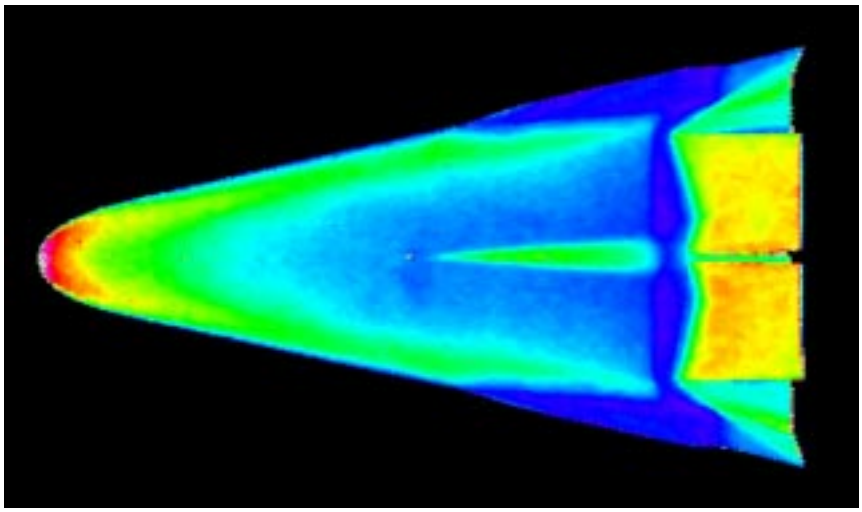

Run # 89
Windward View
Model # 2
BF @ 20°
$\alpha = 40°$
$Re_\infty/ft = 2.4x10^6$
0.0050-in. Trip
@ x/L = 0.5

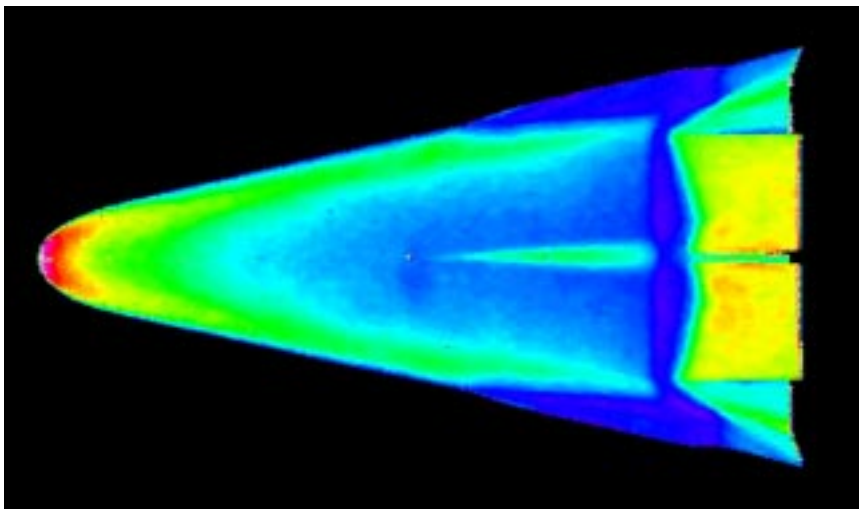

Run # 90
Windward View
Model # 2
BF @ 20°
$\alpha = 40°$
$Re_\infty/ft = 2.2x10^6$
0.0050-in. Trip
@ x/L = 0.5

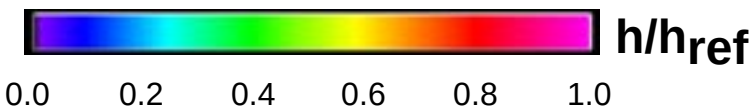

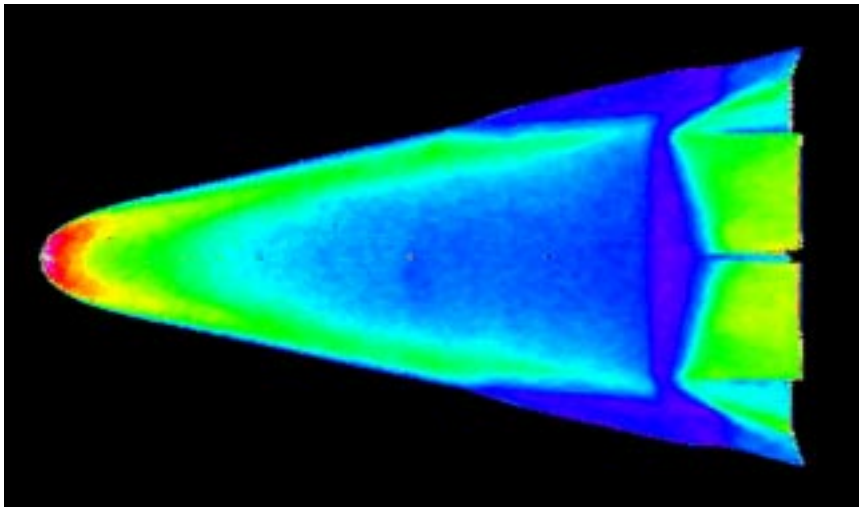

Run # 91
Windward View
Model # 2
BF @ 20°
$\alpha = 40°$
$Re_\infty/ft = 1.6x10^6$
0.0050-in. Trip
@ x/L = 0.5

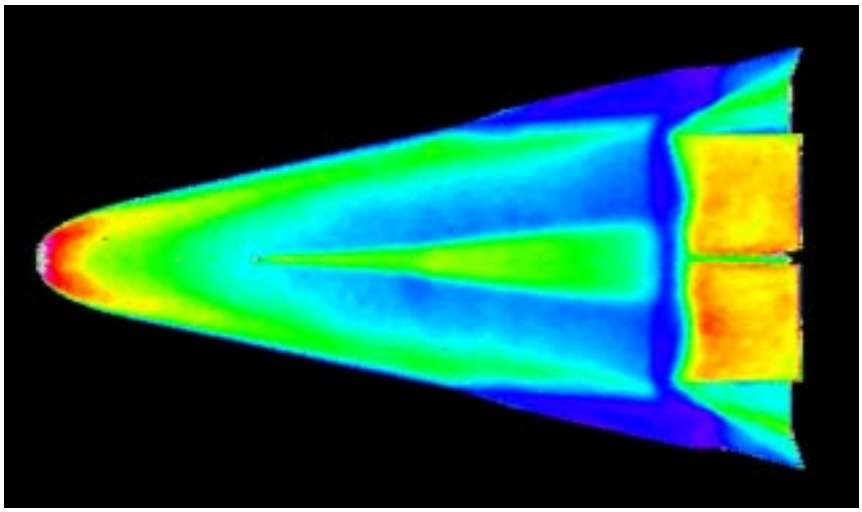

Run # 92
Windward View
Model # 2
BF @ 20°
$\alpha = 40°$
$Re_\infty/ft = 2.4x10^6$
0.0075-in. Trip
@ x/L = 0.3

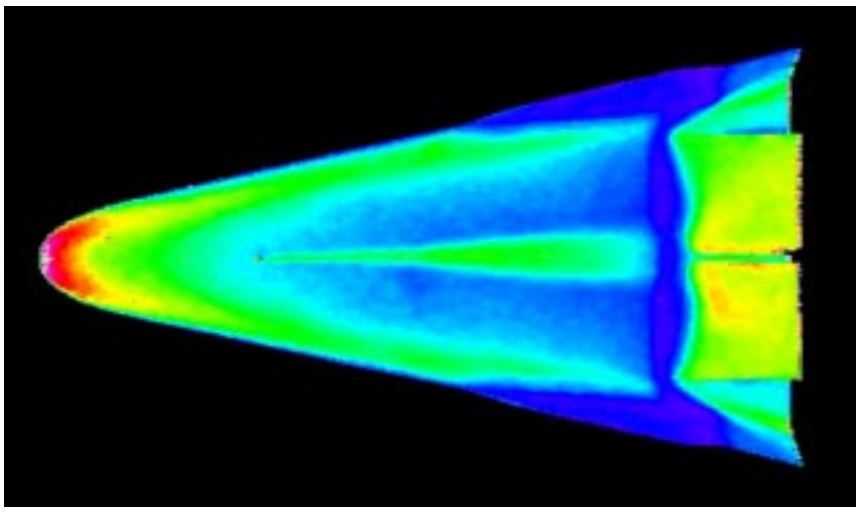

Run # 93
Windward View
Model # 2
BF @ 20°
$\alpha = 40°$
$Re_\infty/ft = 1.9x10^6$
0.0075-in. Trip
@ x/L = 0.3

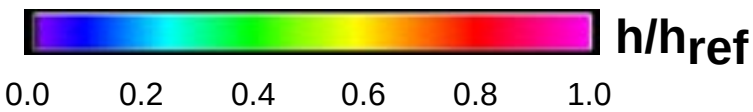

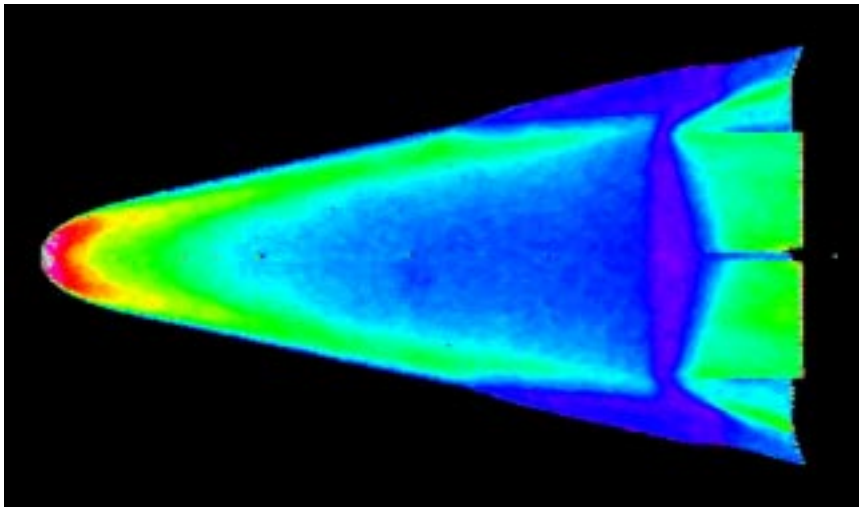

Run # 94
Windward View
Model # 2
BF @ 20°
$\alpha = 40°$
$Re_\infty/ft = 1.1x10^6$
0.0075-in. Trip
@ x/L = 0.3

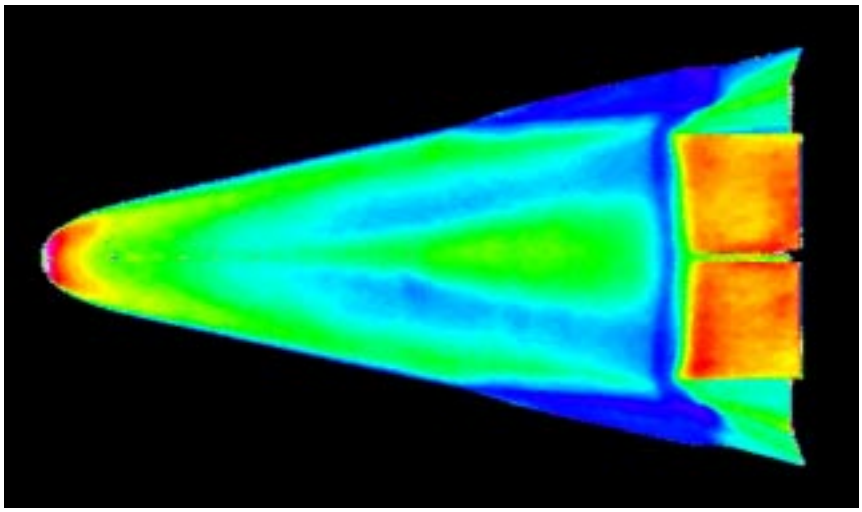

Run # 95
Windward View
Model # 2
BF @ 20°
$\alpha = 40°$
$Re_\infty/ft = 3.8x10^6$
0.0025-in. Trip
@ x/L = 0.1

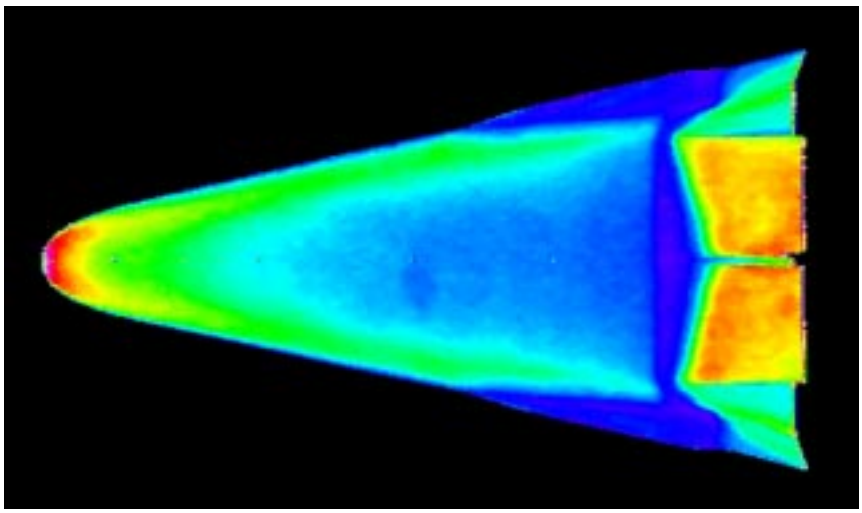

Run # 96
Windward View
Model # 2
BF @ 20°
$\alpha = 40°$
$Re_\infty/ft = 3.3x10^6$
0.0025-in. Trip
@ x/L = 0.1

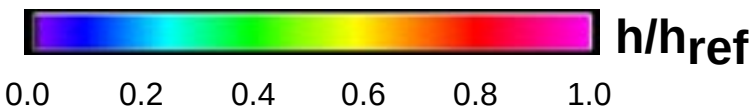

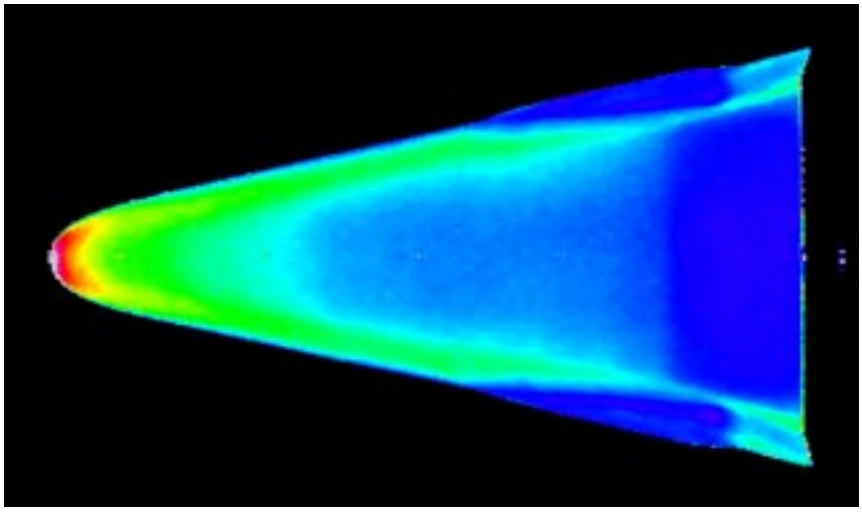

Run # 97
Windward View
Model # 1
BF @ 0°
$\alpha = 40°$
$Re_\infty/ft = 4.4x10^6$
Baseline Repeat

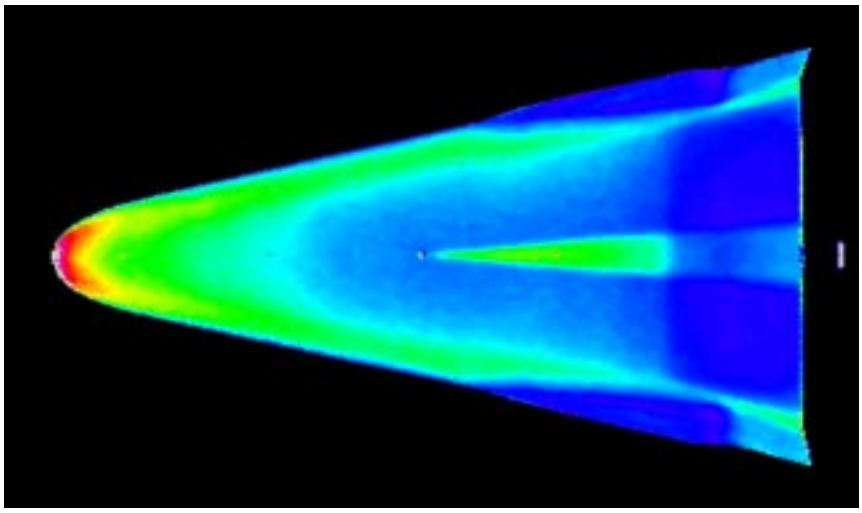

Run # 98
Windward View
Model # 1
BF @ 0°
$\alpha = 40°$
$Re_\infty/ft = 3.8x10^6$
0.0050-in. Trip
@ x/L = 0.5

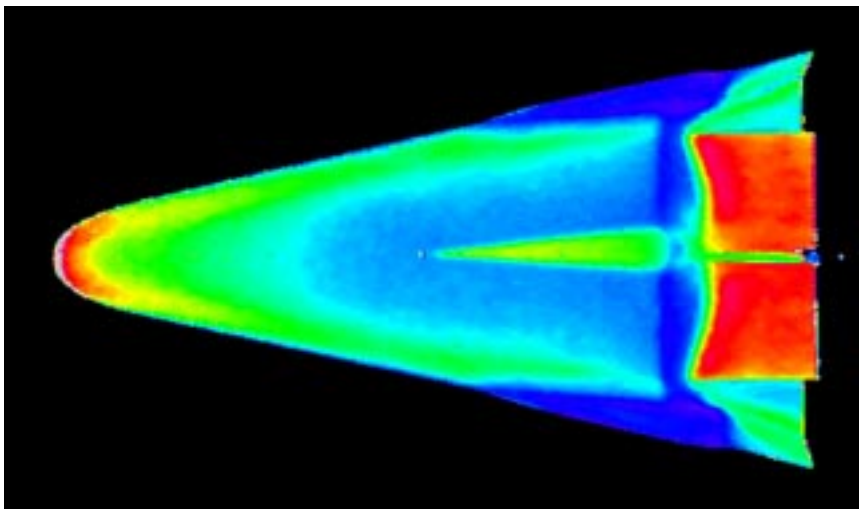

Run # 102
Windward View
Model # 3
BF @ 25°
$\alpha = 40°$
$Re_\infty/ft = 3.8x10^6$
0.0050-in. Trip
@ x/L = 0.5

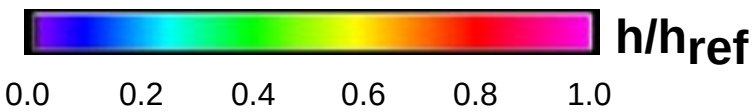

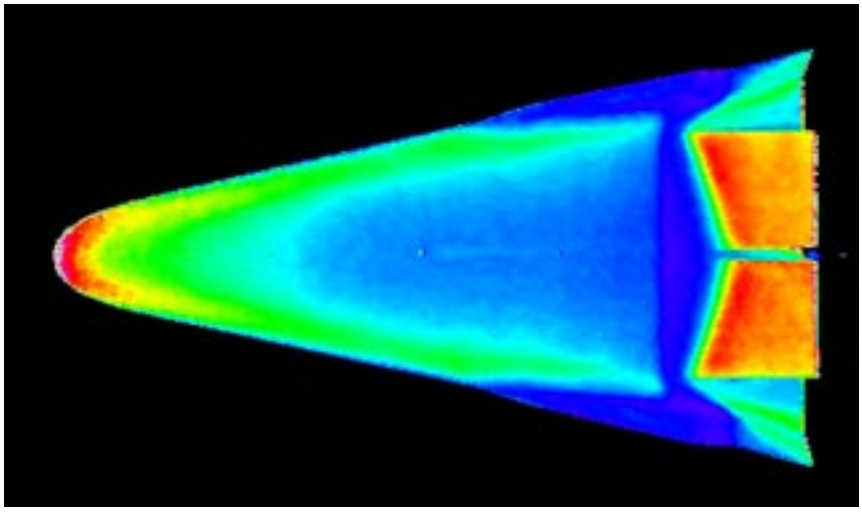

Run # 103
Windward View
Model # 3
BF @ 25°
$\alpha = 40°$
$Re_\infty/ft = 2.5x10^6$
0.0050-in. Trip
@ x/L = 0.5

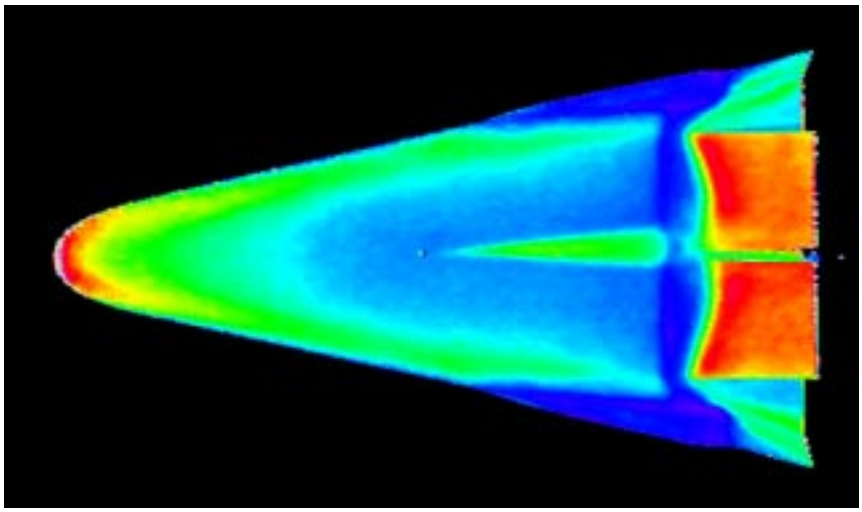

Run # 104
Windward View
Model # 3
BF @ 25°
$\alpha = 40°$
$Re_\infty/ft = 3.3x10^6$
0.0050-in. Trip
@ x/L = 0.5

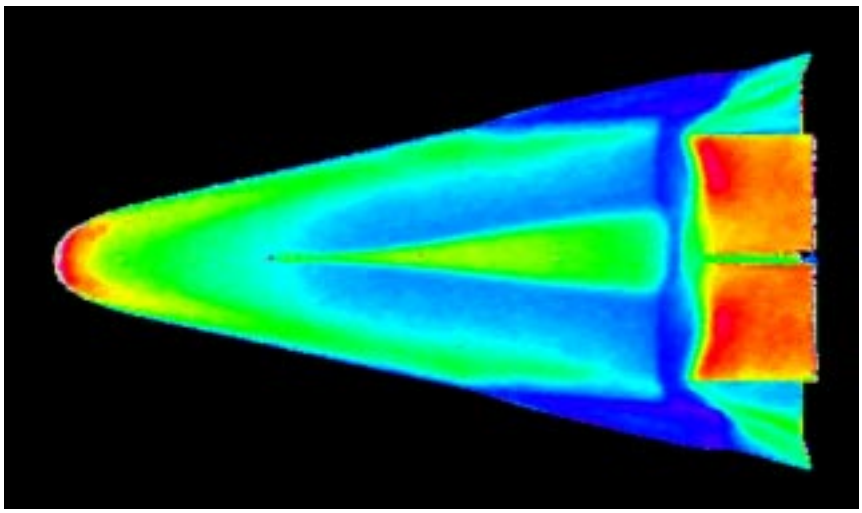

Run # 105
Windward View
Model # 3
BF @ 25°
$\alpha = 40°$
$Re_\infty/ft = 3.3x10^6$
0.0050-in. Trip
@ x/L = 0.3

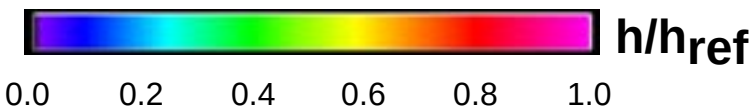

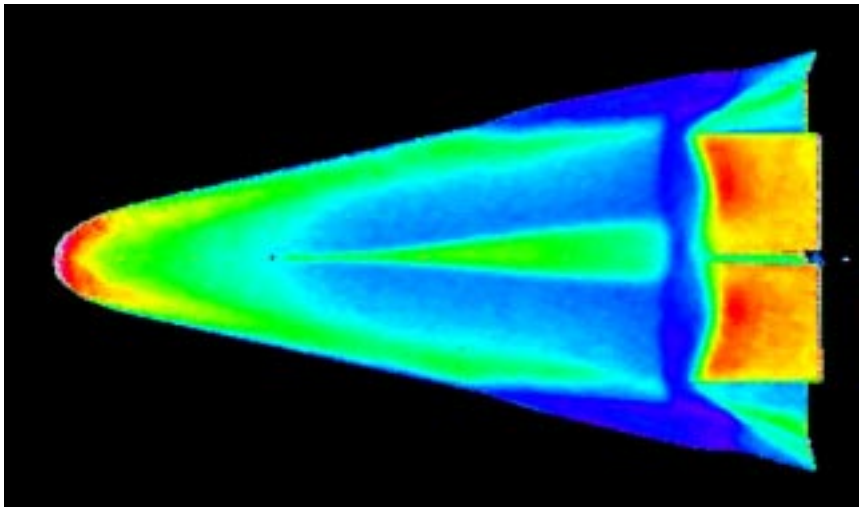

Run # 106
Windward View
Model # 3
BF @ 25°
$\alpha = 40°$
$Re_\infty/ft = 2.2x10^6$
0.0050-in. Trip
@ x/L = 0.3

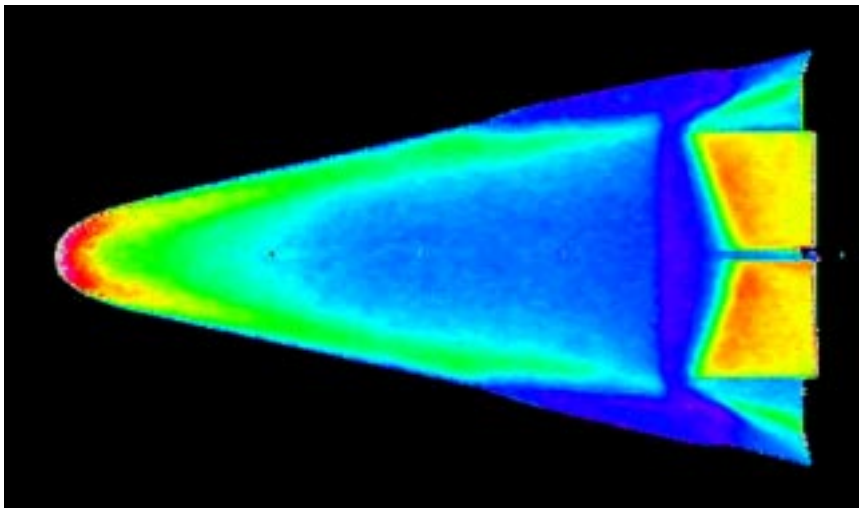

Run # 107
Windward View
Model # 3
BF @ 25°
$\alpha = 40°$
$Re_\infty/ft = 1.6x10^6$
0.0050-in. Trip
@ x/L = 0.3

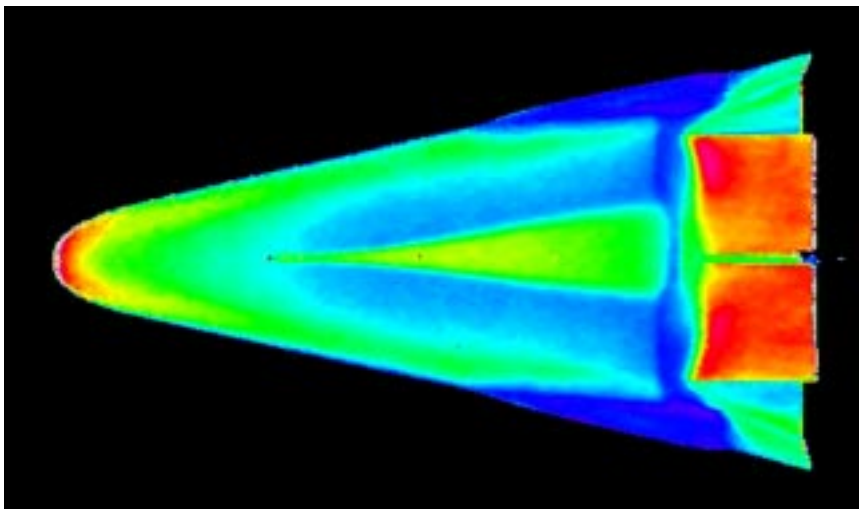

Run # 108
Windward View
Model # 3
BF @ 25°
$\alpha = 40°$
$Re_\infty/ft = 3.8x10^6$
0.0050-in. Trip
@ x/L = 0.3

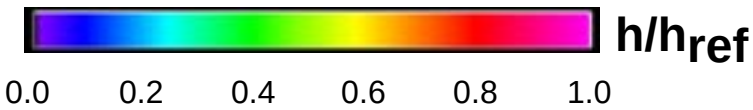

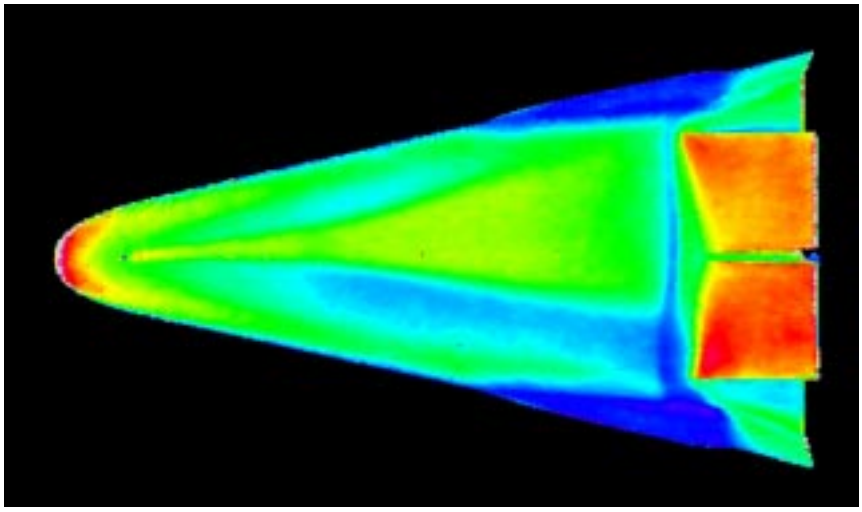

Run # 109
Windward View
Model # 3
BF @ 25°
$\alpha = 40°$
$Re_\infty/ft = 3.8x10^6$
0.0050-in. Trip
@ x/L = 0.1

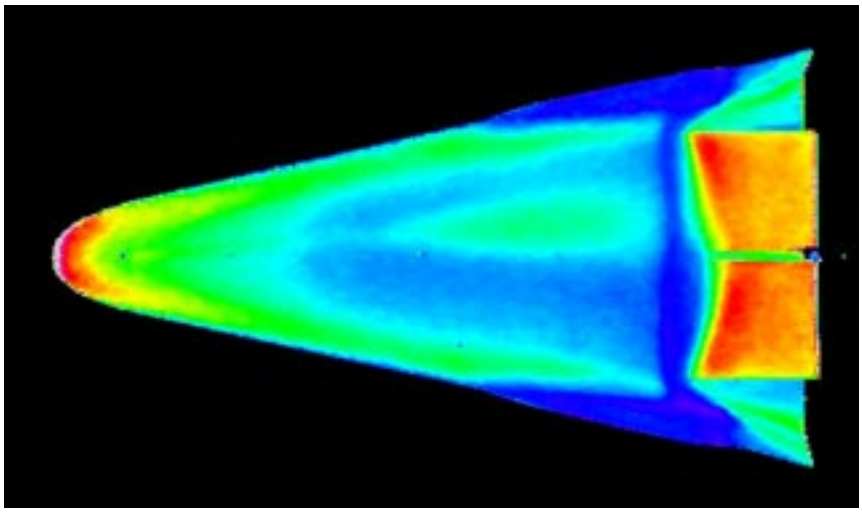

Run # 110
Windward View
Model # 3
BF @ 25°
$\alpha = 40°$
$Re_\infty/ft = 2.5x10^6$
0.0050-in. Trip
@ x/L = 0.1

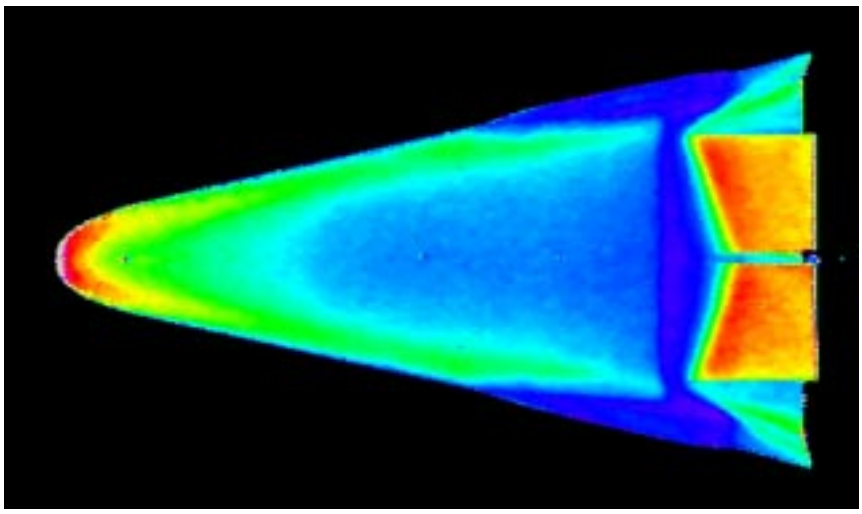

Run # 111
Windward View
Model # 3
BF @ 25°
$\alpha = 40°$
$Re_\infty/ft = 2.2x10^6$
0.0050-in. Trip
@ x/L = 0.1

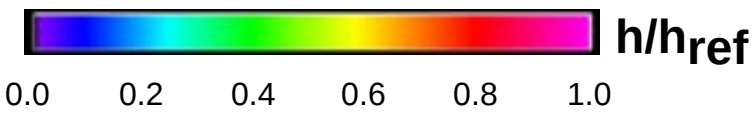

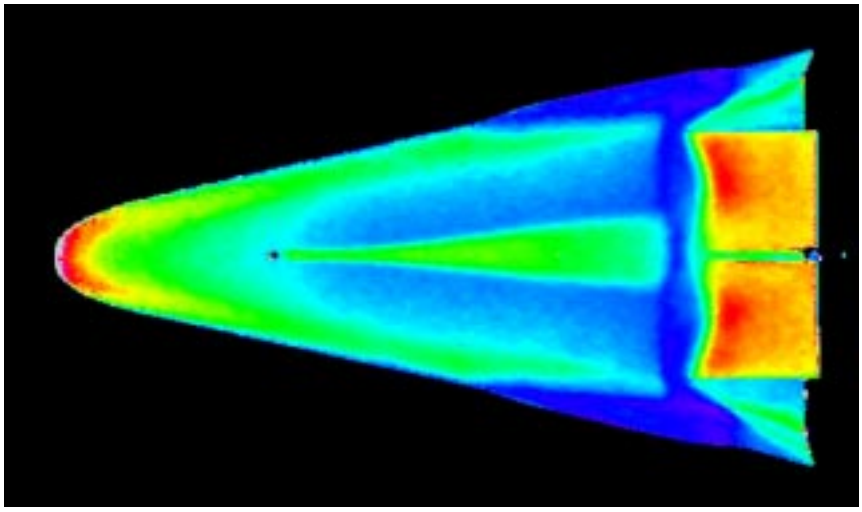

Run # 112
Windward View
Model # 3
BF @ 25°
$\alpha = 40°$
$Re_\infty/ft = 2.2x10^6$
0.0050-in. Trip
@ x/L = 0.3
Width = 0.1-in.

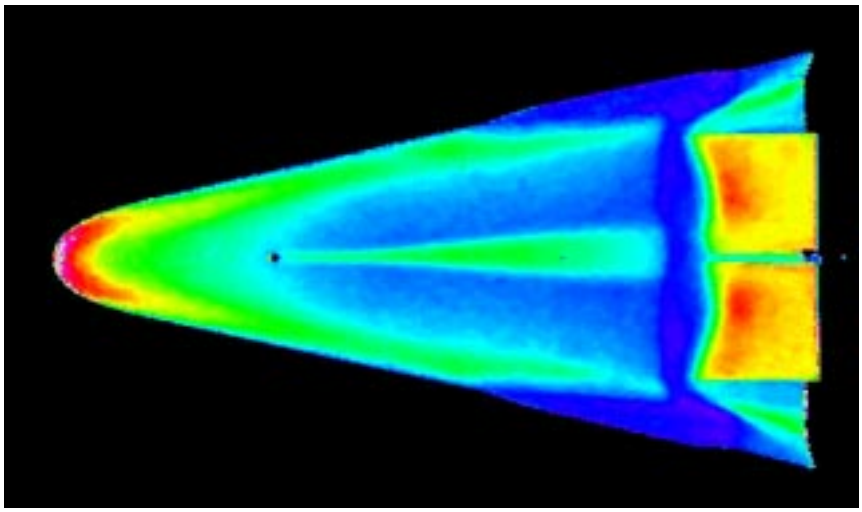

Run # 113
Windward View
Model # 3
BF @ 25°
$\alpha = 40°$
$Re_\infty/ft = 1.6x10^6$
0.0050-in. Trip
@ x/L = 0.3
Width = 0.1-in.

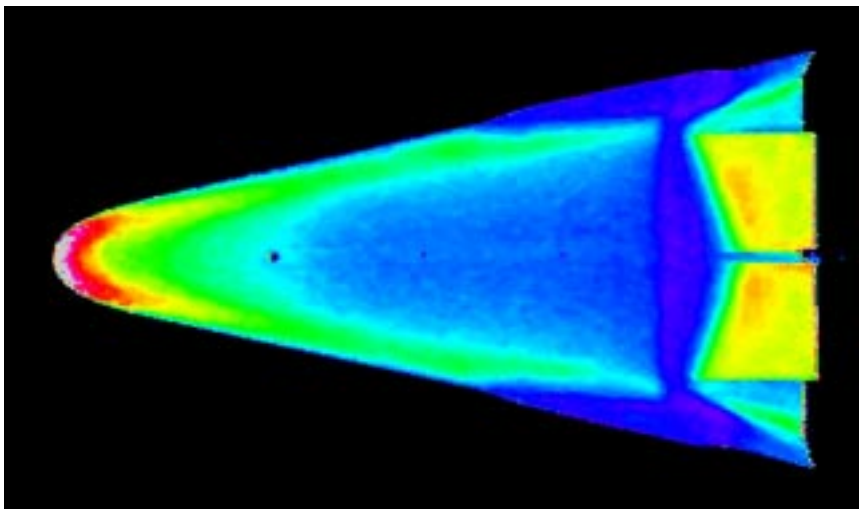

Run # 114
Windward View
Model # 3
BF @ 25°
$\alpha = 40°$
$Re_\infty/ft = 1.1x10^6$
0.0050-in. Trip
@ x/L = 0.3
Width = 0.1-in.

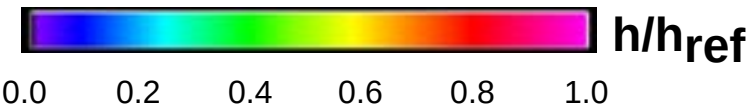

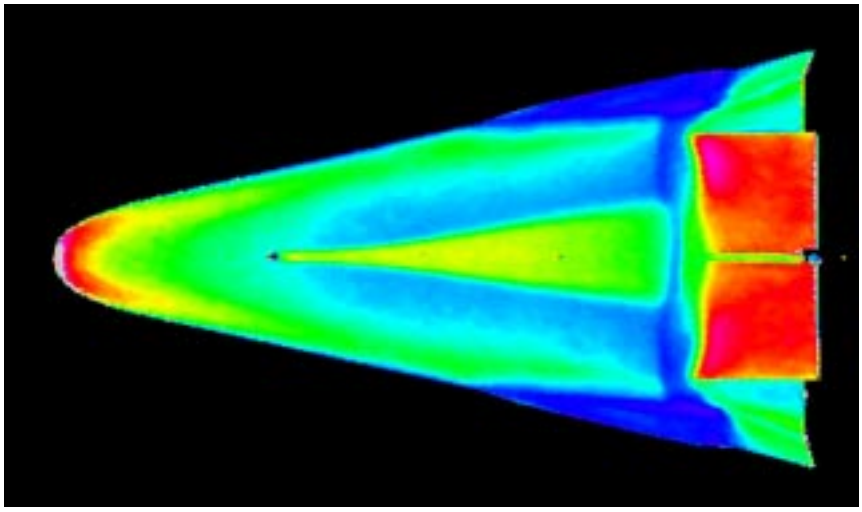

Run # 115
Windward View
Model # 3
BF @ 25°
$\alpha = 40°$
$Re_\infty/ft = 3.8x10^6$
0.0050-in. Trip
@ x/L = 0.3
Width = 0.1-in.

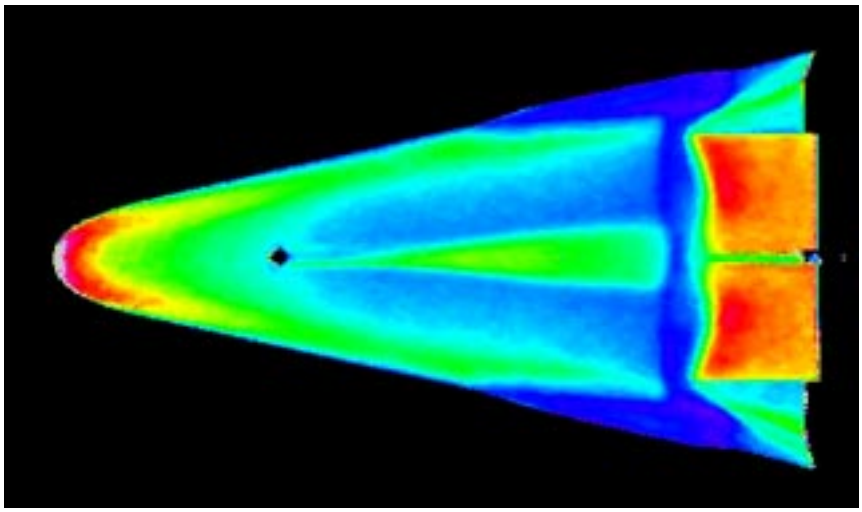

Run # 116
Windward View
Model # 3
BF @ 25°
$\alpha = 40°$
$Re_\infty/ft = 2.2x10^6$
0.0050-in. Trip
@ x/L = 0.3
Width = 0.2-in.

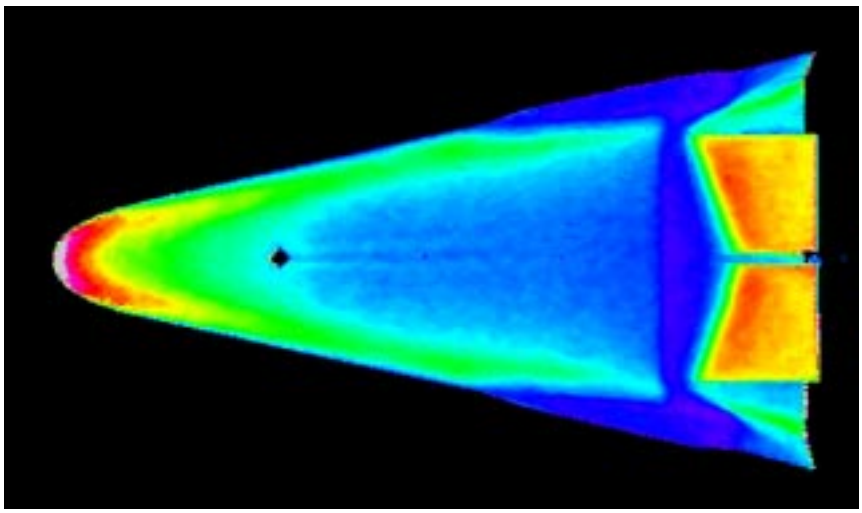

Run # 117
Windward View
Model # 3
BF @ 25°
$\alpha = 40°$
$Re_\infty/ft = 1.6x10^6$
0.0050-in. Trip
@ x/L = 0.3
Width = 0.2-in.

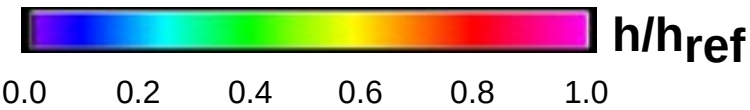

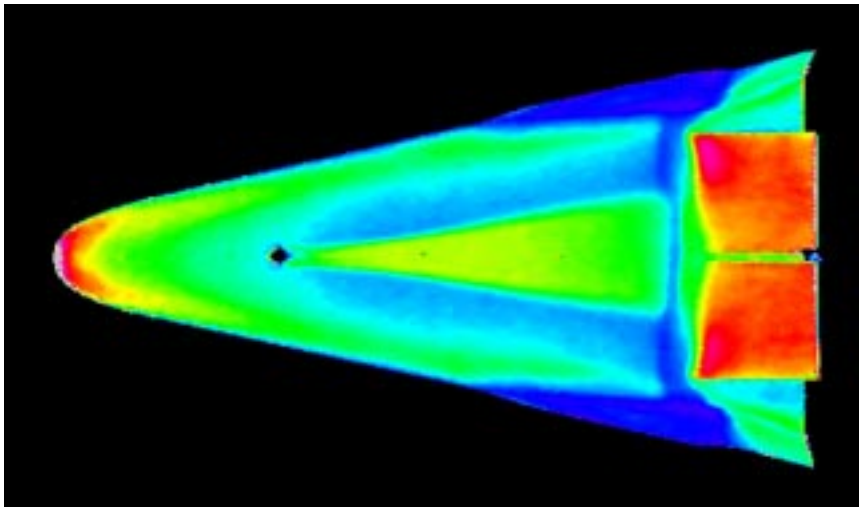

Run # 118
Windward View
Model # 3
BF @ 25°
$\alpha = 40°$
$Re_\infty/ft = 3.8x10^6$
0.0050-in. Trip
@ x/L = 0.3
Width = 0.2-in.

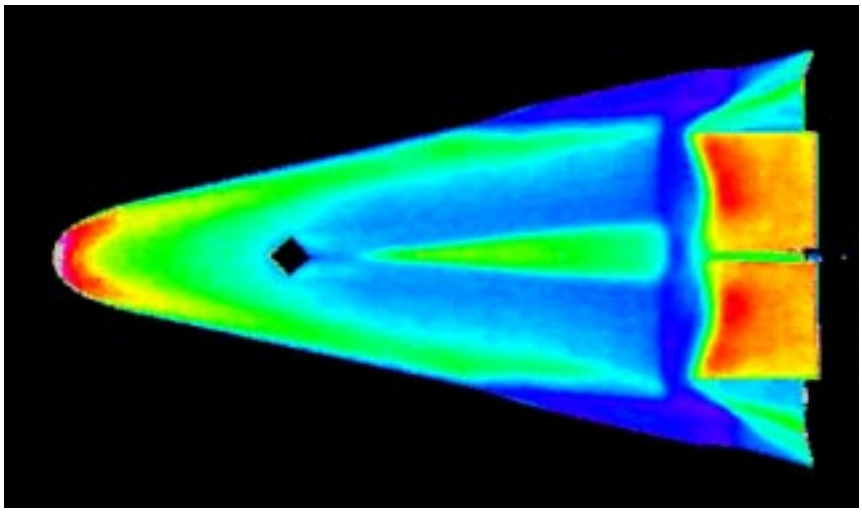

Run # 119
Windward View
Model # 3
BF @ 25°
$\alpha = 40°$
$Re_\infty/ft = 2.2x10^6$
0.0050-in. Trip
@ x/L = 0.3
Width = 0.4-in.

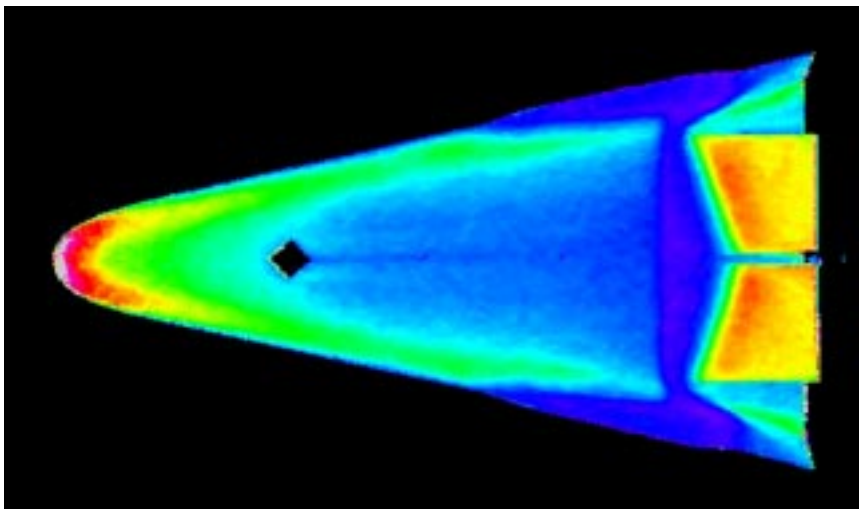

Run # 120
Windward View
Model # 3
BF @ 25°
$\alpha = 40°$
$Re_\infty/ft = 1.6x10^6$
0.0050-in. Trip
@ x/L = 0.3
Width = 0.4-in.

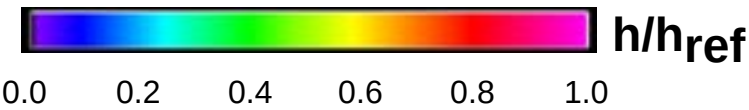

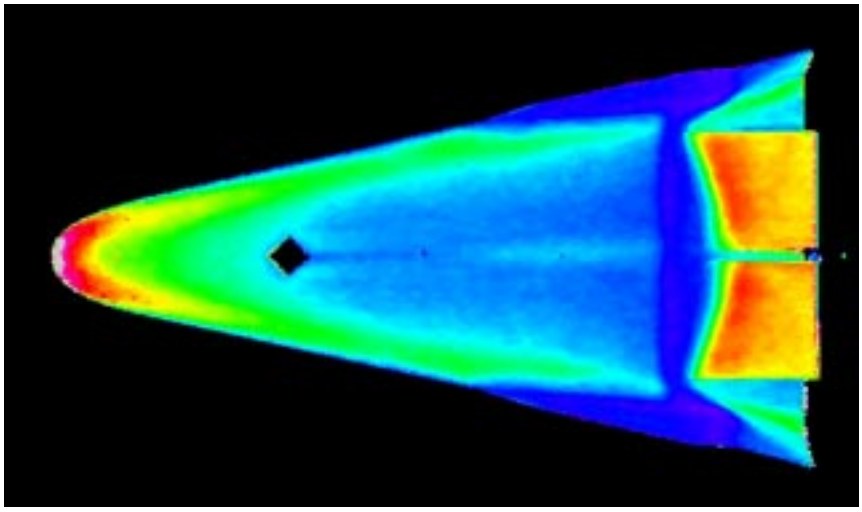

Run # 121
Windward View
Model # 3
BF @ 25°
$\alpha = 40°$
$Re_\infty/ft = 1.9x10^6$
0.0050-in. Trip
@ x/L = 0.3
Width = 0.4-in.

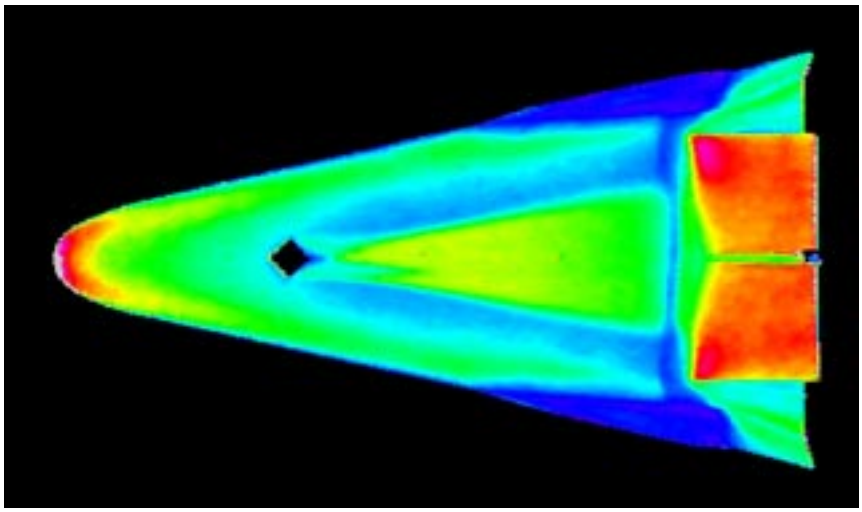

Run # 122
Windward View
Model # 3
BF @ 25°
$\alpha = 40°$
$Re_\infty/ft = 3.8x10^6$
0.0050-in. Trip
@ x/L = 0.3
Width = 0.4-in.

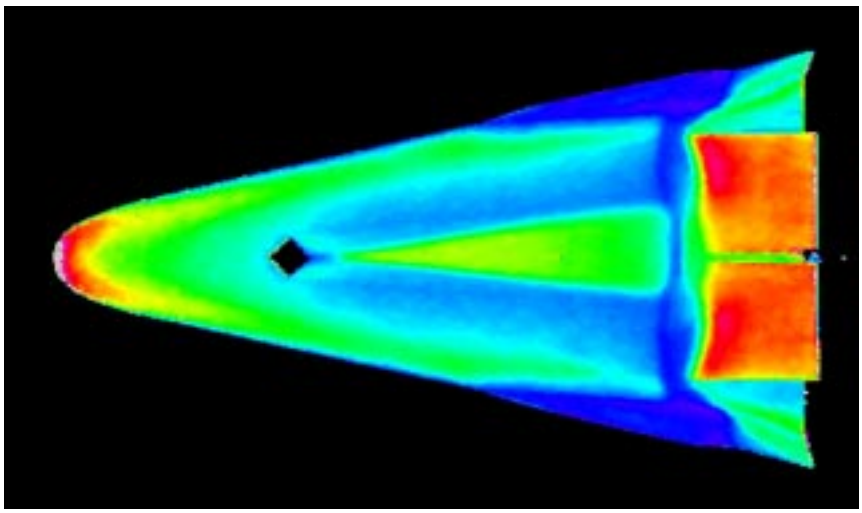

Run # 123
Windward View
Model # 3
BF @ 25°
$\alpha = 40°$
$Re_\infty/ft = 3.3x10^6$
0.0050-in. Trip
@ x/L = 0.3
Width = 0.4-in.

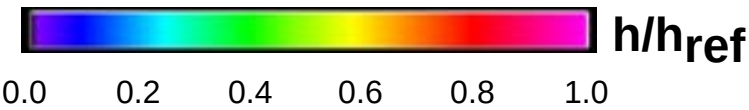

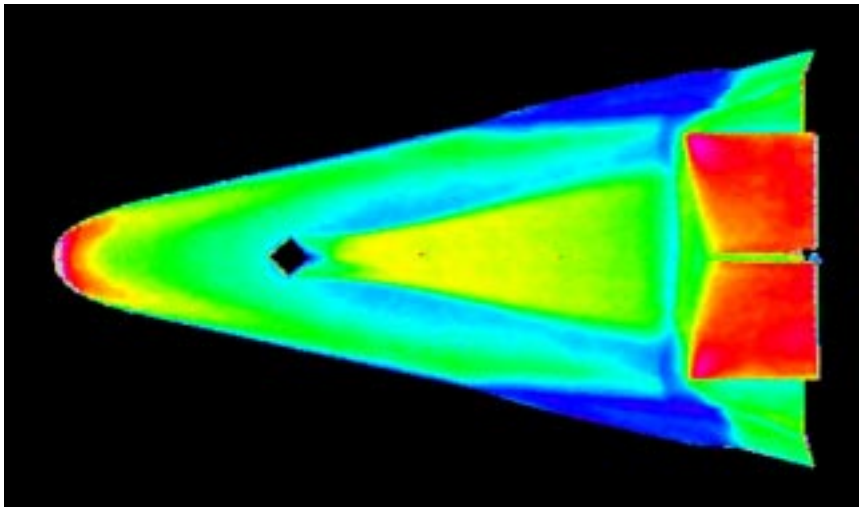

Run # 124
Windward View
Model # 3
BF @ 25°
$\alpha = 40°$
$Re_\infty/ft = 4.4x10^6$
0.0050-in. Trip
@ x/L = 0.3
Width = 0.4-in.

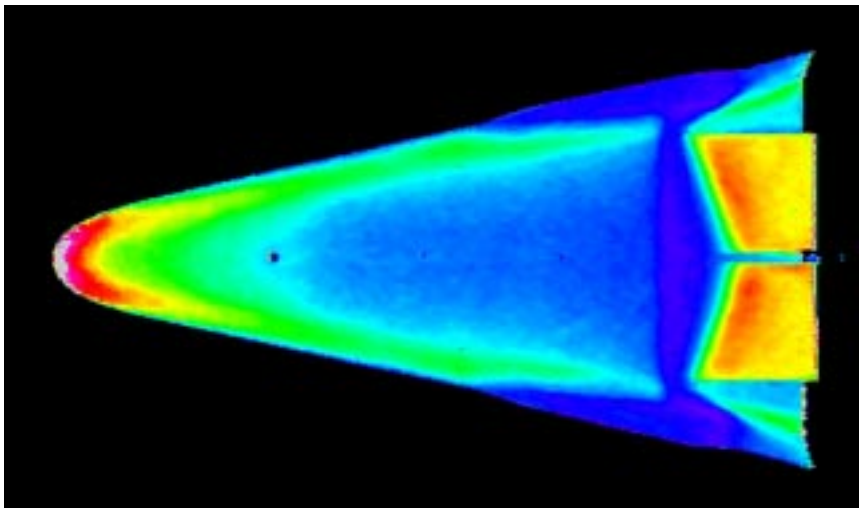

Run # 125
Windward View
Model # 3
BF @ 25°
$\alpha = 40°$
$Re_\infty/ft = 1.6x10^6$
0.0050-in. Trip
@ x/L = 0.3
Width = 0.1-in.
Repeat

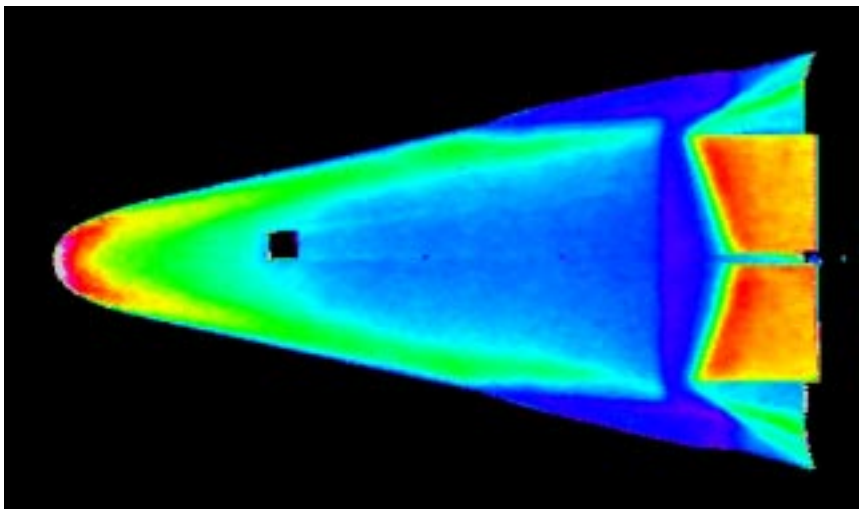

Run # 126
Windward View
Model # 3
BF @ 25°
$\alpha = 40°$
$Re_\infty/ft = 2.2x10^6$
0.0050-in. Trip
@ x/L = 0.3
Width = 0.4-in.
Orientation = 0°

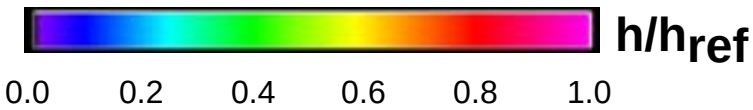

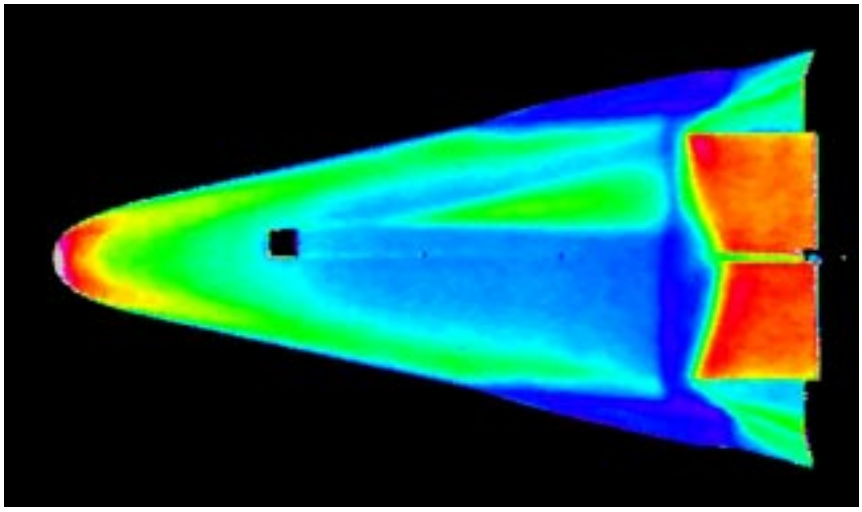

Run # 127
Windward View
Model # 3
BF @ 25°
$\alpha = 40°$
$Re_\infty/ft = 3.3x10^6$
0.0050-in. Trip
@ x/L = 0.3
Width = 0.4-in.
Orientation = 0°

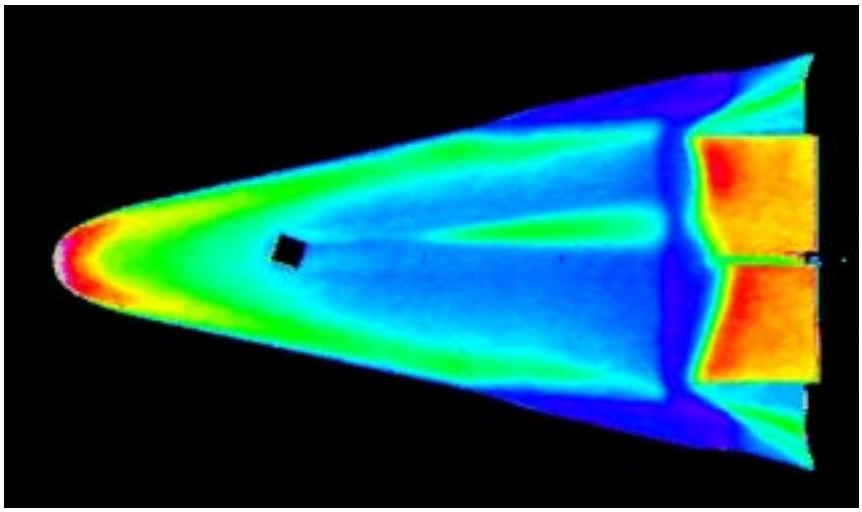

Run # 128
Windward View
Model # 3
BF @ 25°
$\alpha = 40°$
$Re_\infty/ft = 2.2x10^6$
0.0050-in. Trip
@ x/L = 0.3
Width = 0.4-in.
Orientation = 15°

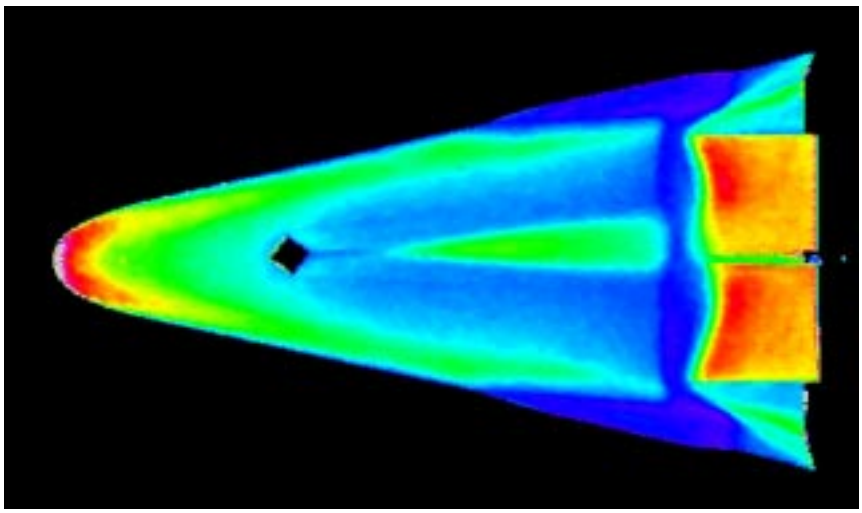

Run # 129
Windward View
Model # 3
BF @ 25°
$\alpha = 40°$
$Re_\infty/ft = 2.2x10^6$
0.0050-in. Trip
@ x/L = 0.3
Width = 0.4-in.
Orientation = 30°

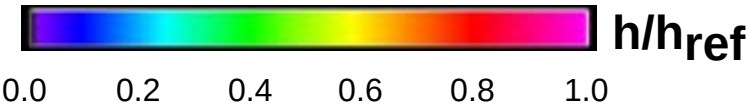

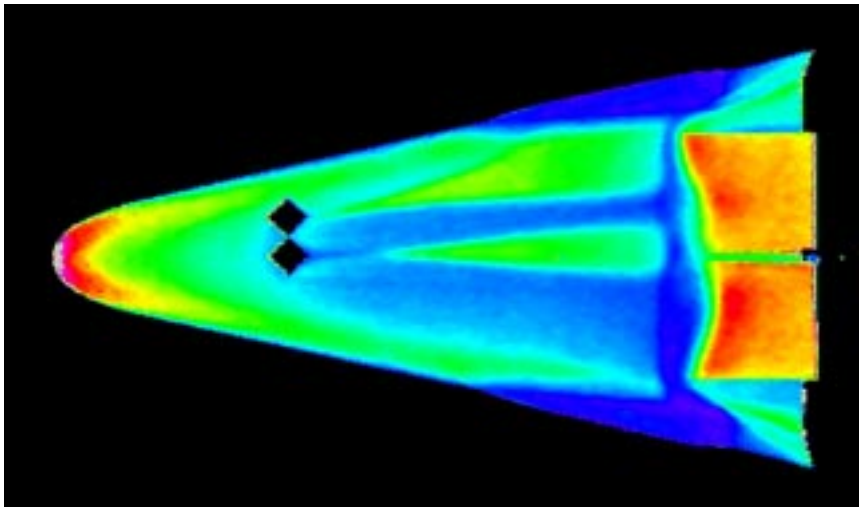

Run # 130
Windward View
Model # 3
BF @ 25°
$\alpha = 40°$
$Re_\infty/ft = 2.2x10^6$
0.0050-in. Trip
@ x/L = 0.3
Width = 0.4-in.
Orientation = 45°

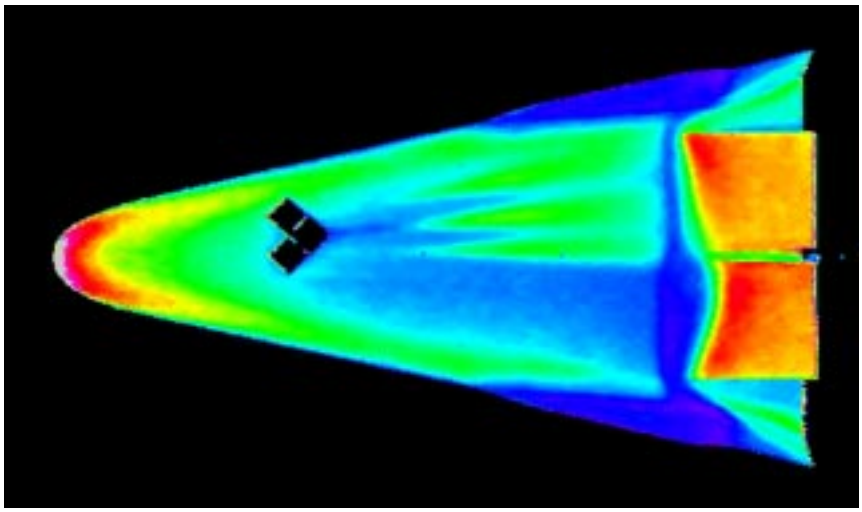

Run # 131
Windward View
Model # 3
BF @ 25°
$\alpha = 40°$
$Re_\infty/ft = 2.2x10^6$
0.0050-in. Trip
@ x/L = 0.3
Width = 0.4-in.
Orientation = 45°

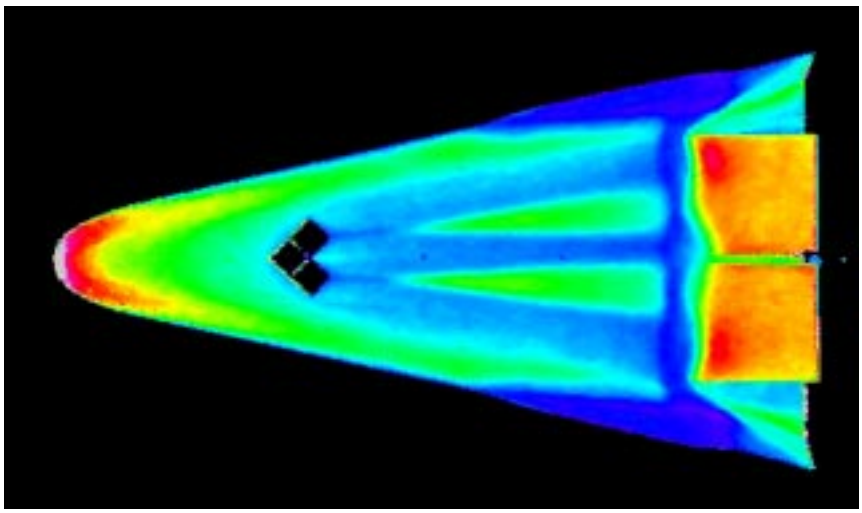

Run # 132
Windward View
Model # 3
BF @ 25°
$\alpha = 40°$
$Re_\infty/ft = 2.2x10^6$
0.0050-in. Trip
@ x/L = 0.3
Width = 0.4-in.
Orientation = 45°

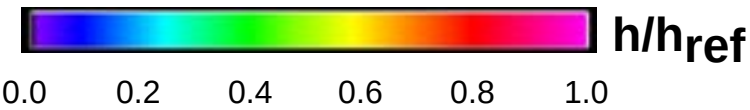

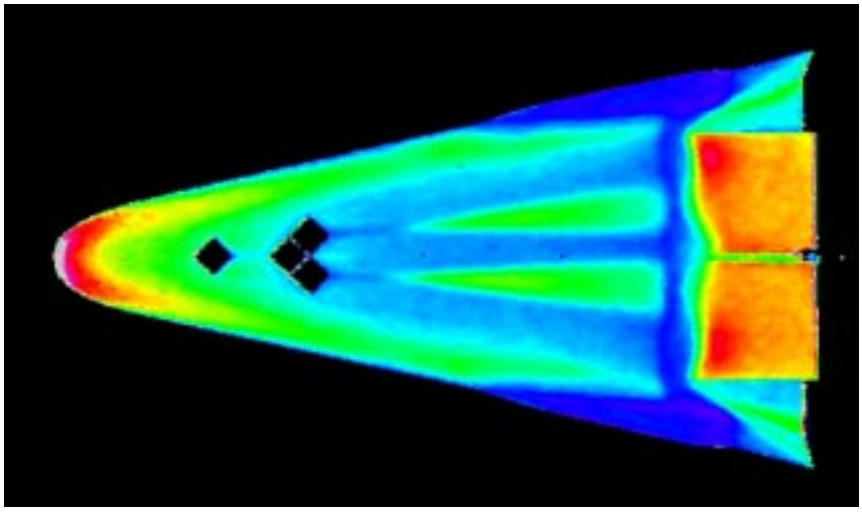

Run # 133
Windward View
Model # 3
BF @ 25°
$\alpha = 40°$
$Re_\infty/ft = 2.2x10^6$
0.0050-in. Trip
@ x/L = 0.3
Width = 0.4-in.
Orientation = 45°

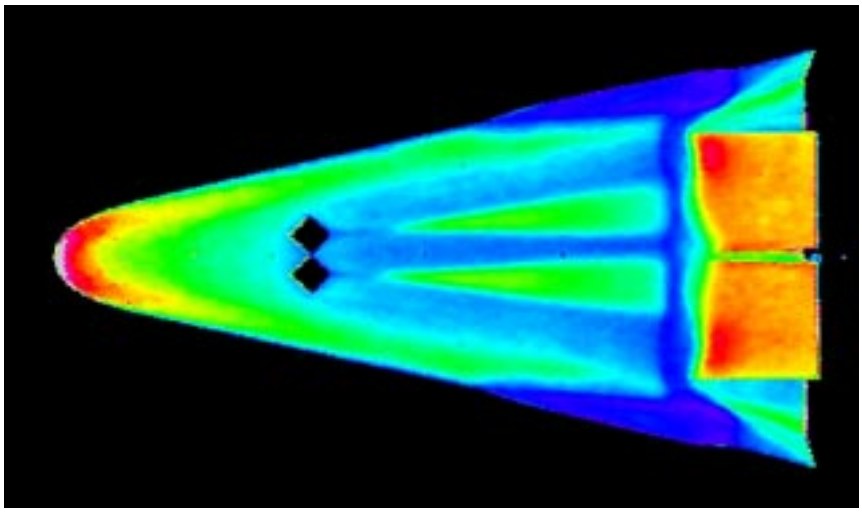

Run # 134
Windward View
Model # 3
BF @ 25°
$\alpha = 40°$
$Re_\infty/ft = 2.2x10^6$
0.0050-in. Trip
@ x/L = 0.3
Width = 0.4-in.
Orientation = 45°

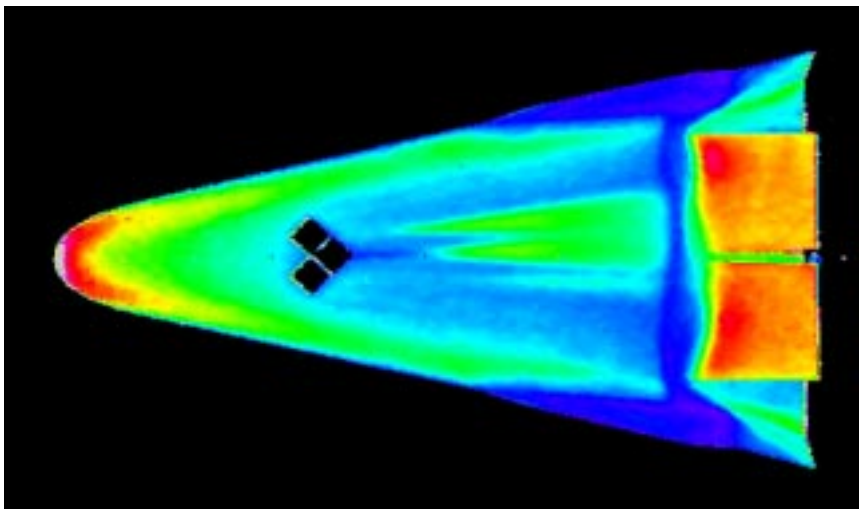

Run # 135
Windward View
Model # 3
BF @ 25°
$\alpha = 40°$
$Re_\infty/ft = 2.2x10^6$
0.0050-in. Trip
@ x/L = 0.3
Width = 0.4-in.
Orientation = 45°

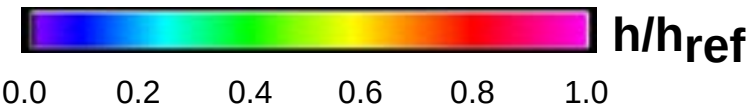

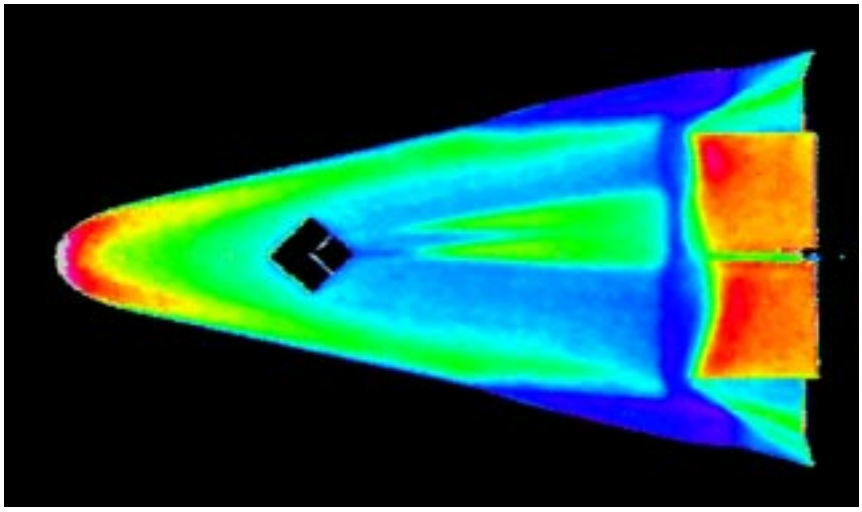

Run # 136
Windward View
Model # 3
BF @ 25°
$\alpha = 40°$
$Re_\infty/ft = 2.2x10^6$
0.0050-in. Trip
@ x/L = 0.3
Width = 0.4-in.
Orientation = 45°

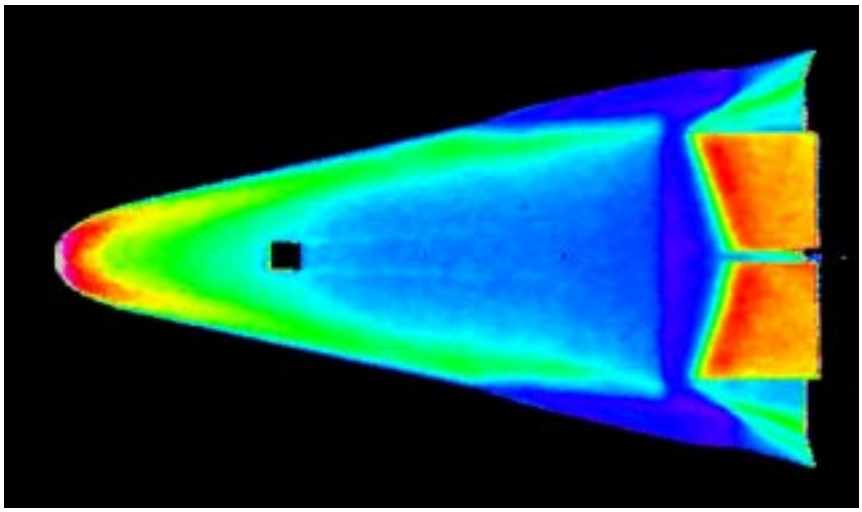

Run # 137
Windward View
Model # 3
BF @ 25°
$\alpha = 40°$
$Re_\infty/ft = 2.2x10^6$
0.0050-in. Trip
@ x/L = 0.3
Width = 0.4-in.
Orientation = 0°

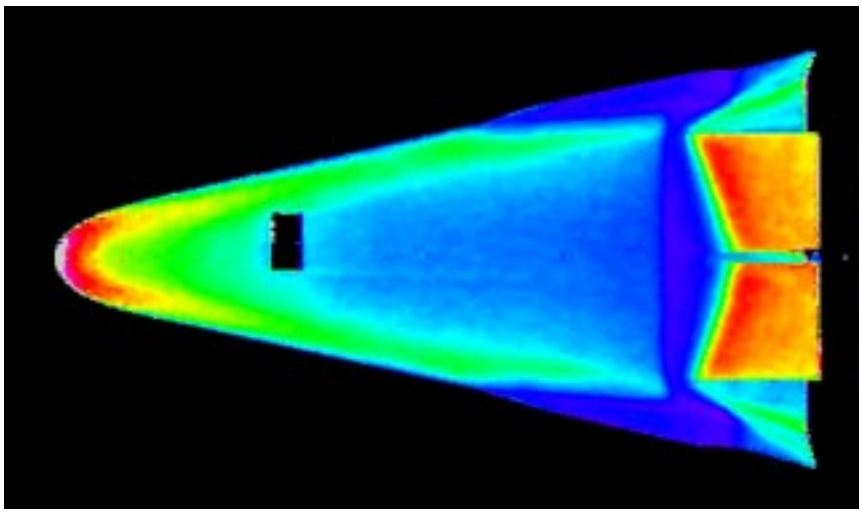

Run # 138
Windward View
Model # 3
BF @ 25°
$\alpha = 40°$
$Re_\infty/ft = 2.2x10^6$
0.0050-in. Trip
@ x/L = 0.3
Width = 0.4-in.
Orientation = 0°

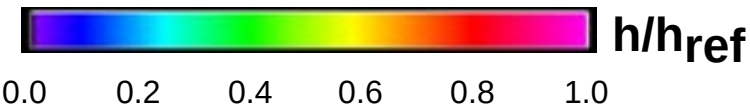

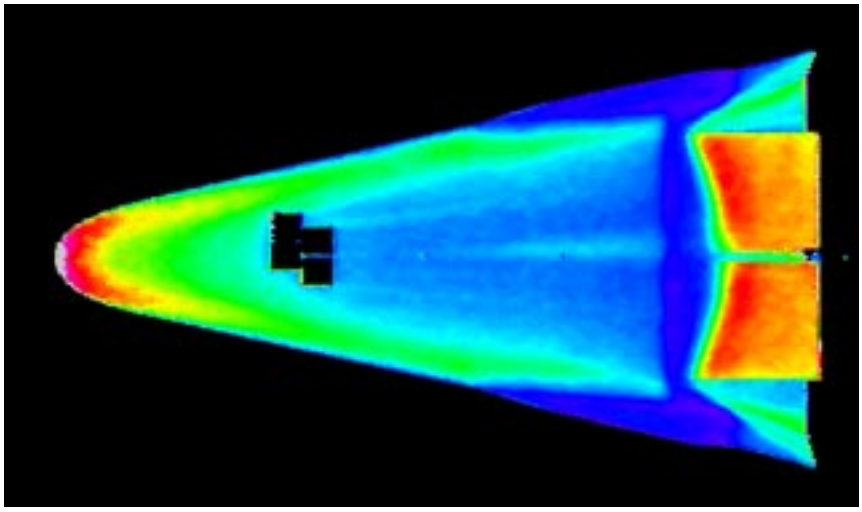

Run # 139
Windward View
Model # 3
BF @ 25°
$\alpha = 40°$
$Re_\infty/ft = 2.2x10^6$
0.0050-in. Trip
@ x/L = 0.3
Width = 0.4-in.
Orientation = 0°

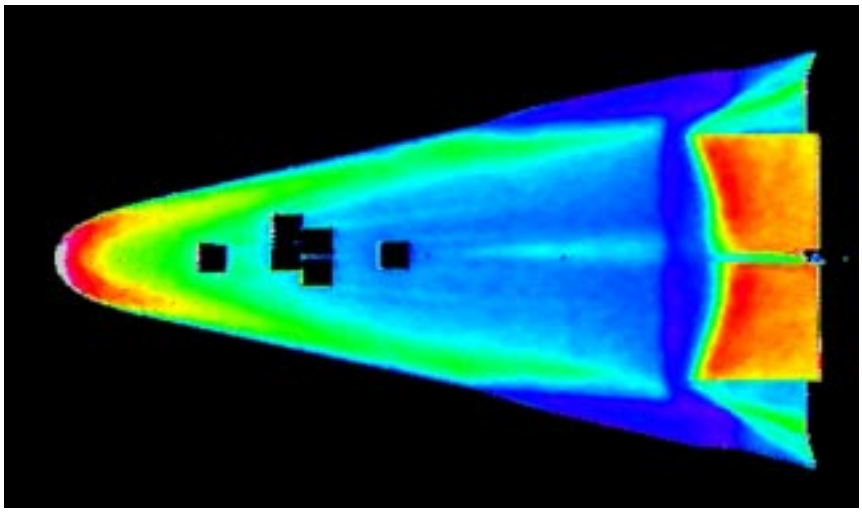

Run # 140
Windward View
Model # 3
BF @ 25°
$\alpha = 40°$
$Re_\infty/ft = 2.2x10^6$
0.0050-in. Trip
@ x/L = 0.3
Width = 0.4-in.
Orientation = 0°

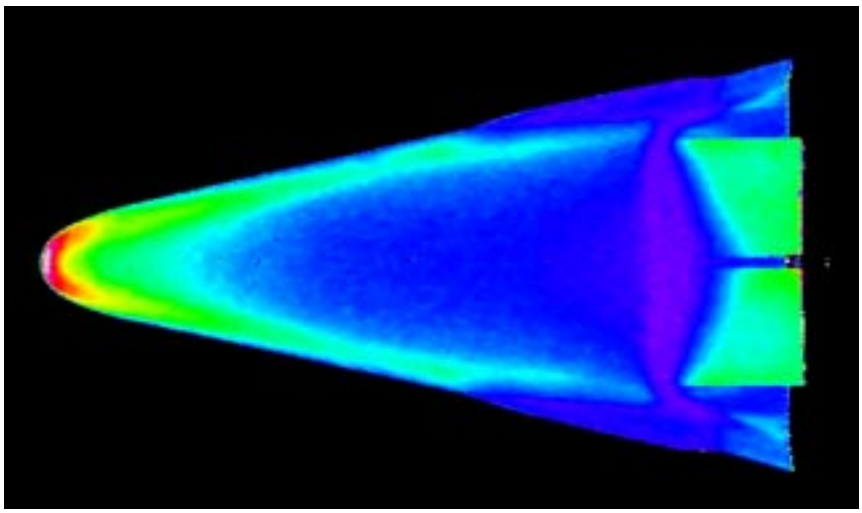

Run # 141
Windward View
Model # 3
BF @ 25°
$\alpha = 30°$
$Re_\infty/ft = 1.2x10^6$

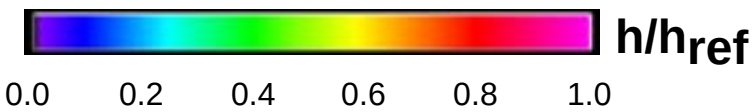

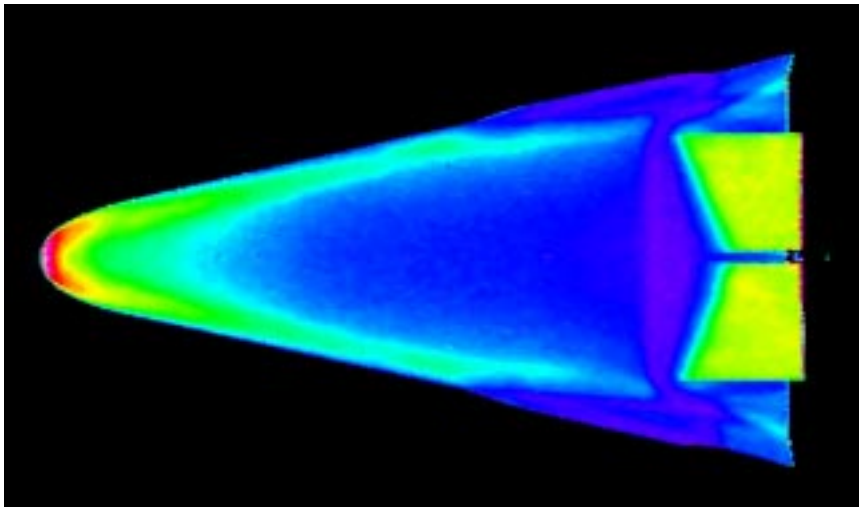

Run # 142
Windward View
Model # 3
BF @ 25°
$\alpha = 30°$
$Re_\infty/ft = 2.2x10^6$

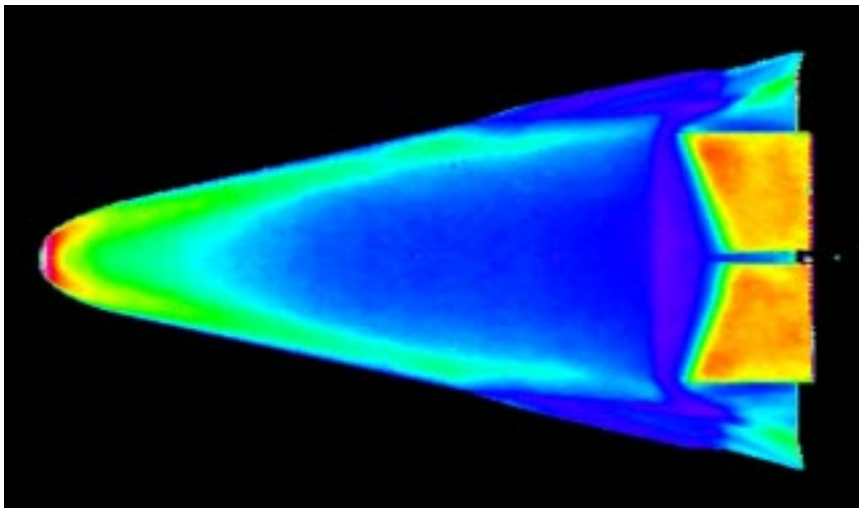

Run # 143
Windward View
Model # 3
BF @ 25°
$\alpha = 30°$
$Re_\infty/ft = 4.4x10^6$

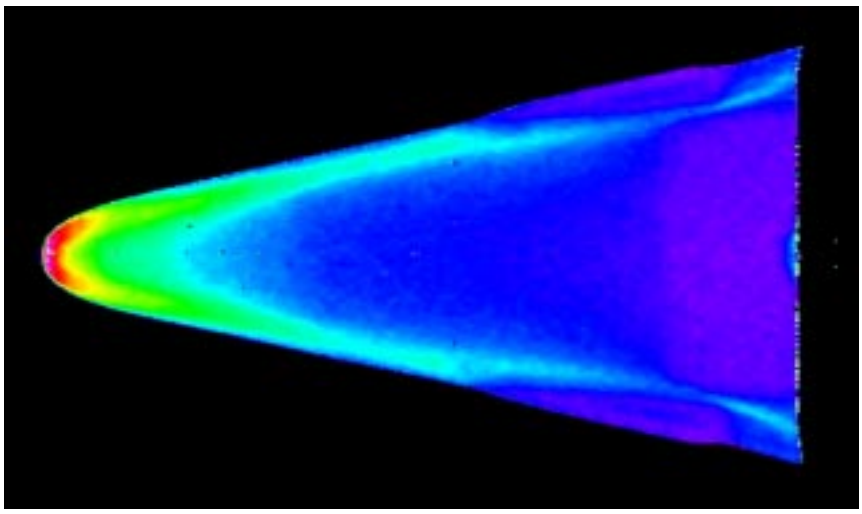

Run # 144
Windward View
Model # 1
BF @ 0°
$\alpha = 30°$
$Re_\infty/ft = 1.1x10^6$

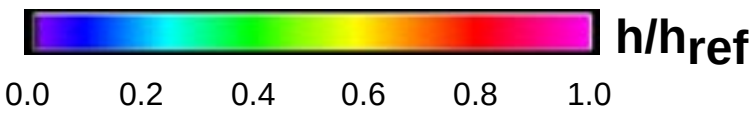

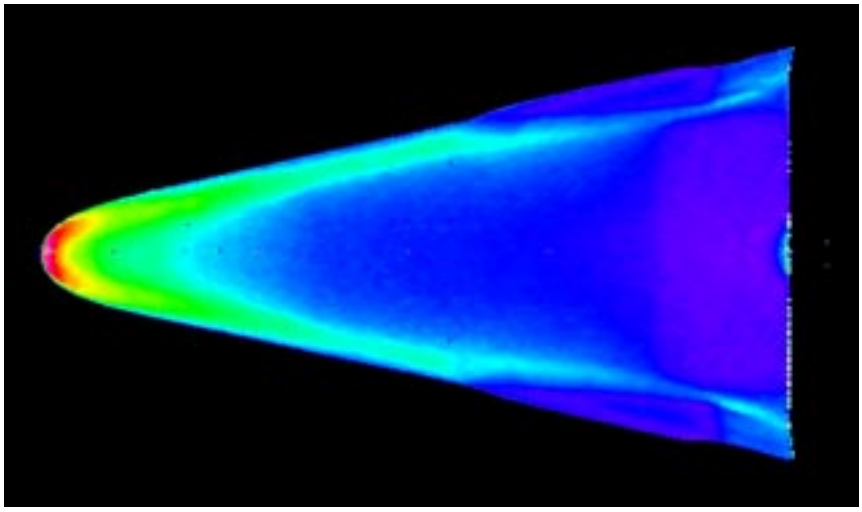

Run # 145
Windward View
Model # 1
BF @ 0°
$\alpha = 30°$
$Re_\infty/ft = 2.2x10^6$

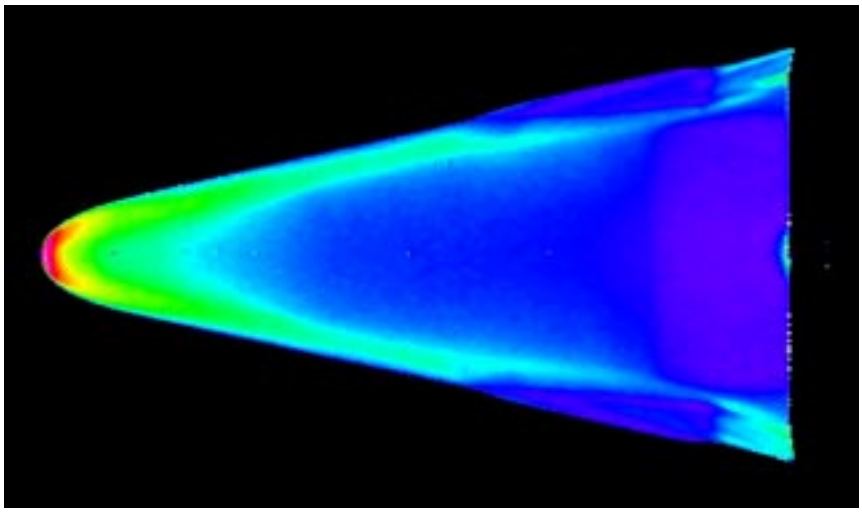

Run # 146
Windward View
Model # 1
BF @ 0°
$\alpha = 30°$
$Re_\infty/ft = 4.4x10^6$

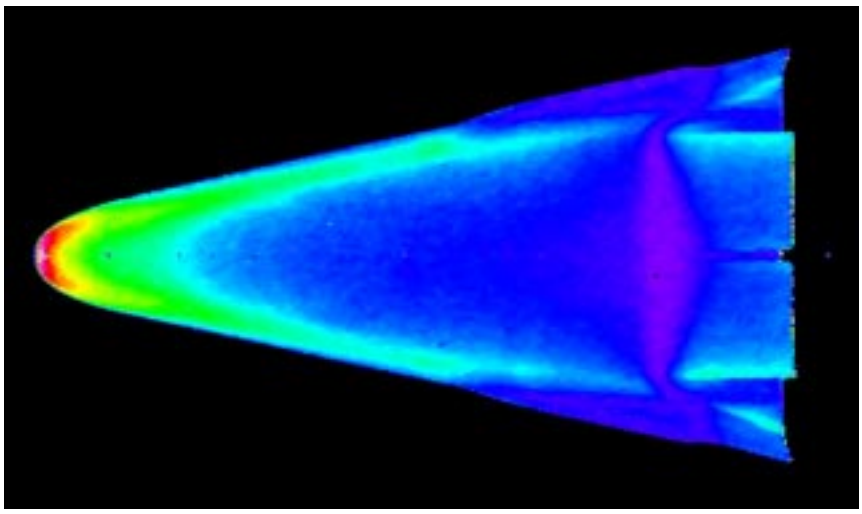

Run # 147
Windward View
Model # 2
BF @ 20°
$\alpha = 30°$
$Re_\infty/ft = 1.1x10^6$
0.0025-in. Trip
@ x/L = 0.1

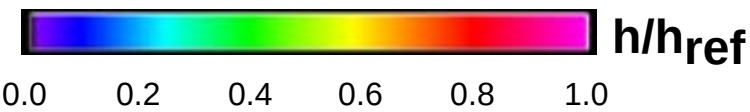

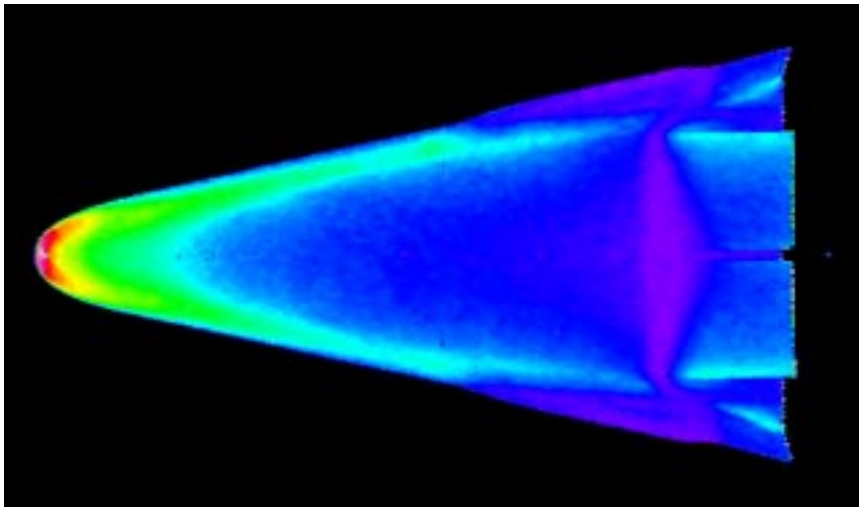

Run # 148
Windward View
Model # 2
BF @ 20°
$\alpha = 30°$
$Re_\infty/ft = 1.1 \bullet x10^6$

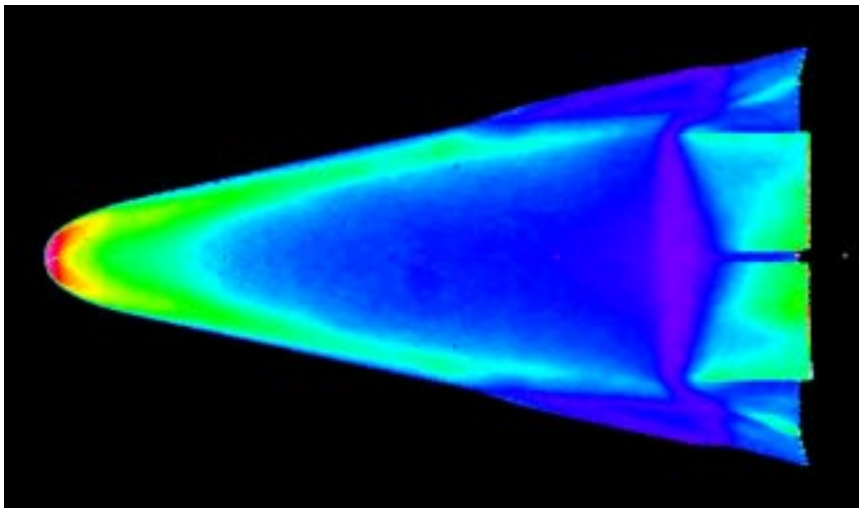

Run # 149
Windward View
Model # 2
BF @ 20°
$\alpha = 30°$
$Re_\infty/ft = 2.2x10^6$

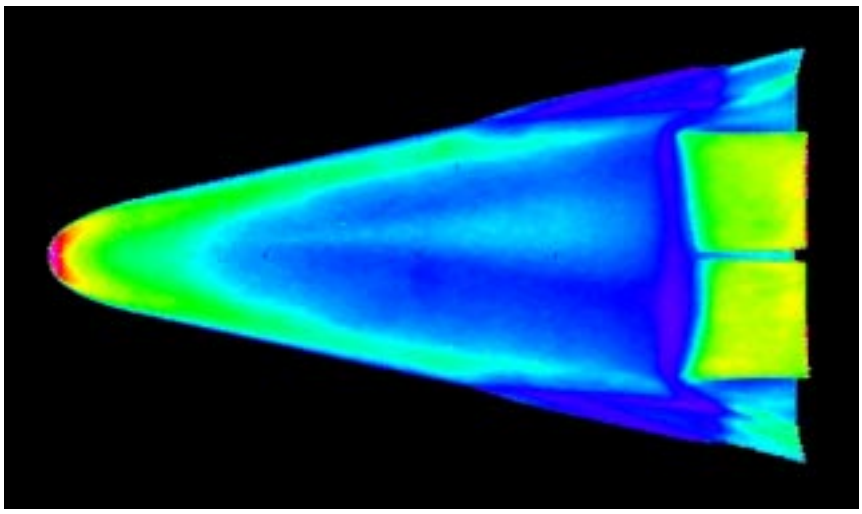

Run # 150
Windward View
Model # 2
BF @ 20°
$\alpha = 30°$
$Re_\infty/ft = 4.4x10^6$

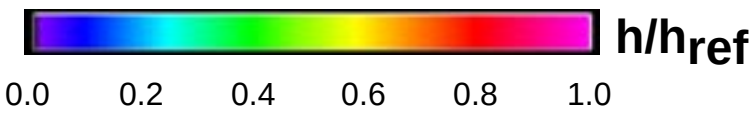

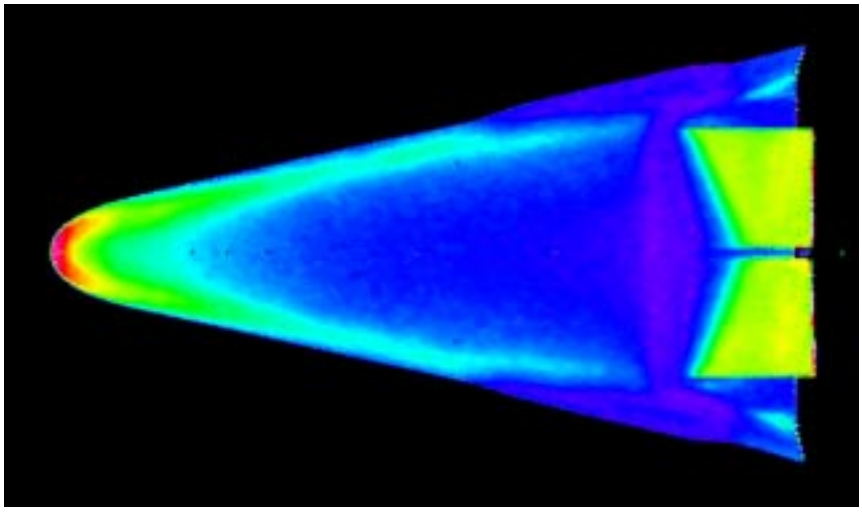

Run # 151
Windward View
Model # 4
BF @ 30°
$\alpha = 30°$
$Re_\infty/ft = 1.1x10^6$

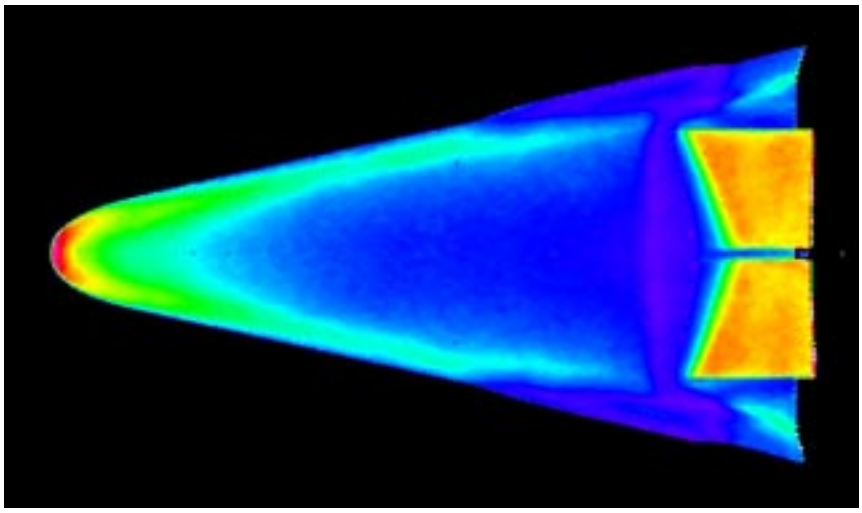

Run # 152
Windward View
Model # 4
BF @ 30°
$\alpha = 30°$
$Re_\infty/ft = 2.2x10^6$

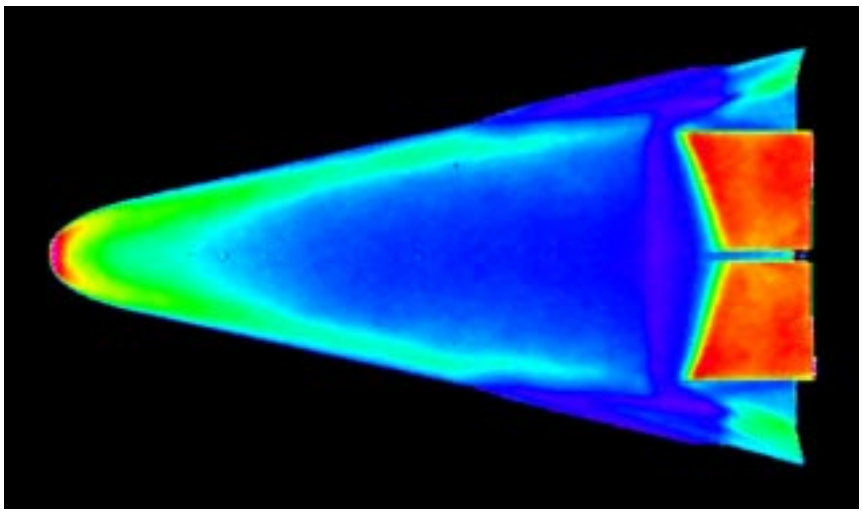

Run # 153
Windward View
Model # 4
BF @ 30°
$\alpha = 30°$
$Re_\infty/ft = 4.4x10^6$

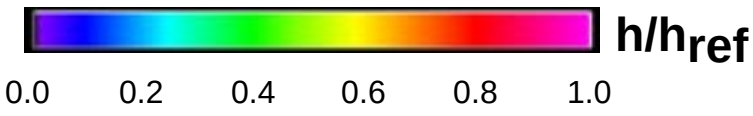

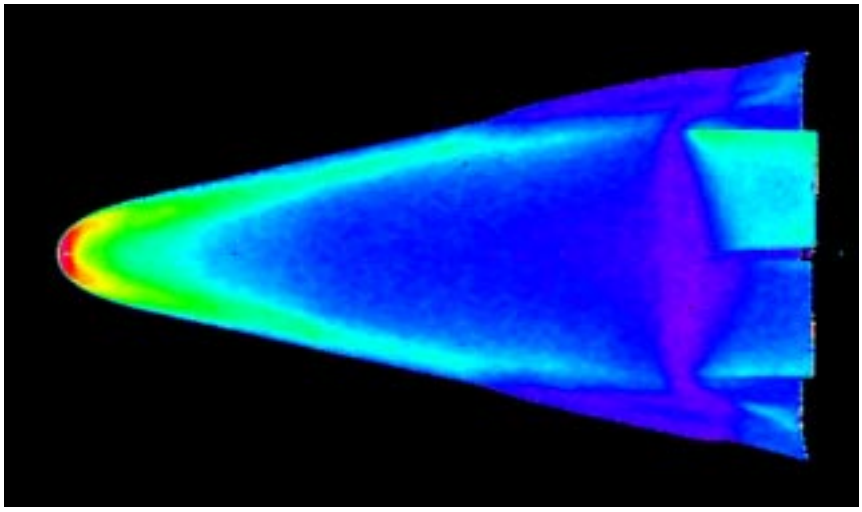

Run # 154
Windward View
Model # 5
RBF @ 20°
LBF @ 25°
$\alpha = 30°$
$Re_\infty/ft = 1.1x10^6$

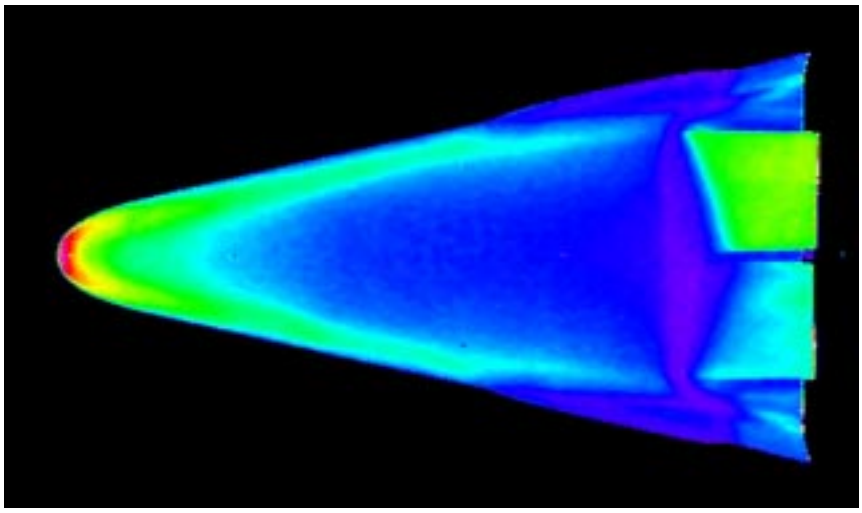

Run # 156
Windward View
Model # 5
RBF @ 20°
LBF @ 25°
$\alpha = 30°$
$Re_\infty/ft = 2.2x10^6$

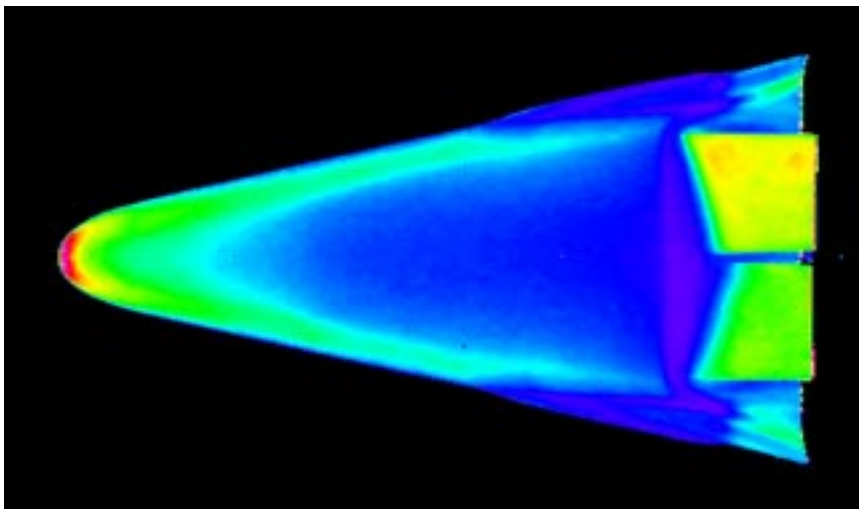

Run # 157
Windward View
Model # 5
RBF @ 20°
LBF @ 25°
$\alpha = 30°$
$Re_\infty/ft = 4.4x10^6$

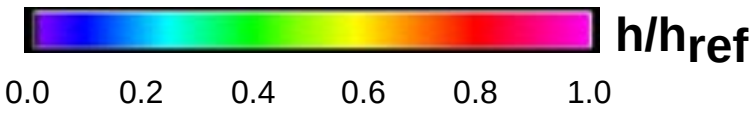

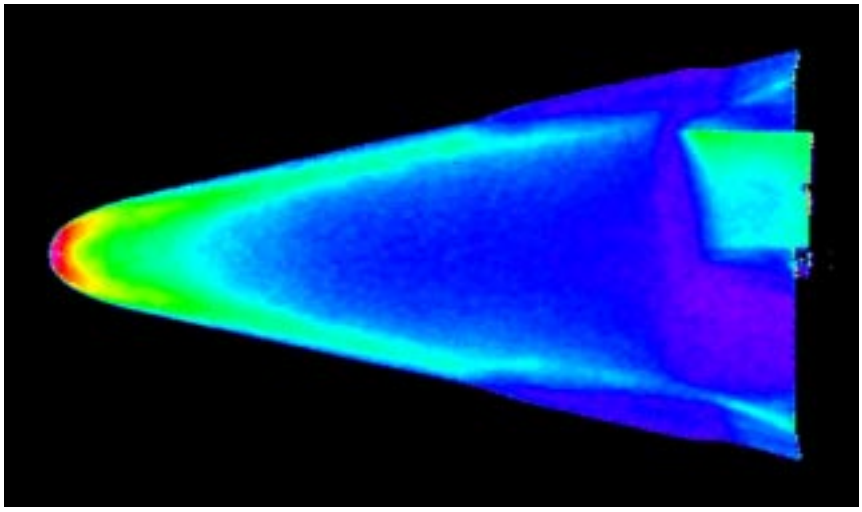

Run # 158
Windward View
Model # 6
RBF @ 0°
LBF @ 25°
$\alpha = 30°$
$Re_\infty/ft = 1.1x10^6$

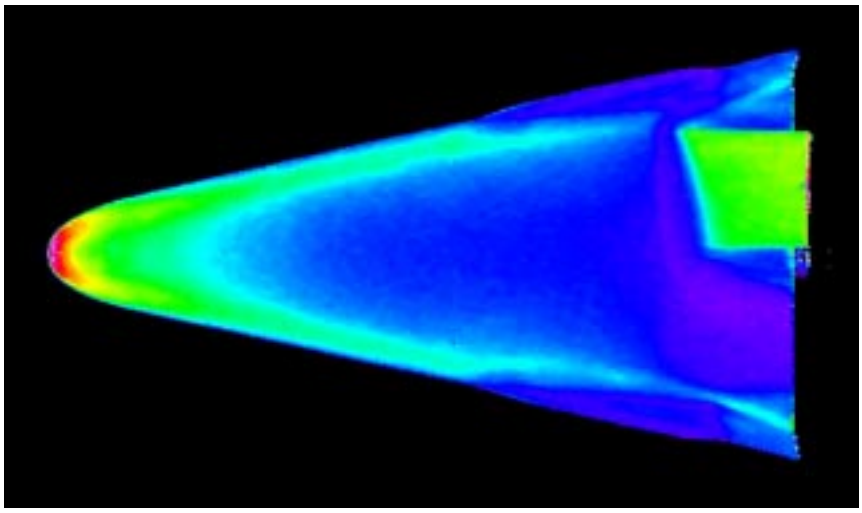

Run # 159
Windward View
Model # 6
RBF @ 0°
LBF @ 25°
$\alpha = 30°$
$Re_\infty/ft = 2.2x10^6$

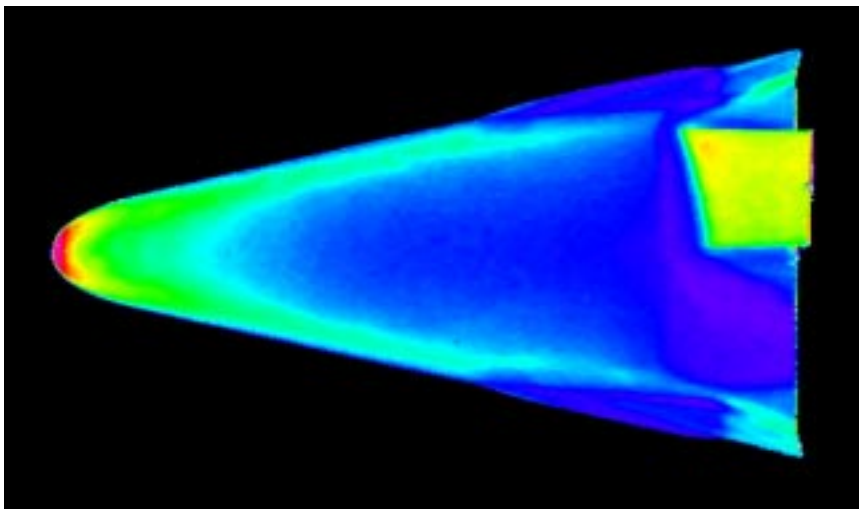

Run # 160
Windward View
Model # 6
RBF @ 0°
LBF @ 25°
$\alpha = 30°$
$Re_\infty/ft = 4.4x10^6$

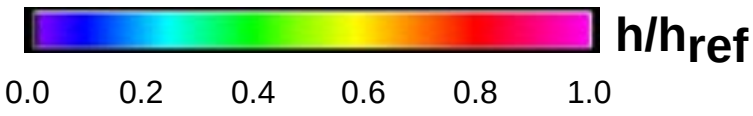

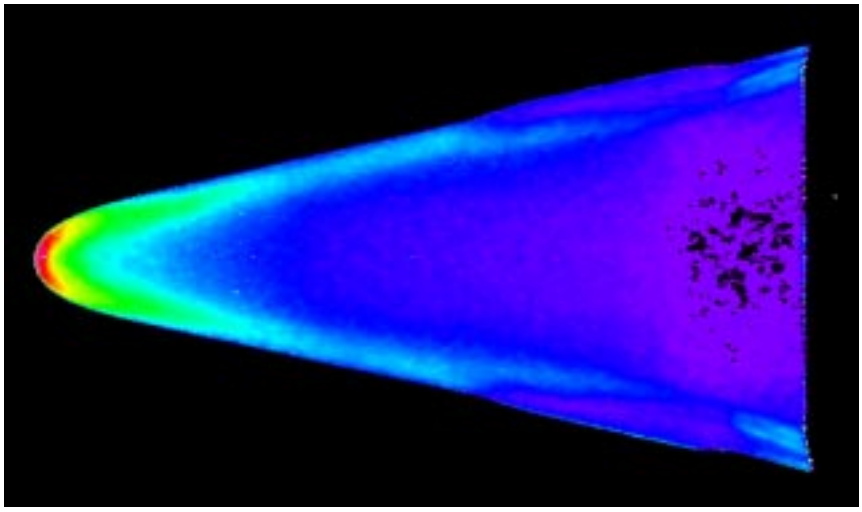

Run # 161
Windward View
Model # 1
BF @ 0°
$\alpha = 20°$
$Re_\infty/ft = 1.1x10^6$

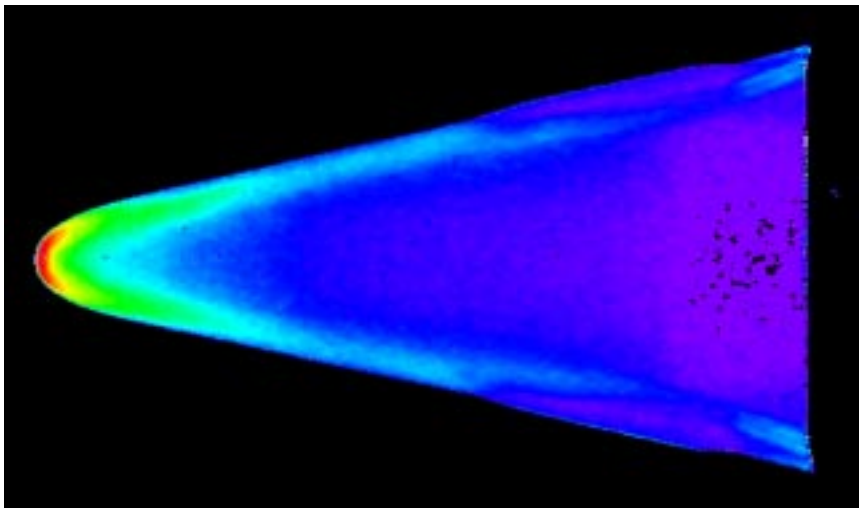

Run # 162
Windward View
Model # 1
BF @ 0°
$\alpha = 20°$
$Re_\infty/ft = 1.1x10^6$
Repeat

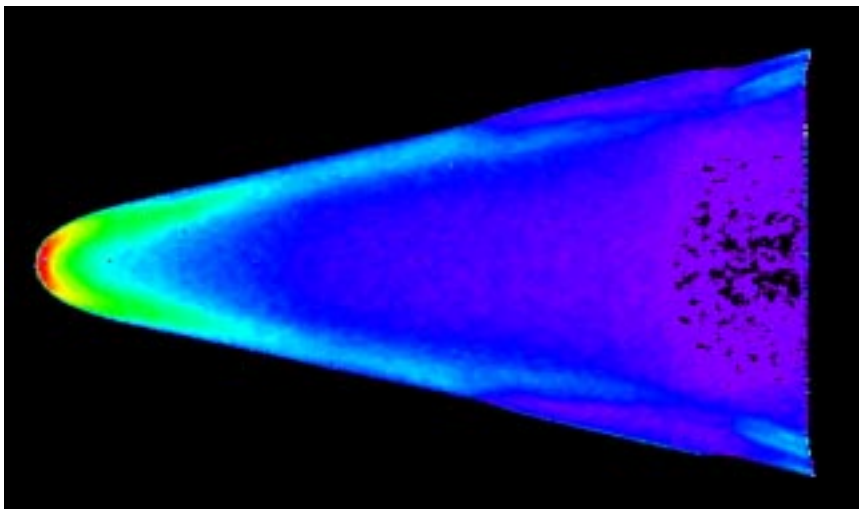

Run # 163
Windward View
Model # 1
BF @ 0°
$\alpha = 20°$
$Re_\infty/ft = 1.1x10^6$
Repeat

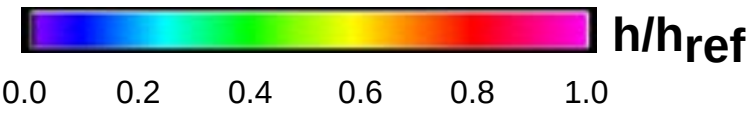

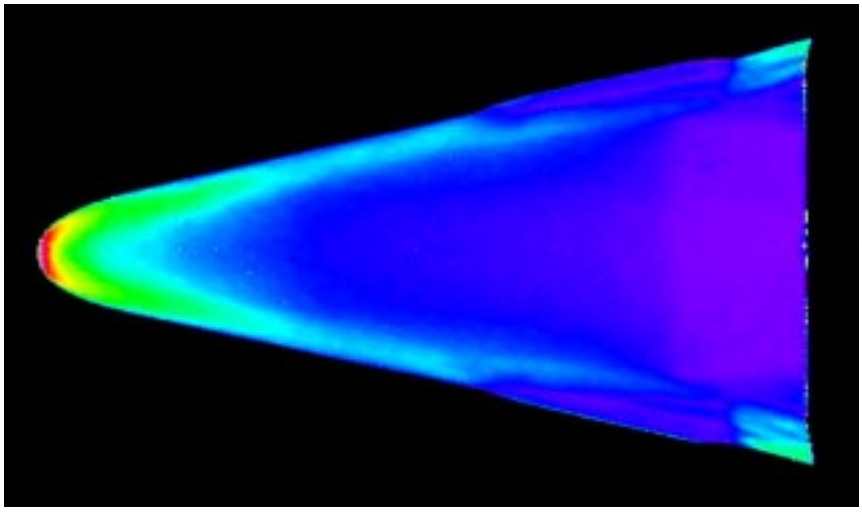

Run # 164
Windward View
Model # 1
BF @ 0°
$\alpha = 20°$
$Re_\infty/ft = 4.4x10^6$

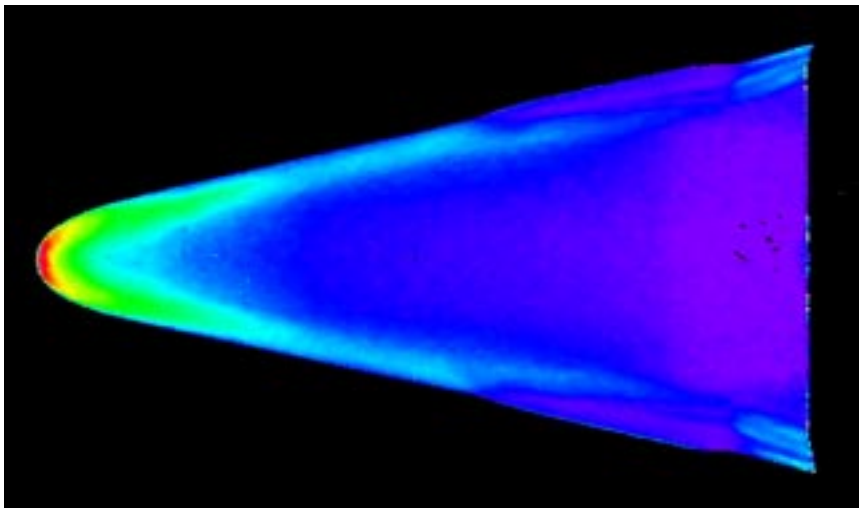

Run # 165
Windward View
Model # 1
BF @ 0°
$\alpha = 20°$
$Re_\infty/ft = 2.2x10^6$

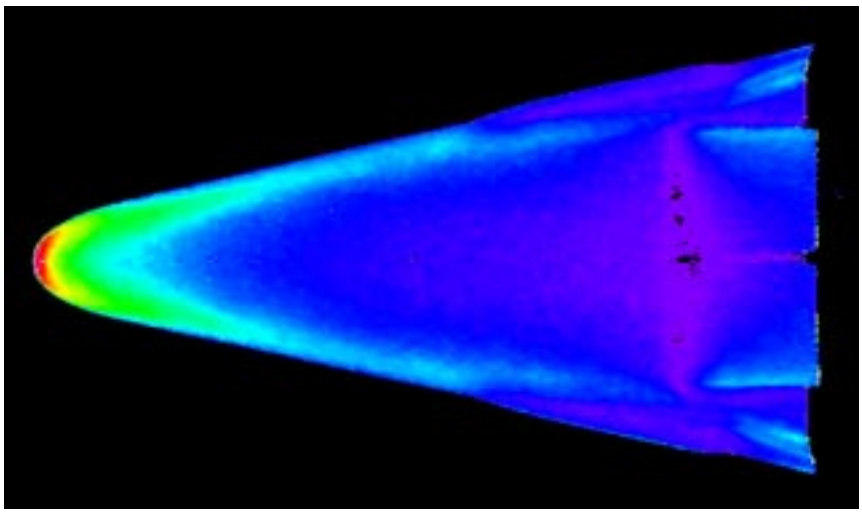

Run # 166
Windward View
Model # 2
BF @ 20°
$\alpha = 20°$
$Re_\infty/ft = 1.1x10^6$

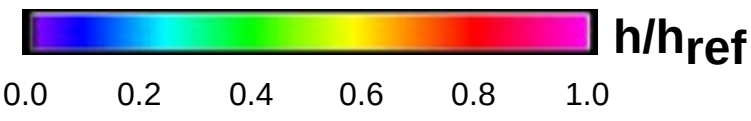

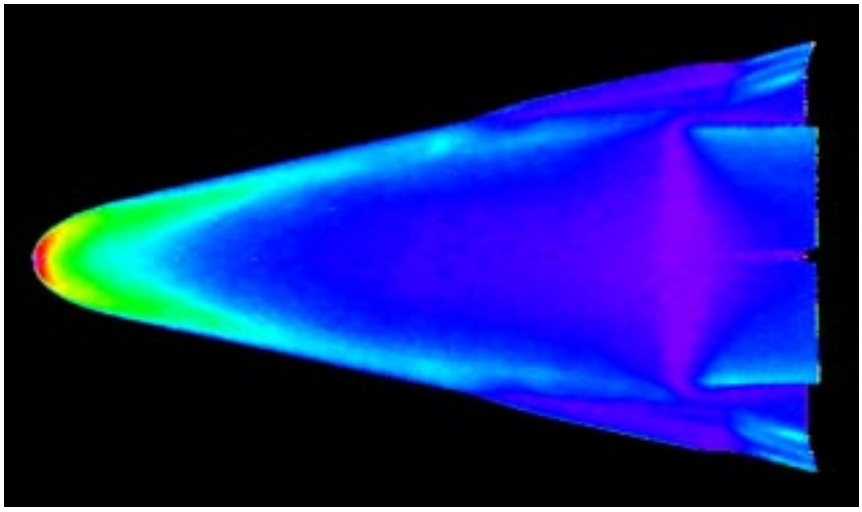

Run # 167
Windward View
Model # 2
BF @ 20°
$\alpha = 20°$
$Re_\infty/ft = 2.2x10^6$

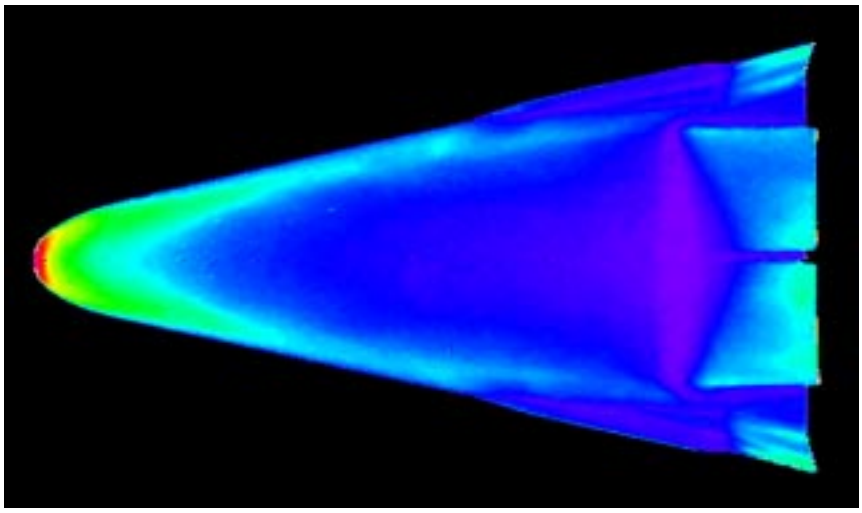

Run # 168
Windward View
Model # 2
BF @ 20°
$\alpha = 20°$
$Re_\infty/ft = 4.4x10^6$

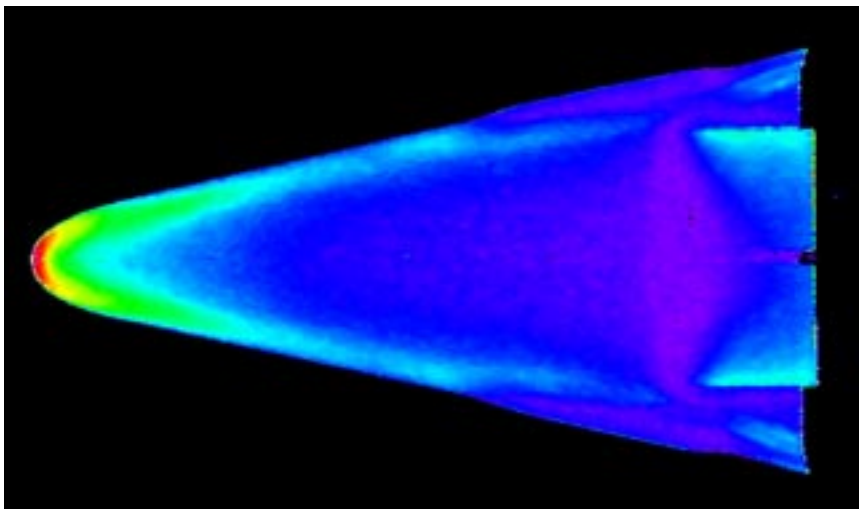

Run # 169
Windward View
Model # 3
BF @ 25°
$\alpha = 20°$
$Re_\infty/ft = 1.1x10^6$

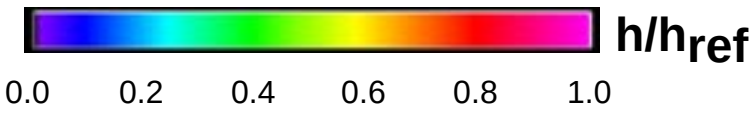

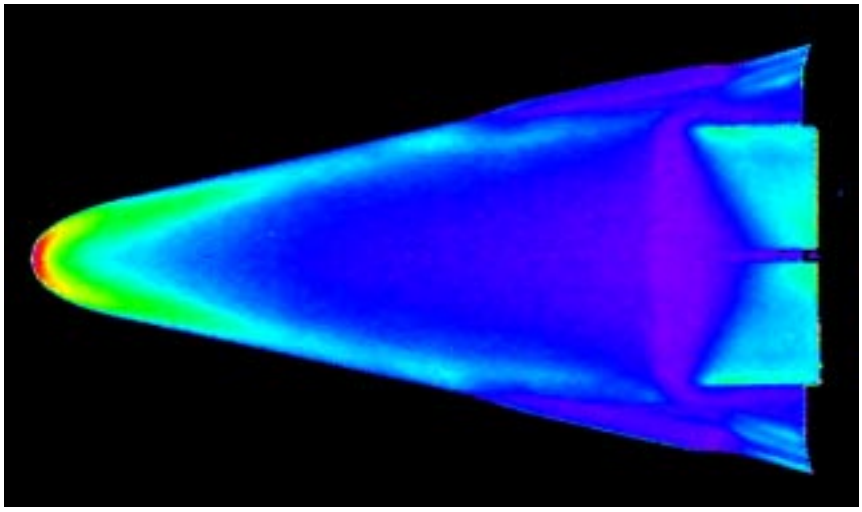

Run # 170
Windward View
Model # 3
BF @ 25°
$\alpha = 20°$
$Re_\infty/ft = 2.2x10^6$

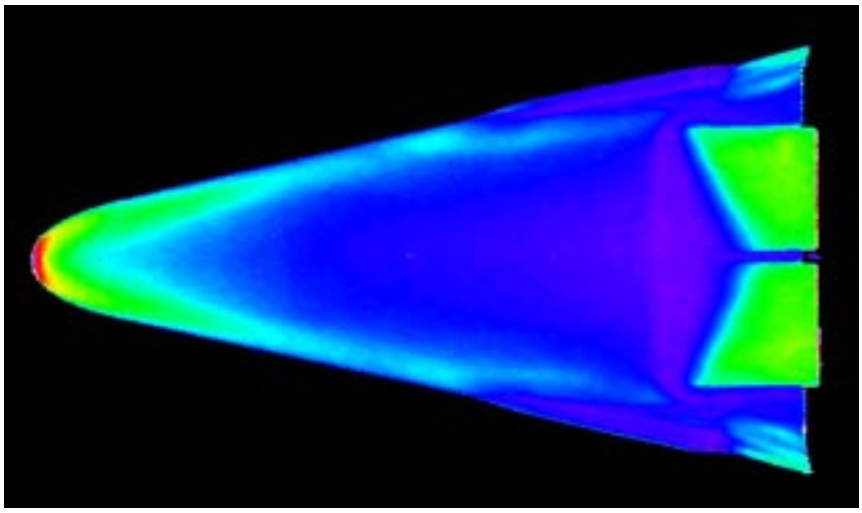

Run # 171
Windward View
Model # 3
BF @ 25°
$\alpha = 20°$
$Re_\infty/ft = 4.4x10^6$

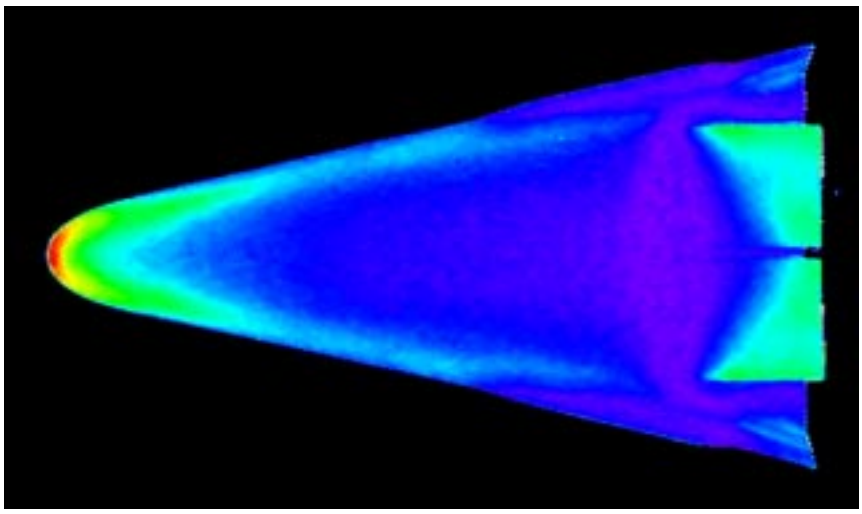

Run # 172
Windward View
Model # 4
BF @ 30°
$\alpha = 20°$
$Re_\infty/ft = 1.1x10^6$

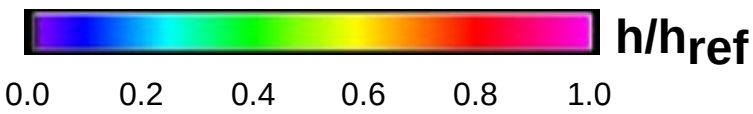

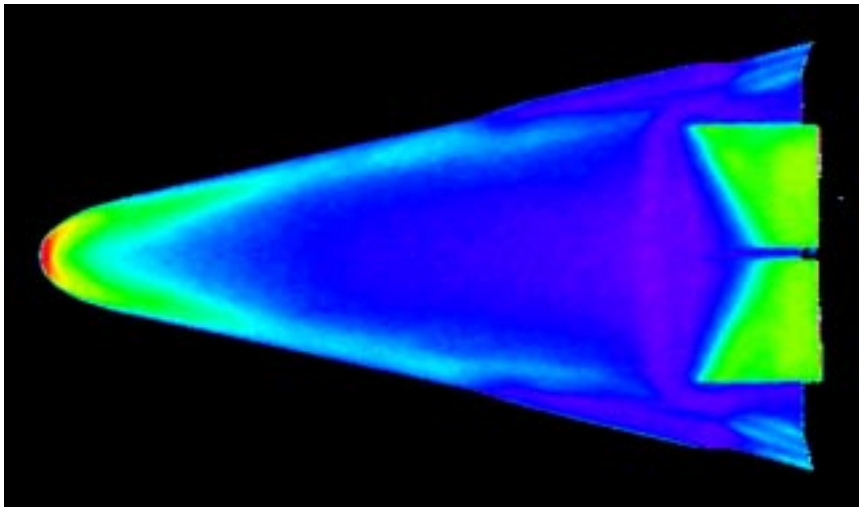

Run # 173
Windward View
Model # 4
BF @ 30°
$\alpha = 20°$
$Re_\infty/ft = 2.2x10^6$

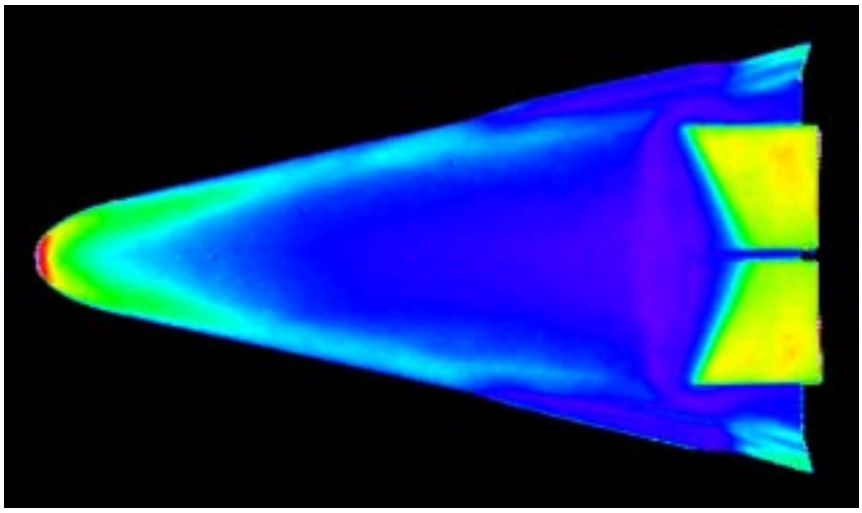

Run # 174
Windward View
Model # 4
BF @ 30°
$\alpha = 20°$
$Re_\infty/ft = 4.4x10^6$

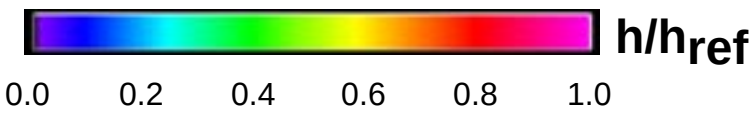

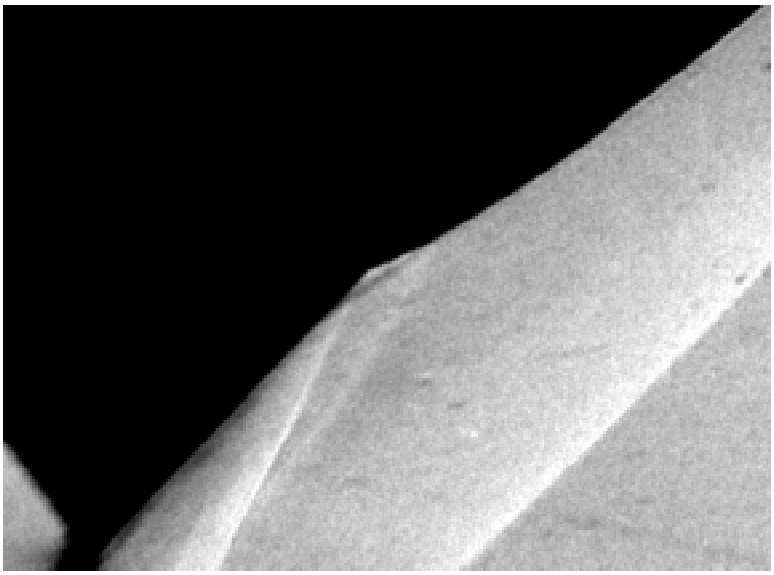

TEST 6739
$\alpha = 40^{\circ}$
BF@ 25°

RUN 1
$Re_{\infty}/ft = 2.2X10^{6}$

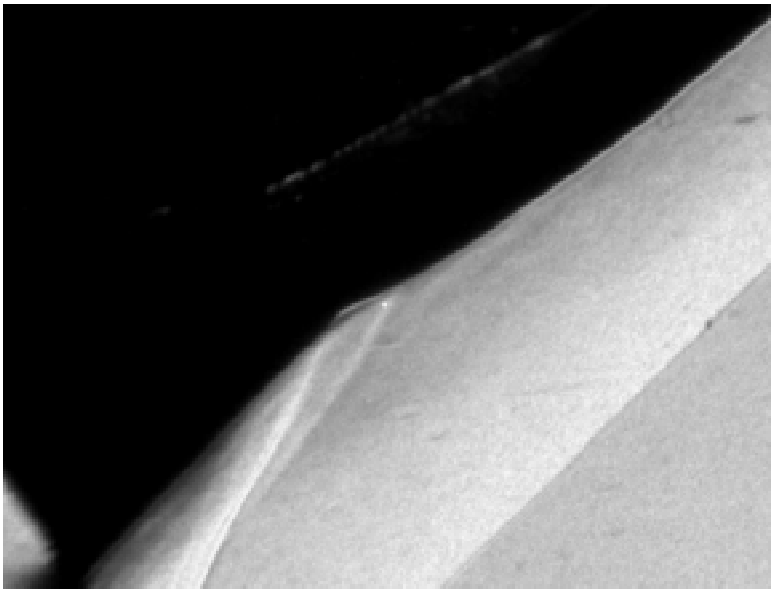

TEST 6739
$\alpha = 40^{\circ}$
BF@ 25°

RUN 2
$Re_{\infty}/ft = 4.4X10^{6}$

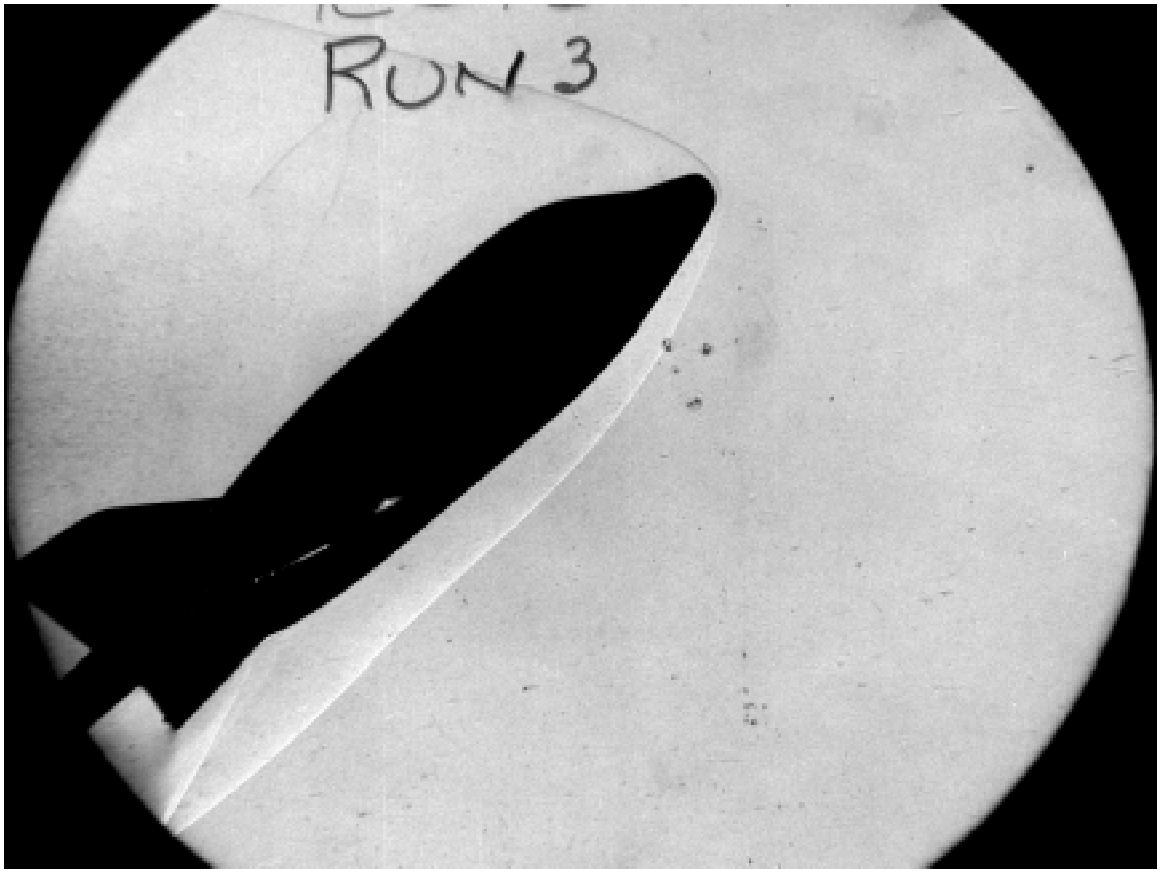

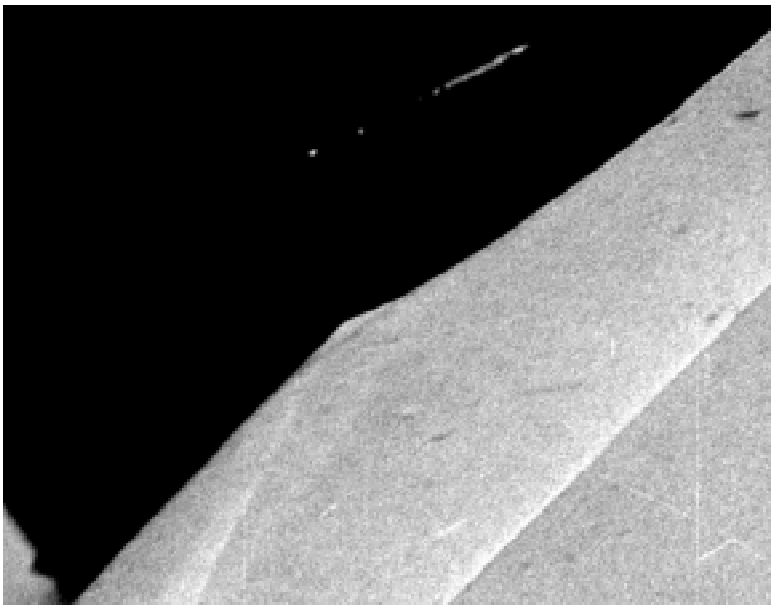

TEST 6739
$\alpha = 40^{\circ}$
BF@ 25°

RUN 3
$Re_{\infty}/ft = 1.1X10^{6}$

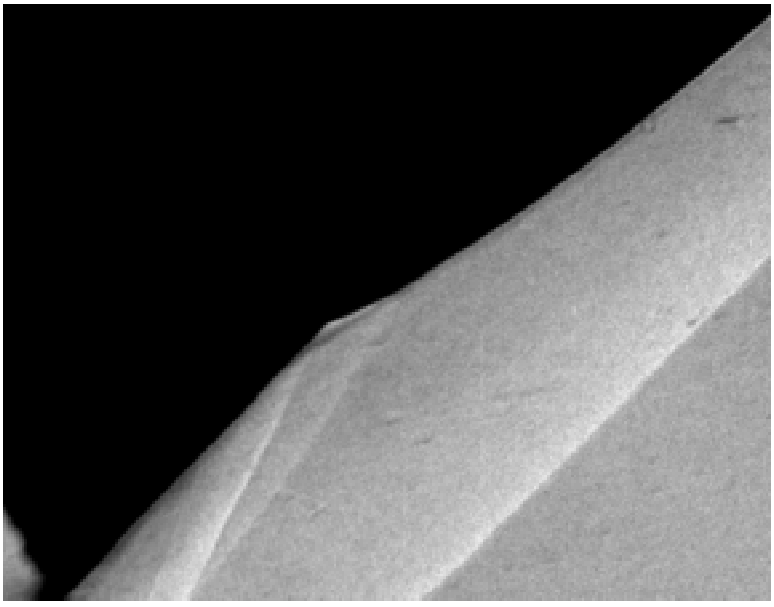

TEST 6739
$\alpha = 40^{\circ}$
BF@ 25°

RUN 4
$Re_{\infty}/ft = 2.2X10^{6}$

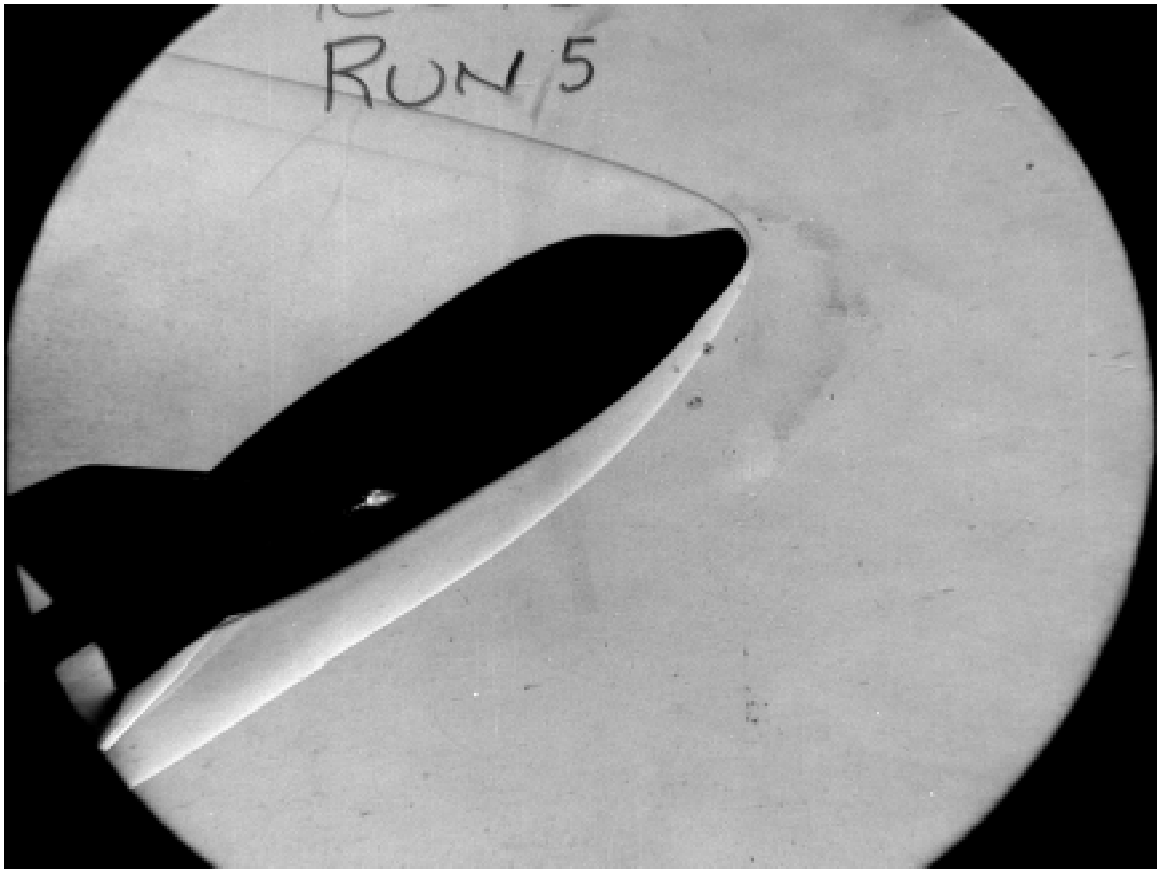

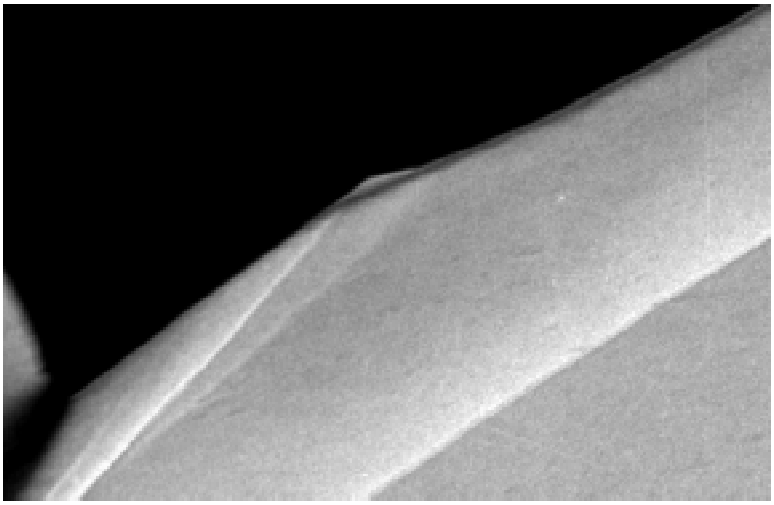

TEST 6739
$\alpha = 30^{\circ}$
BF@ 25°

RUN 5
$Re_{\infty}/ft = 2.2X10^{6}$

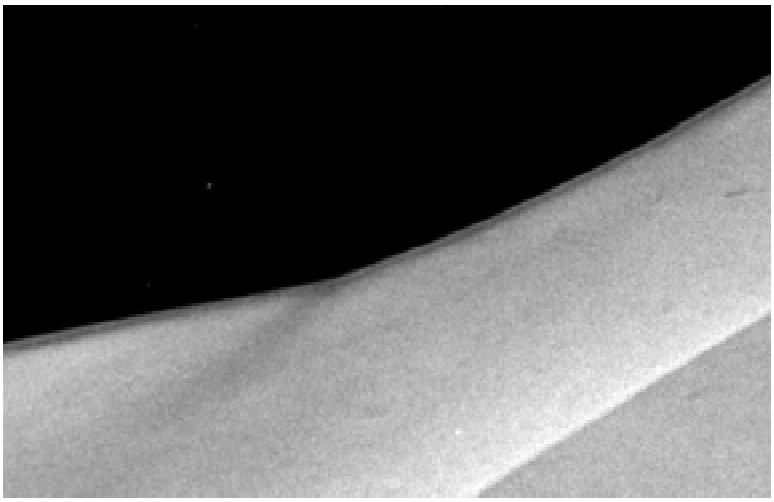

TEST 6739
$\alpha = 30^{\circ}$
BF@ 0°

RUN 6
$Re_{\infty}/ft = 2.2X10^{6}$

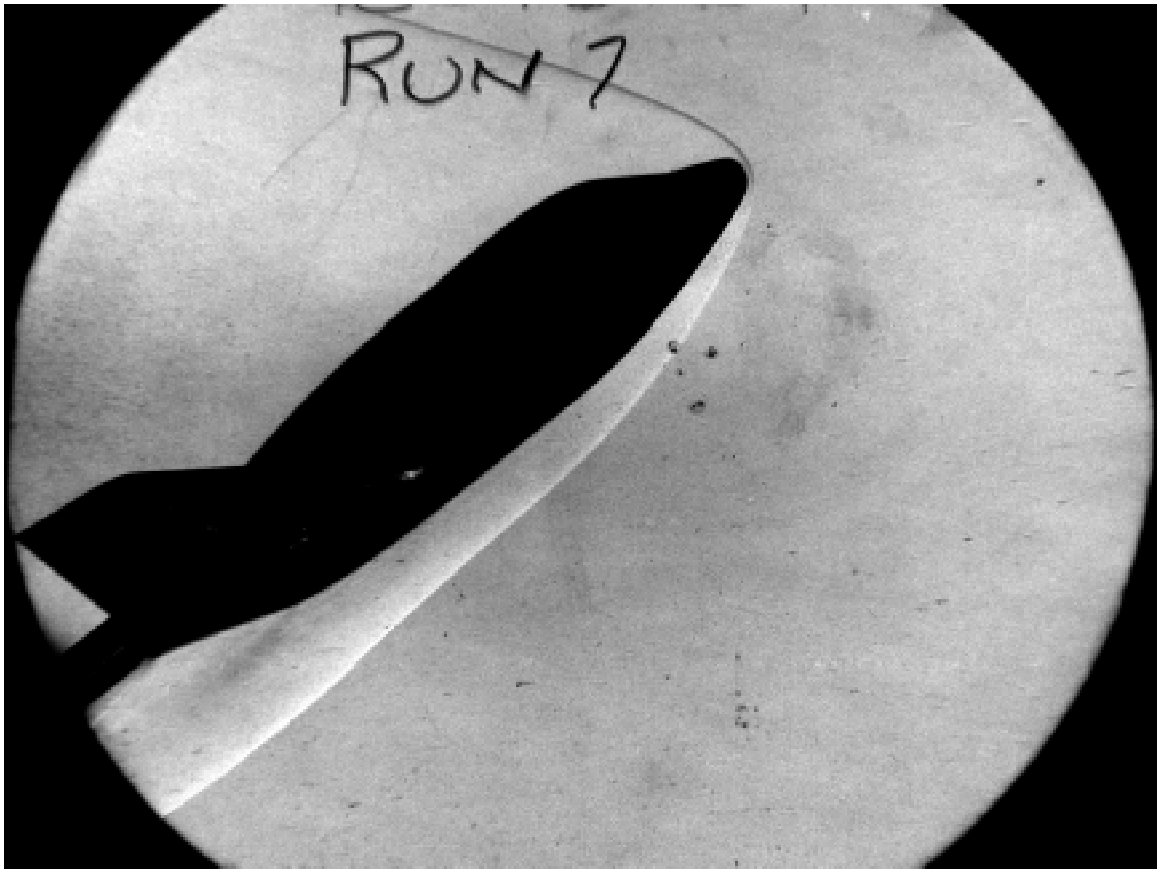

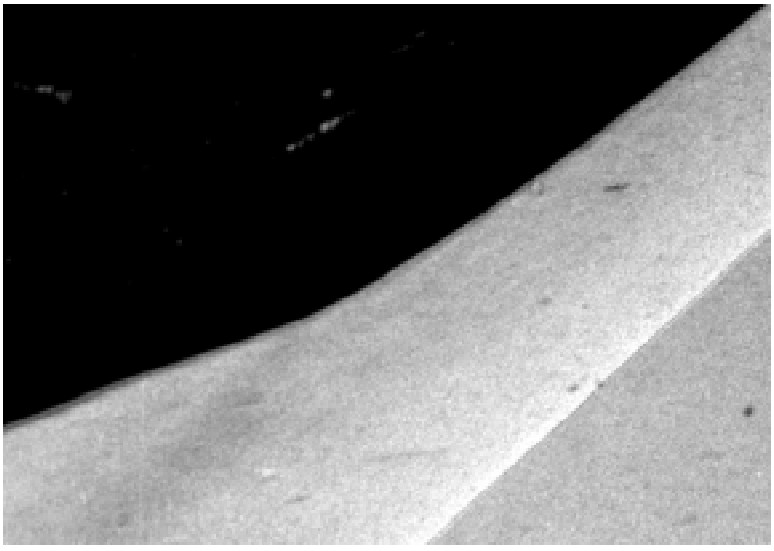

TEST 6739
$\alpha = 40^{\circ}$
BF@ 0°

RUN 7
$Re_{\infty}/ft = 2.2X10^{6}$

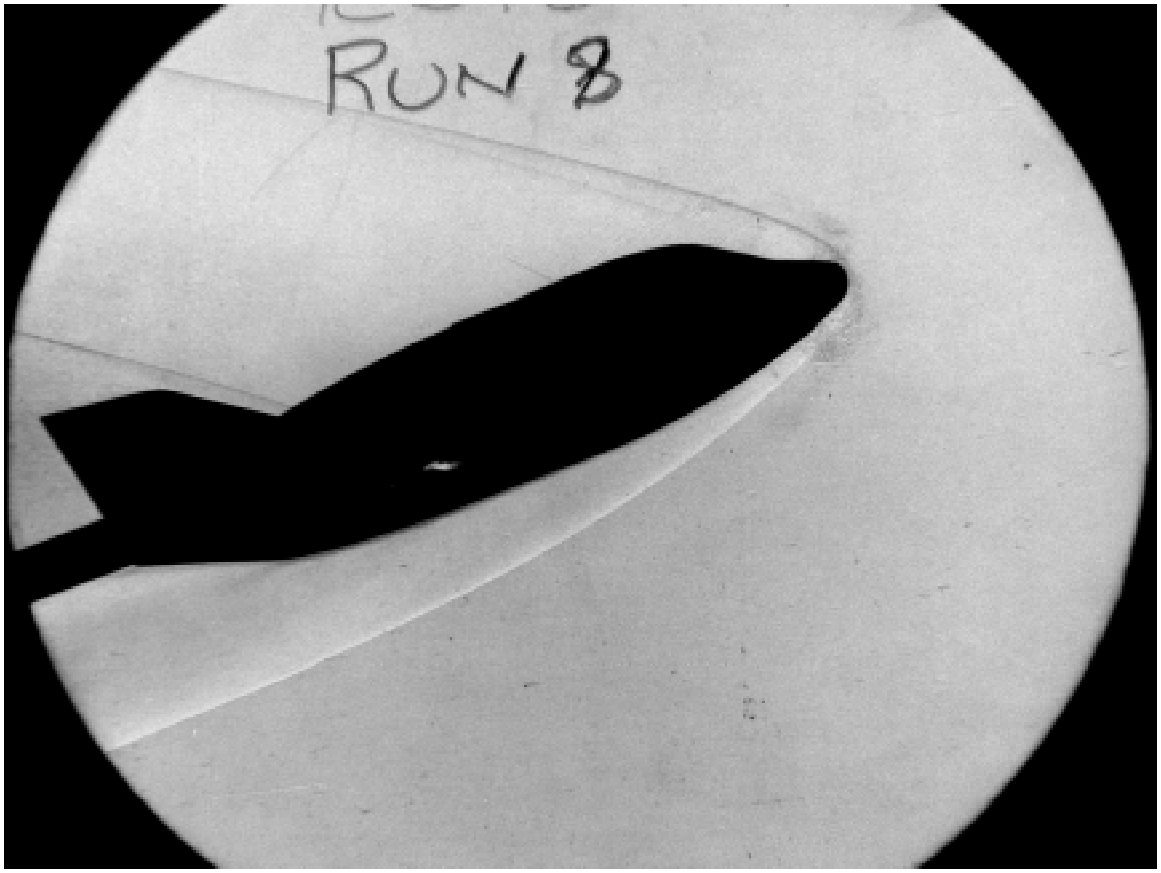

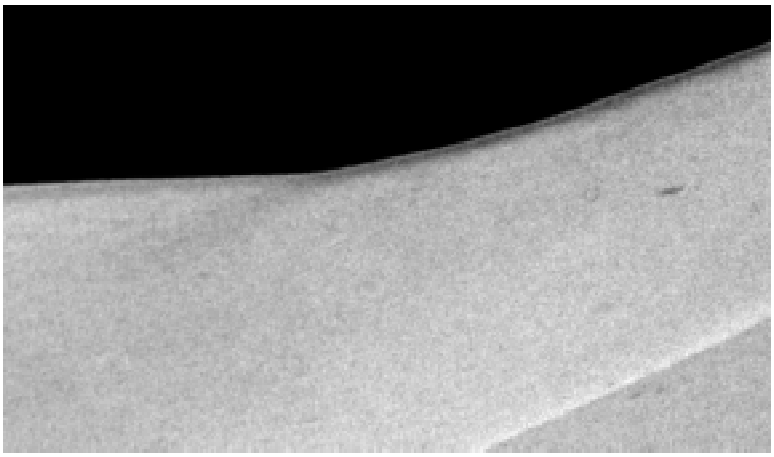

TEST 6739
$\alpha = 20^{\circ}$
BF@ 0°

RUN 8
$Re_{\infty}/ft = 2.2X10^{6}$

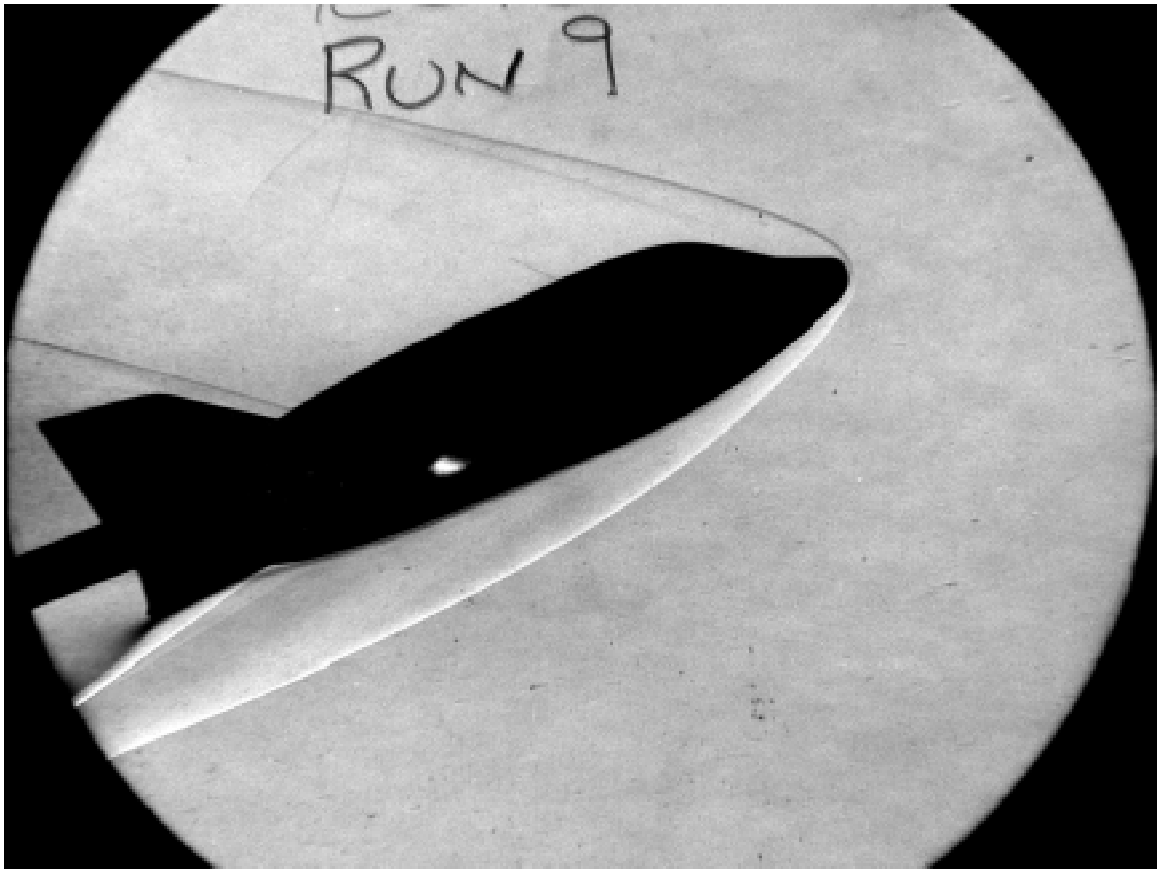

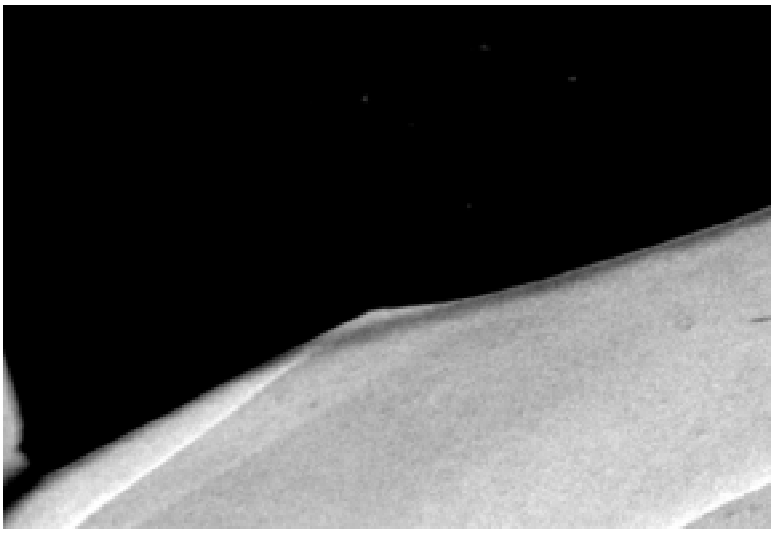

TEST 6739
$\alpha = 20^{\circ}$
BF@ 25°

RUN 9
$Re_{\infty}/ft = 2.2X10^{6}$

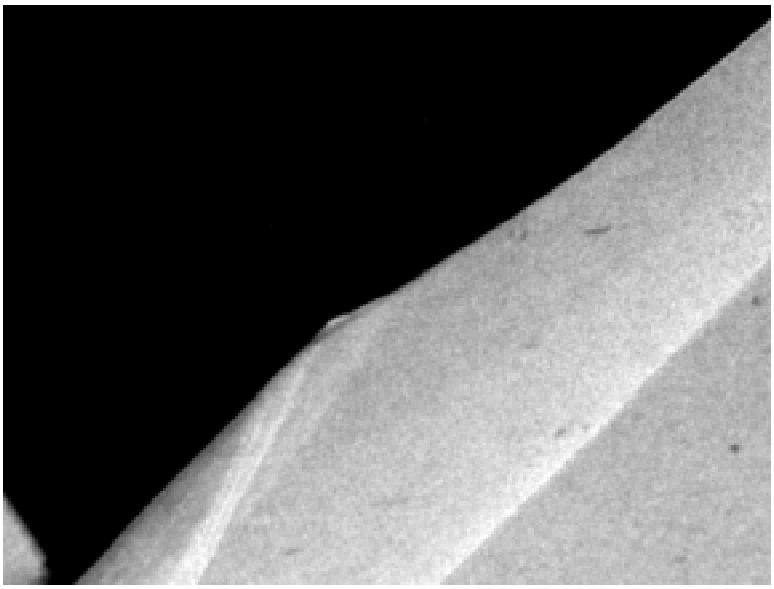

TEST 6739
$\alpha = 40^{\circ}$
BF@ 25°

RUN 10
$Re_{\infty}/ft = 2.2X10^{6}$
Trip@ x/L=0.3, W=0.4", k=0.005"

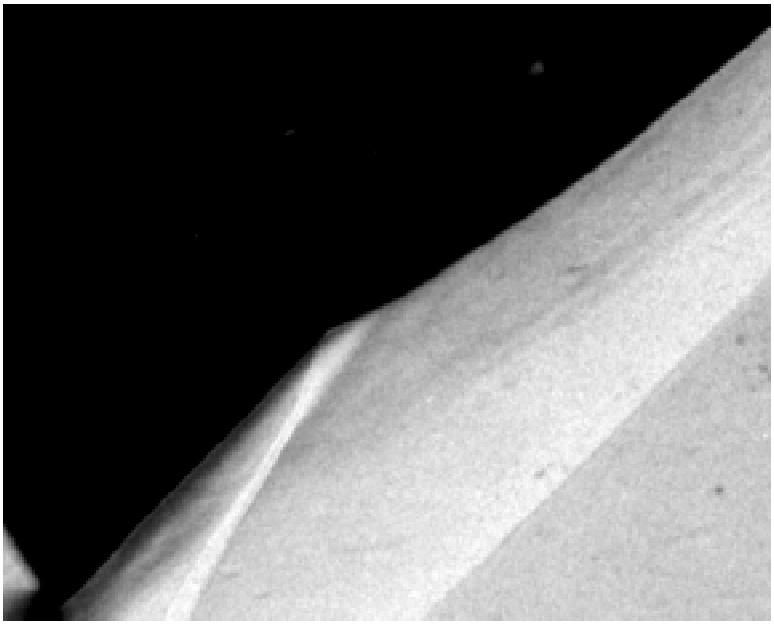

TEST 6739 RUN 11

$\alpha = 40^{\circ}$ $Re_{\infty}/ft = 4.4X10^{6}$

BF@ 25° Trip@ x/L=0.3, W=0.4", k=0.005" (peeled up)

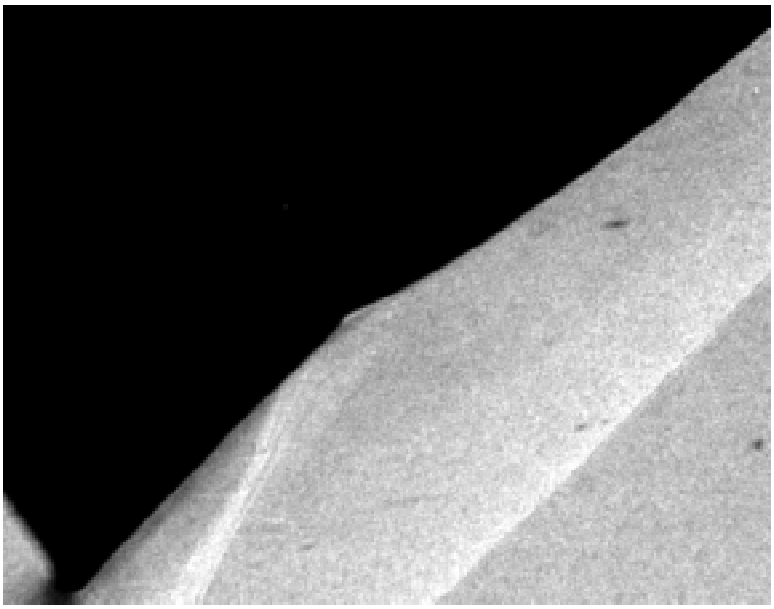

TEST 6739
$\alpha = 40^{\circ}$
BF@ 25°

RUN 12
$Re_{\infty}/ft = 2.2X10^{6}$
Trip@ x/L=0.2, W=0.05", k=0.005"

WINDWARD VIEW

LEEWARD VIEW

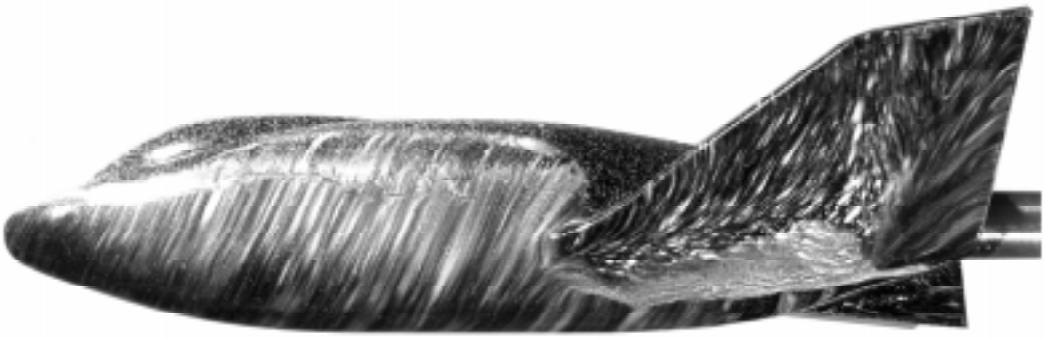

SIDE VIEW

TEST 6739
$\alpha = 40^{\circ}$
BF@ 25°

RUN 1
$Re_{\infty}/ft = 2.2X10^{6}$

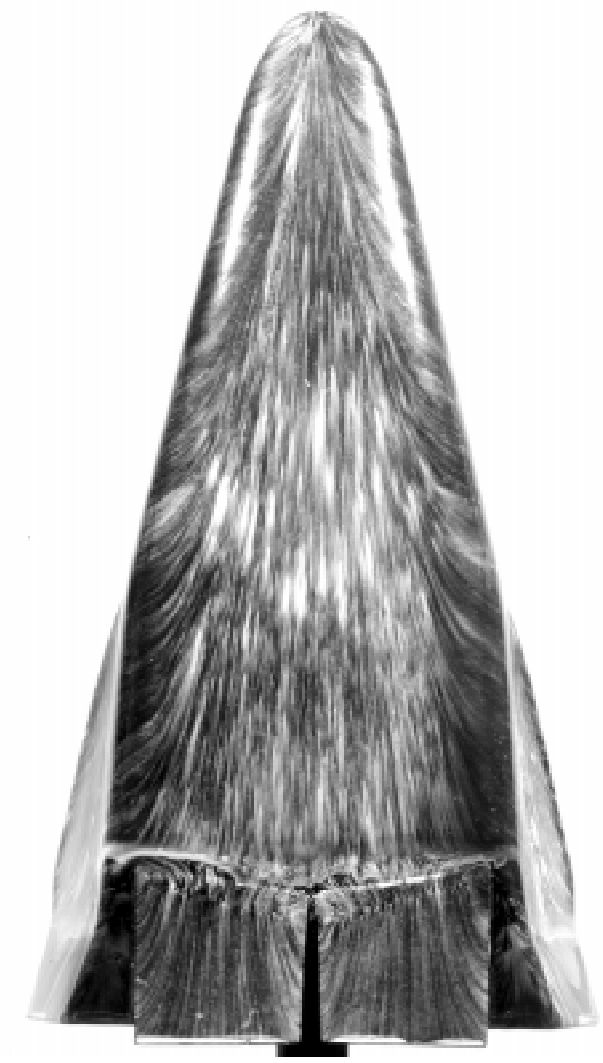

WINDWARD VIEW

LEEWARD VIEW

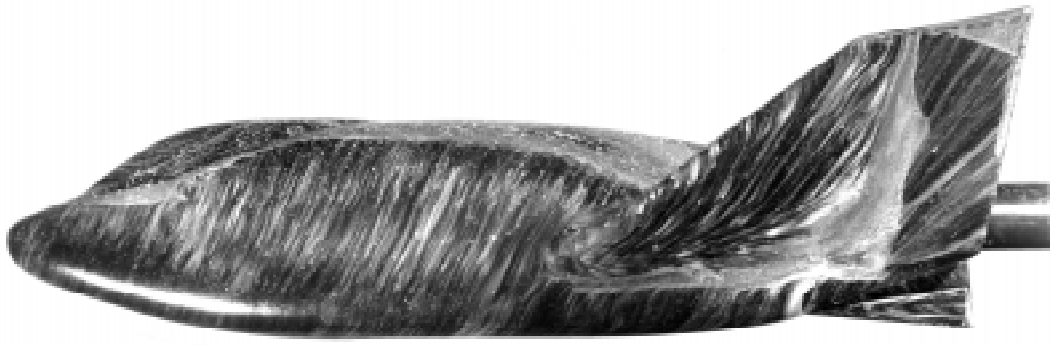

SIDE VIEW

TEST 6739
$\alpha = 40^{\circ}$
BF@ 25°

RUN 2
$Re_{\infty}/ft = 4.4X10^{6}$

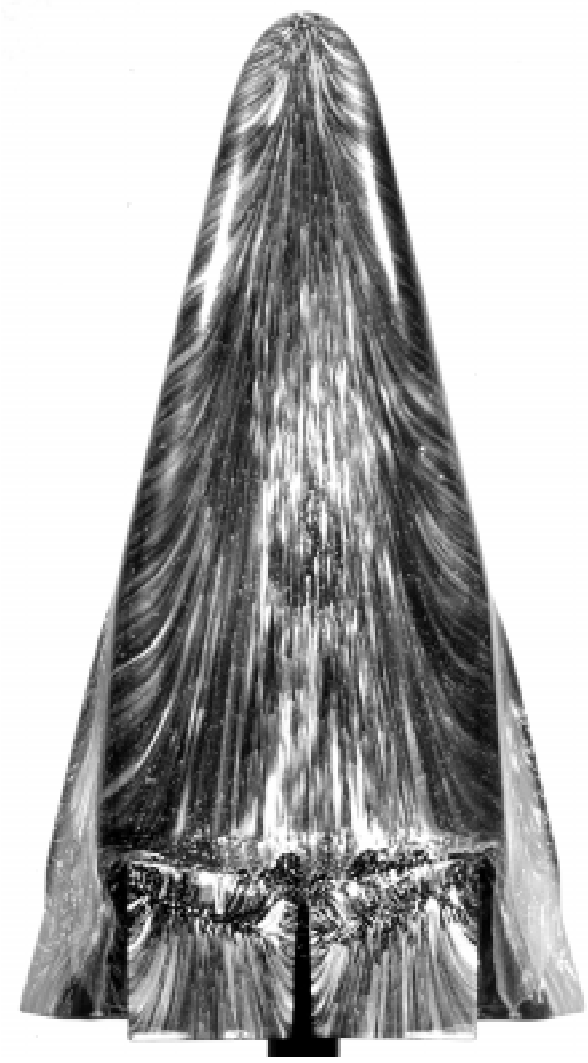

WINDWARD VIEW

LEEWARD VIEW

SIDE VIEW

TEST 6739
$\alpha = 40^{\circ}$
BF @ 25°

RUN 3
$Re_{\infty}/ft = 1.1X10^{6}$

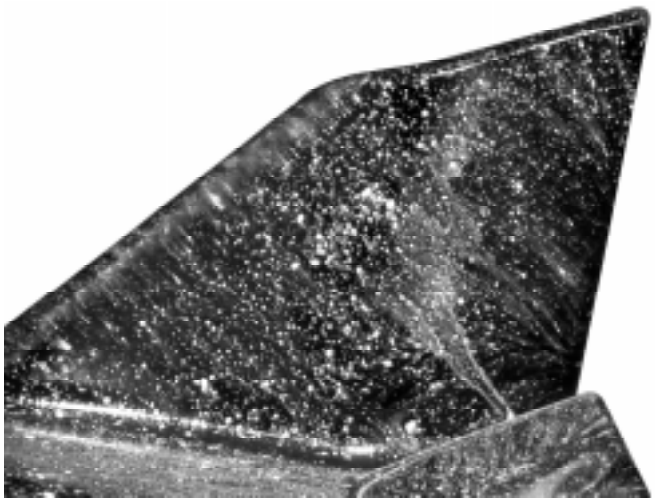

OBLIQUE LEESIDE VIEW

LEESIDE VIEW

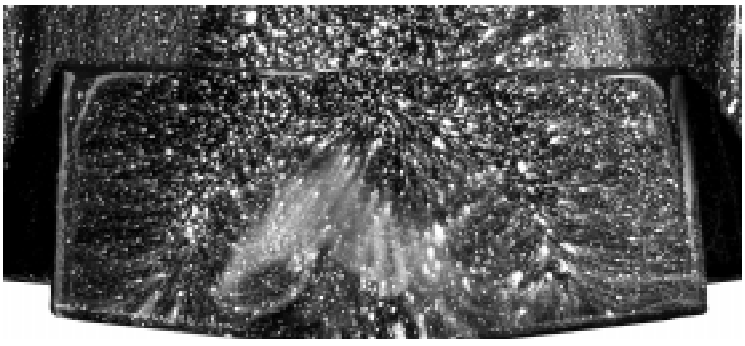

MAGNIFIED LEESIDE VIEW

TEST 6739
$\alpha = 40^{\circ}$
BF@ 25°

RUN 4
$Re_{\infty}/ft = 2.2X10^{6}$
Repeat of RUN 1

WINDWARD VIEW

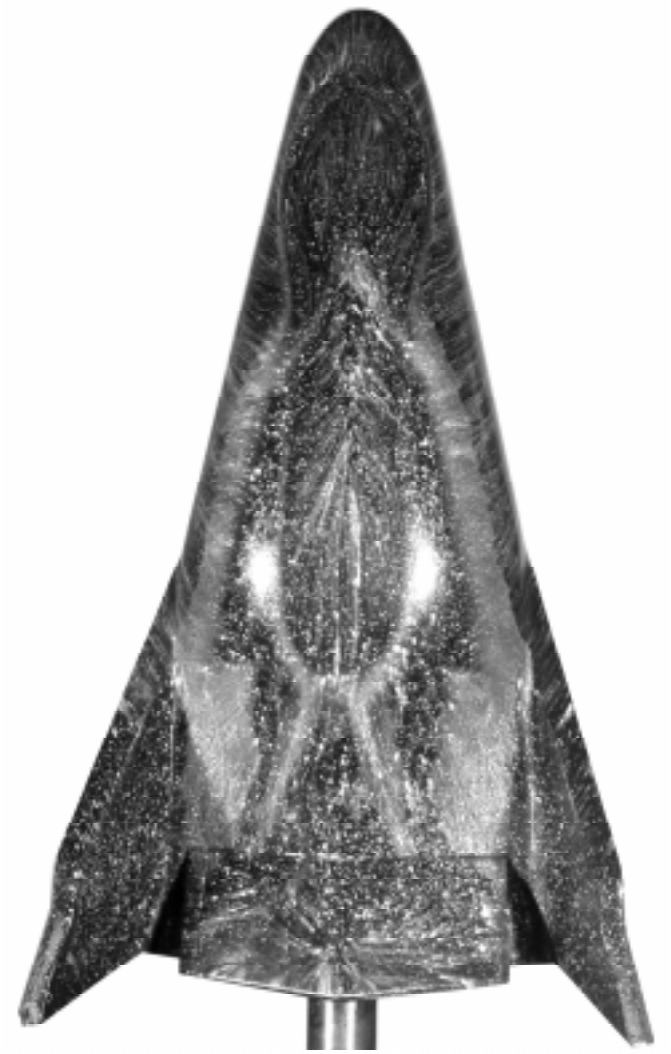

LEEWARD VIEW

SIDE VIEW

TEST 6739
$\alpha = 30^{\circ}$
BF@ 25°

RUN 5
$Re_{\infty}/ft = 2.2X10^{6}$

WINDWARD VIEW

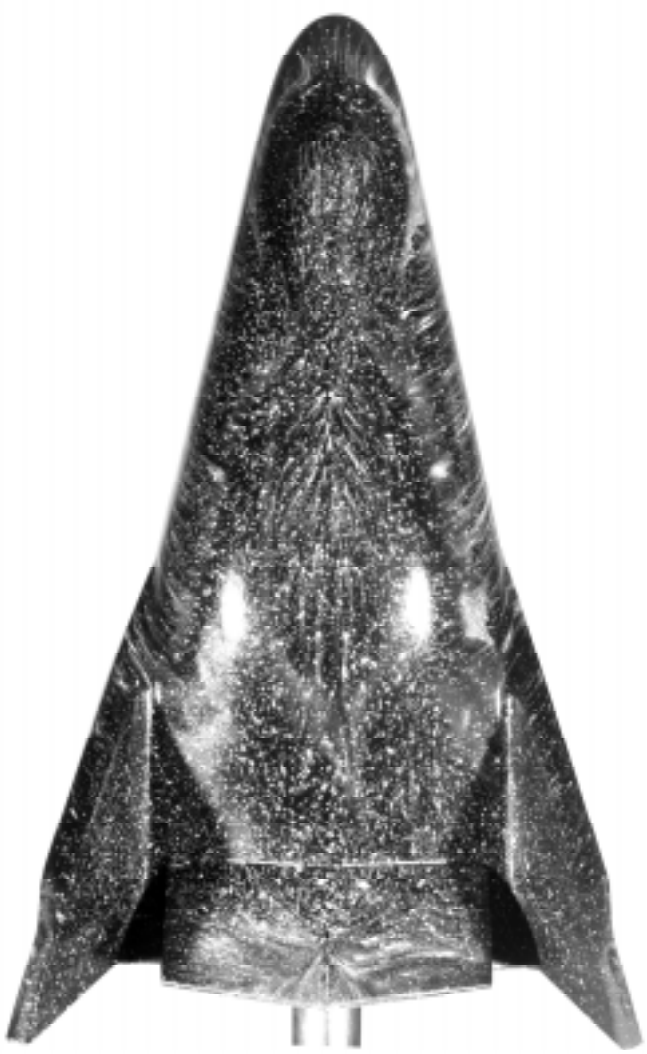

LEEWARD VIEW

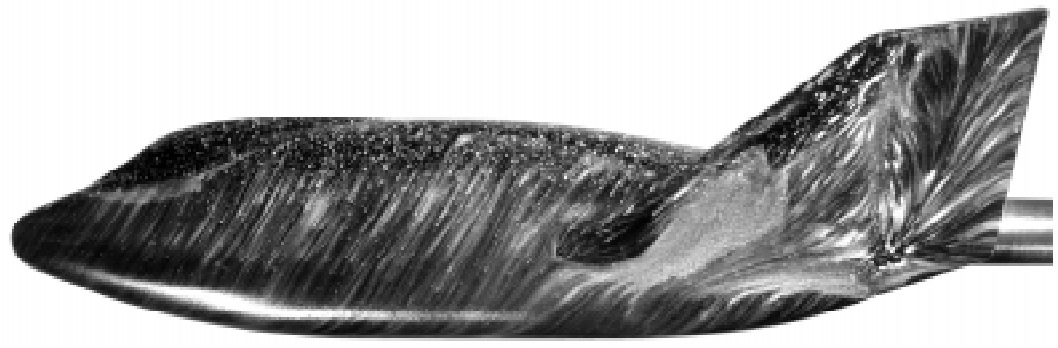

SIDE VIEW

TEST 6739
$\alpha = 30^{\circ}$
BF@ 0°

RUN 6
$Re_{\infty}/ft = 2.2X10^{6}$

WINDWARD VIEW

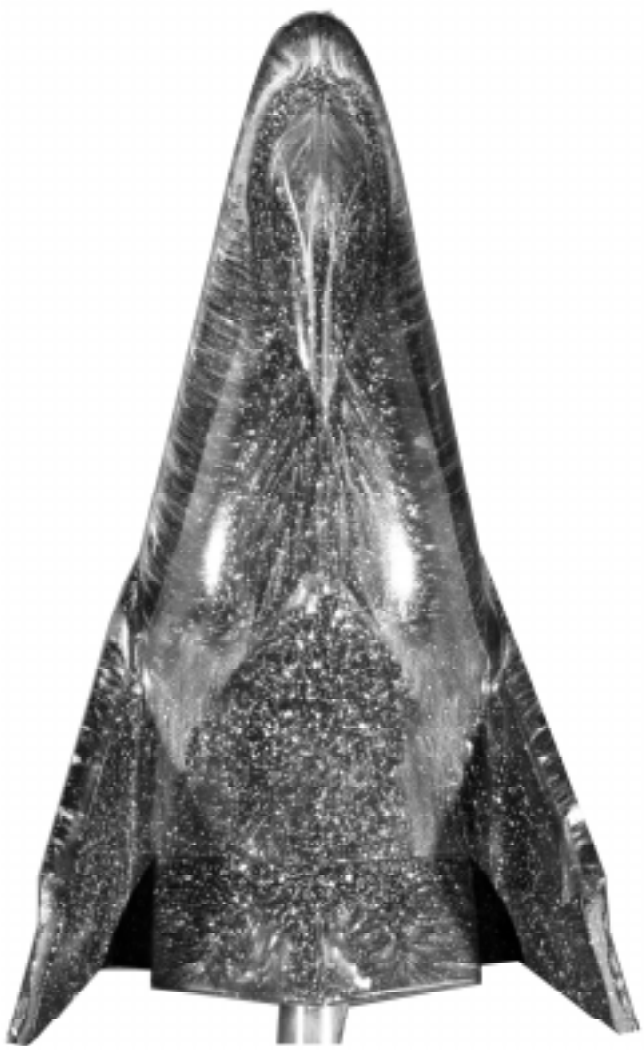

LEEWARD VIEW

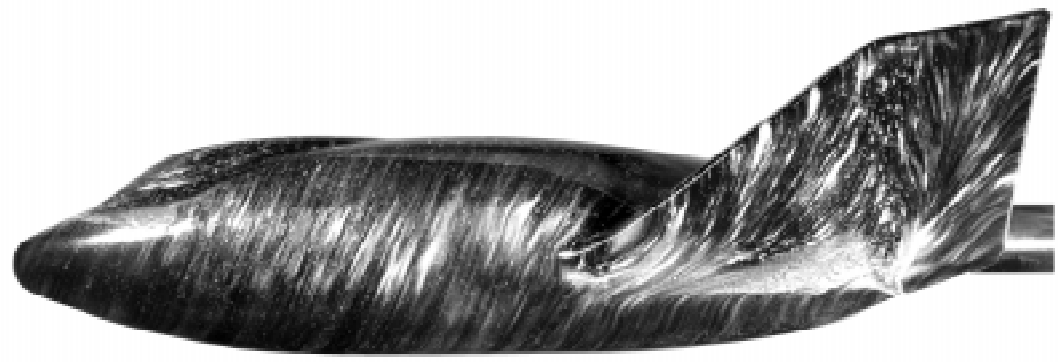

SIDE VIEW

TEST 6739
$\alpha = 40^{\circ}$
BF@ 0°

RUN 7
$Re_{\infty}/ft = 2.2X10^{6}$

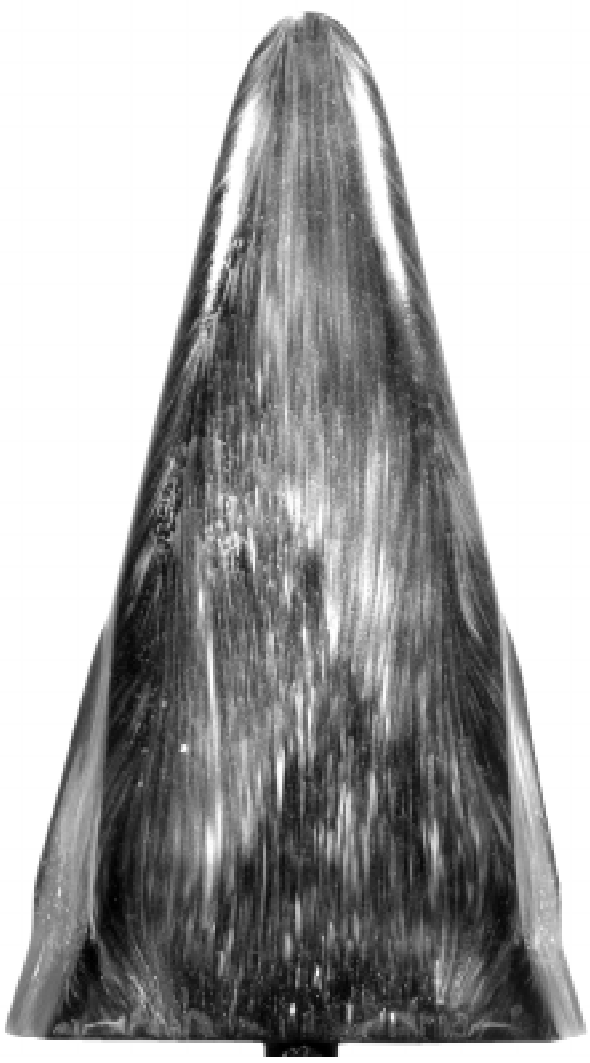

WINDWARD VIEW

LEEWARD VIEW

SIDE VIEW

TEST 6739
$\alpha = 20^{\circ}$
BF@ 0°

RUN 8
$Re_{\infty}/ft = 2.2X10^{6}$

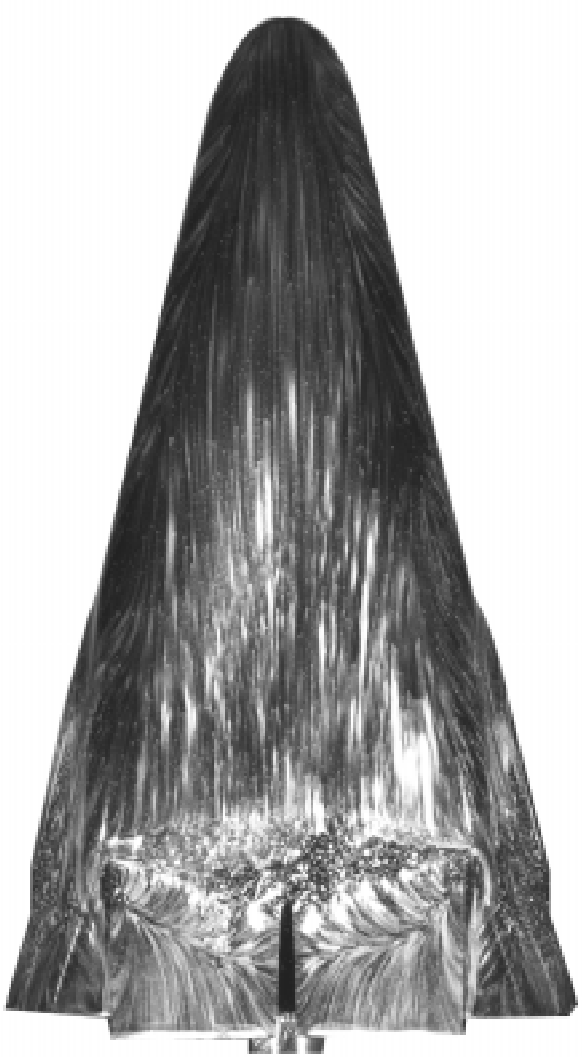

WINDWARD VIEW

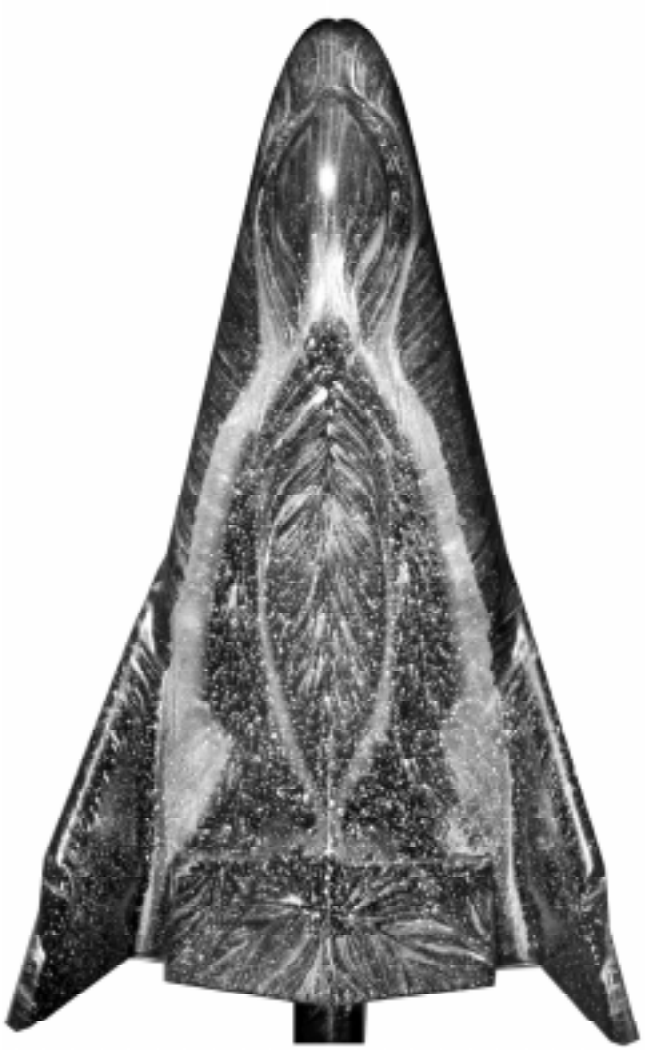

LEEWARD VIEW

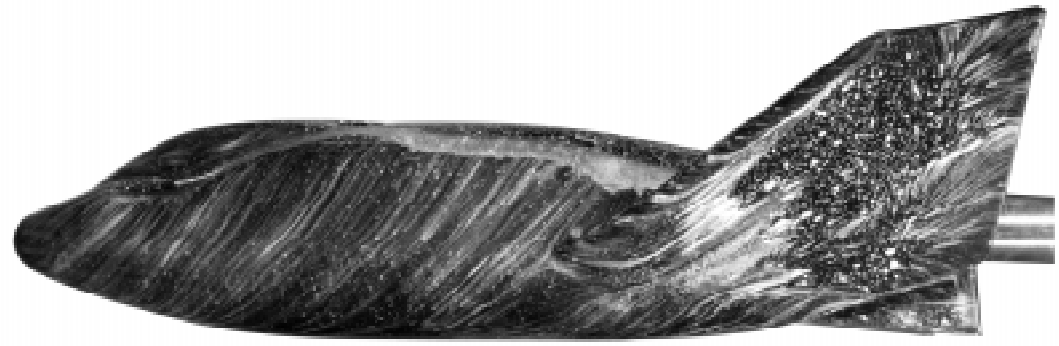

SIDE VIEW

TEST 6739
$\alpha = 20^{\circ}$
BF@ 25°

RUN 9
$Re_{\infty}/ft = 2.2X10^{6}$

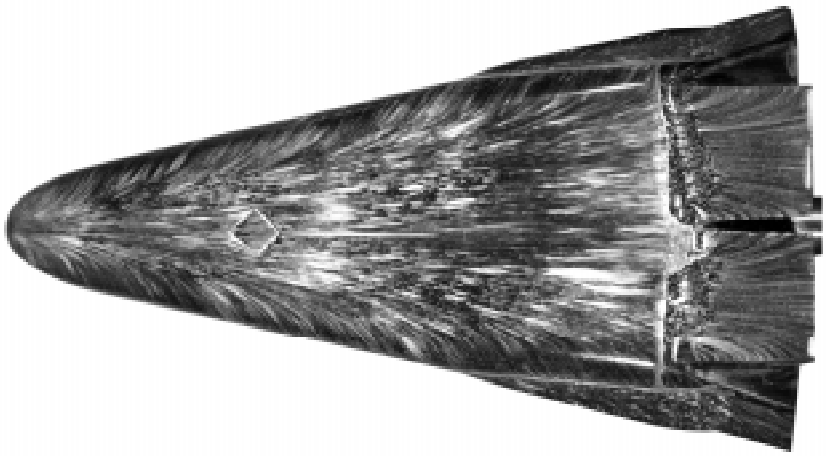

TEST 6739 RUN 10
α = 40° Re_∞/ft = 2.2X10^6
BF@ 25° Trip@ x/L=0.3, W=0.4", k=0.005”

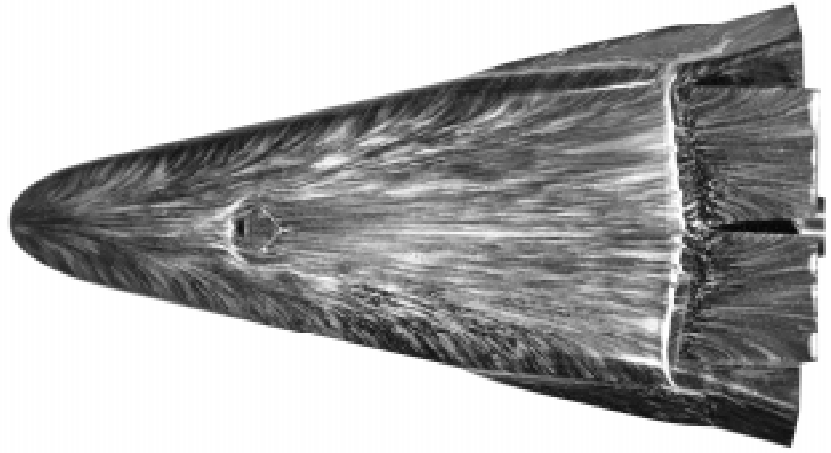

TEST 6739 RUN 11
α = 40° Re_∞/ft = 4.4X10^6
BF@ 25° Trip@ x/L=0.3, W=0.4", k=0.005” (peeled up)

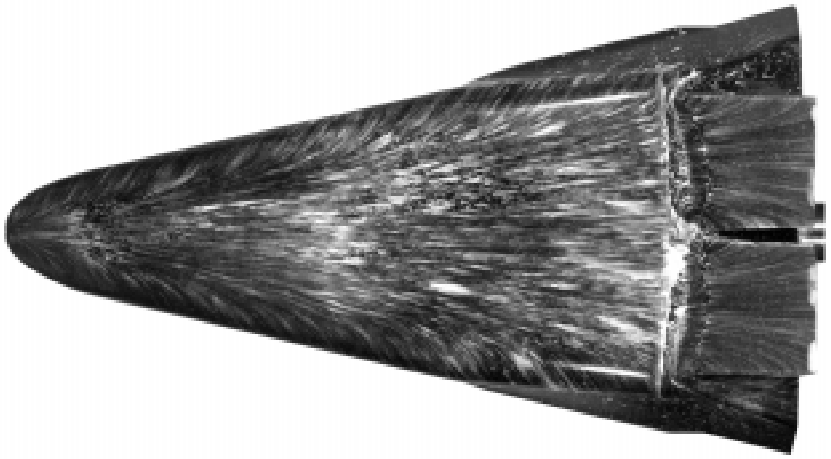

TEST 6739 RUN 12
α = 40° Re_∞/ft = 2.2X10^6
BF@ 25° Trip@ x/L=0.2, W=0.05", k=0.005”

REPORT DOCUMENTATION PAGE

Form Approved
OMB No. 0704-0188

1. AGENCY USE ONLY (Leave blank)	2. REPORT DATE	3. REPORT TYPE AND DATES COVERED
	September 1997	Technical Memorandum

4. TITLE AND SUBTITLE
Results of Aerothermodynamic and Boundary-Layer Transition Testing of 0.0362-Scale X-38 (Rev. 3.1) Vehicle in NASA Langley 20-Inch Mach 6 Tunnel

5. FUNDING NUMBERS
906-42-00-50

6. AUTHOR(S)
Scott A. Berry, Thomas J. Horvath, V. Eric Roback, and George B. Williams, Jr.

7. PERFORMING ORGANIZATION NAME(S) AND ADDRESS(ES)
NASA Langley Research Center
Hampton, VA 23681-2199

8. PERFORMING ORGANIZATION REPORT NUMBER

9. SPONSORING/MONITORING AGENCY NAME(S) AND ADDRESS(ES)
National Aeronautics and Space Administration
Washington, DC 20546-0001

10. SPONSORING/MONITORING AGENCY REPORT NUMBER
NASA TM-112857

11. SUPPLEMENTARY NOTES
Berry, Horvath, Roback, and Williams: Langley Research Center, Hampton, VA

12a. DISTRIBUTION/AVAILABILITY STATEMENT
Unclassified–Unlimited
Subject Category 34
Availability: NASA CASI (301) 621-0390

12b. DISTRIBUTION CODE

13. ABSTRACT (Maximum 200 words)
The aeroheating characteristics of the X-38 Revision 3.1 lifting-body configuration have been experimentally examined in the Langley 20-Inch Mach 6 Tunnel. Global surface heat transfer distributions, surface streamline patterns, and shock shapes were measured on a 0.0362-scale model of a proposed Space Station Crew Return Vehicle at Mach 6 in air. Parametric variations include angles-of-attack of 20°, 30°, and 40°; Reynolds numbers based on model length of 0.9 to 3.7 million; and body-flap deflections of 0°, 20°, 25°, and 30°. The effects of discrete roughness elements, which included trip height, location, size, and orientation, as well as multiple-trip parametrics, were investigated. This document is intended to serve as a quick release of preliminary data to the X-38 program; analysis is limited to observations of the experimental trends in order to expedite dissemination.

14. SUBJECT TERMS
Experimental reentry heat transfer; Boundary-layer transition;
Phospor thermography technique; Lifting-body aerothermodynamics

15. NUMBER OF PAGES
99

16. PRICE CODE
A05

17. SECURITY CLASSIFICATION OF REPORT	18. SECURITY CLASSIFICATION OF THIS PAGE	19. SECURITY CLASSIFICATION OF ABSTRACT	20. LIMITATION OF ABSTRACT
Unclassified	Unclassified	Unclassified	